Ph. D. Thesis

Satyajyoti Senapati

July 2005

BIOSYNTHESIS AND IMMOBILIZATION OF NANOPATICLES AND THEIR APPLICATIONS

SATYAJYOTI SENAPATI

JULY 2005

BIOSYNTHESIS AND IMMOBILIZATION OF NANOPARTICLES AND THEIR APPLICATIONS

A THESIS

SUBMITTED TO THE

UNIVERSITY OF PUNE

FOR THE DEGREE OF

DOCTOR OF PHILOSOPHY

IN

CHEMISTRY

BY

SATYAJYOTI SENAPATI

CATALYSIS DIVISION
NATIONAL CHEMICAL LABORATORY
PUNE 411 008
INDIA

JULY 2005

DECLARATION BY RESEARCH GUIDE

Certified that the work incorporated in the thesis entitled: "**Biosynthesis and immobilization of nanoparticles and their applications**", submitted by Mr. Satyajyoti Senapati, for the Degree of ***Doctor of Philosophy***, was carried out by the candidate under my supervision at Catalysis Division, National Chemical Laboratory, Pune 411 008, India. Such material as has been obtained from other sources has been duly acknowledged in the thesis.

Dr. Rajiv Kumar
(Research Supervisor)

DECLARATION BY RESEARCH SCHOLAR

I hereby declare that the thesis entitled " **Biosynthesis and immobilization of nanoparticles and their applications**", submitted for the Degree of ***Doctor of Philosophy*** to the University of Pune, has been carried out by me at Catalysis Division, National Chemical Laboratory, Pune 411 008, India, under the supervision of Dr. Rajiv Kumar. The work is original and has not been submitted in part or full by me for any other degree or diploma to this or any other University.

Satyajyoti Senapati

…….Dedicated to My Beloved Parents

Acknowledgement

It is my great pleasure to acknowledge my research supervisor Dr. Rajiv Kumar who introduced me to a fascinating realm of chemistry. His invaluable guidance, constant inspiration, unending support and constructive criticism helped me a lot to focus my views in proper perspective. I am grateful to him for giving me liberty to carry out my research work independently throughout the course of this programme. My deepest personal regards are due for him forever.

I wish to express my sincere gratitude to Dr. Absar Ahmad and Dr. M. I. Khan, Biochemical Sciences Division, who was my mentor in understanding the subject of microbiology and biochemistry. I am most indebted to them for their constant encouragement and motivation. My heartfelt thanks to Dr. Murali Sastry, Materials Chemistry Division, for his motivation, subtle guidance, fruitful discussion and constant help in exploring the new field of nanotechnology. His tireless enthusiasm has always been a source of inspiration for me.

I am thankful to Dr. S. Sivasanker and Dr. A. V. Ramaswamy, former Head of Catalysis Division, and Dr. Aditi Pant, former Head of Biochemistry Sciences Division, NCL, for providing divisional facilities. Special thanks are to Dr. A. P. Singh, Dr. Kinage, Dr. C. S. Gopinath, Dr. P. Manikandan, Dr. Halligudi, Dr. P. N. Joshi, Ms. V. Samuel, and all other scientific and non-scientific staff of Catalysis Division for their help and cooperation during my tenure as research scholar. I am also grateful to all scientific, Dr. S. Rao and Dr. Sushma and non-scientific staff of Biochemical Sciences Division for their valuable help and cooperation.

I sincerely acknowledge Dr. Sainkar, and Mr. Gaikawad for SEM and Dr. Mohan Bhadhade, Mrs. Renu Parischa and Mr. Rajesh Gunade for TEM for their valuable help in every possible way through fruitful discussions.

I am very much thankful to my senior labmates Dr. Priyabrata Mukherjee, Dr. Subhash Chandra Laha, Dr. Chitta Ranjan Patra and Dr. Deendayal Mandal, Dr. Anirban Ghosh, and my junior labmates Mahesh Kadgaonkar, Amit Deshmukh, Raina Gupta, Rajesh Upadhyay, Sonu Ram Sankar and Pranjal Kalita for their helpful hand, sympathetic ears and making the lab feel like a family. Special thanks to Atul, Anil, Feroz, Atul Sonawane, Priya, Syed, Srikant, Shabab, Shadab, Asutosh, Harish, Nitin, Anish, Vandana, Venkatesh, Chidambaram, Sachin Shah, Shylesh, Surendran, Shainaz, Shrikant, Selva, Pai, Satyanarayan, Prasant, Shanbag, Dhanashree, Shankar, Rohit, Niparkar, Tejas and all other research scholars in Catalysis Division for their constant support throughout my stay in NCL. Many thanks to the summer trainees, who helped me with my experiments at various time.

I would like to express my deep felt gratitude to my colleagues and friends, Kausikda, Subarnada, Saptarshida, Rajada, Arindamda, Mahuadi, Bikashda, Somnathda, Sujatadi, Debasisda, Tarunda, Anuradha, Saikat, Debasis Samanta, Prabal, Sukhen, Annytda, Babuda, Subhoda, Bibhas, Rupa, Debdut, Kartick, Soumitra, Prabhas, Chaitali, Arijit, Sougata, Pradip, Chanchal, Sidhuda, Mukul, Rita, Rahman, Anamitra, Pallabi, Pradip Ghosh, Sanmitra, Ambarish, Tanushree, Chinmay, Bhaskar, Maitry, Prakashda, Sahoo, Dumbre, Subramanium, Ashwini, Sumant, Debu, Kannan, Balchandra, Mahima, Sushim, Manas, Arindam, Jadab, Sasanka, Pranjal Barua, Sanjib, Diganta, Khirud, Lakhi, Sofia, Gitali, Rahul, Ankur, Upendra and Major for the wonderful time I had with them. It gives me great pleasure to thank my old friends, Rajesh, Biltu, Shyamalendu, Nilotpal, Sarbajit, Debojit, Amitava, Hari, Soumendra, Basu, Narendra, Debi, Abhijit, Ramada, Digantada, Susmita and Jhuma from whom I have received unfailing support and encouragement during many years of studies, that they have shown to me in their own special way. My sincere appreciation to Nirmalya, Nabanita, Mou, Tickla, Nupur, Amrita, Ranjanda Alokda, Boudi, Rudra, Dibyo, and my other friends for making my stay at NCL a very comfortable and memorable one.

I also take this golden opportunity to convey my earnest respect to my schoolteachers Mr. Jiten Kar and Mr. Badal Ranjan Barua, my graduation tutors Dr. Bibhas Das Purakayastha and Dr. Alok Debroy, and the professors of Department of Chemistry, Gauhati University, Prof. Saibal Bhattacherjee and Dr. Birinchi Kumar Das for their extraordinary way of teaching that build up my research career in science.

It gives me great pleasure to thank Ma, Baba, Dada, Chorda, Mohor, Boudi, Jethu, Boroma, Kaku for their love, unfailing support, tremendous patience, trust and encouragement they have shown in their own way during my long period of studies. They have been a constant source of strength and inspiration for me. My due thanks to Pompi, Mom, Jona and Monida who has so much love and faith in me.

Finally, my thanks are due to Council of Scientific and Industrial Research, Government of India, for awarding the research fellowship, and to Dr. P. Ratnasamy, former Director, Dr. S. Sivaram, Director, and Dr. B. D. Kulkarni, Deputy Director, National Chemical Laboratory, to carry out my research work and extending all possible infrastructural facilities, and to allow me to submit this work in the form of a thesis for the award of Ph.D. degree.

July 2005 Satyajyoti Senapati

CONTENTS

List of Figures

List of Tables

List of Abbreviations

AAS	Atomic Absorption Spectroscopy
ATP	Adenosine Triphosphate
BE	Binding Energy
CDBA	Cetyldimethylbenzylammonium Chloride
CVD	Chemical Vapor Deposition
Conv.	Conversion
2D	Two Dimension
3D	Three Dimension
DDSA	Dodecynyl Succinic Anhydride
DMP	Tridimethylaminomethyl Phenol
DNA	Deoxyribonucleic acid
e.g.	For Example
eV	Electron Volt
fcc	Face Centered Cubic
FIB	Focused Ion Beam
FID	Flame Ionizing Detector
Fig.	Figure
FT	Fourier Transform
FTIR	Fourier Transform Infrared
g	Gram
GC	Gas Chromatography
GCMS	Gas Chromatography Mass Spectroscopy
h	Hour
kDa	Kilo Dalton
LCD	Light Emitting Diode
M	Molar
mA	Miliampere
MCM	Mobile's Crystalline Material
MGYP	Malt Extract-Glucose-Yeast Extract-Peptone
min	Minute
mL	Mililitre

μL	Microlitre
mM	Milimolar
MNA	Methyl Nadic Anhydride
NADH	Nicotinamide Adenine Dinucleotide (reduced)
NCIM	National Collection of Industrial Microorganisms
nm	Nanometer
PAGE	Polyacrylamide Gel Electrophoresis
PDA	Potato-Dextrose-Agar
RNA	Ribonucleic acid
rpm	Revolution Per Minute
SAD	Selected Area Diffraction
SAED	Selected Area Electron Diffraction
Sel.	Selectivity
SEM	Scanning Electron Microscopy
TCD	Thermal Conductivity Detector
TEM	Transmission Electron Microscopy
TEOS	Tetraethylorthosilicate
UV-Vis	Ultraviolet-Visible
V	Volt
Viz.	Namely
W/O	Water in Oil
W/V	Weight/Volume
XRD	X-rays Diffraction
XPS	X-ray Photoelectron Spectroscopy

1.1. INTRODUCTION

Over the last few years, the scientific and engineering communities have been witnessing an impressive progress in the field of nanoscience and nanotechnology. Nanotechnology deals with small structures and small-sized materials of dimensions in the range of few nanometers to less than 100 nanometers. The unit of nanometer derives its prefix *nano* from a Greek word meaning extremely small. One nanometer (10^{-9} of a meter) is roughly the length occupied by five silicon or ten hydrogen atoms aligned in a line. In comparison, the hydrogen atom is about 0.1 nanometer, a virus may be about 100 nanometers, a red blood corpuscle approximately 7,000 nanometers in diameter and an average human hair is 10,000 nanometers wide.

1.1.1. What is Nanoscience and Nanotechnology?

"Nanoscience" is the study of phenomena exhibited by materials at atomic and molecular level of dimensions ranging from a few nanometers to less than 100 nanometers. In chemistry, this range of sizes has been associated with colloids, micelles, polymer molecules, and similar structures such as very large molecules, or aggregates of many molecules. In physics and electrical engineering, nanoscience is most often associated with quantum behavior, and the behavior of electrons in nanoscale structures. Biology and biochemistry have also been deeply associated with nanoscience as components of the cell; most interesting structures of biology such as DNA, RNA and subcellular organelles can be considered as nanostructures.[1]

"Nanotechnology" is the application of science to control matter at the molecular level. At this level, the properties are significantly different from that of bulk materials. It is also referred to as the term for designing, characterization, production and application of structures, devices and systems by controlling shape and size at nanometer scale.[2] In

other words, nanoscience and technology is a field that focuses on (i) the development of synthetic methods and surface analytical tools for building structures and materials, (ii) to understand the change in chemical and physical properties due to miniaturization, and (iii) the use of such properties in the development of novel and functional materials and devices.[3] Nanoscience offers an exciting possibility to study a state of matter, which is intermediate between bulk and isolated atoms or molecules, as well as the effect of spatial confinement on electron behavior. It also provides an opportunity to explore the problems related to surface or interface because of their interfacial nature.[4]

It has been well known that living cells are the best examples of machines that operate at the nano level and perform a number of jobs ranging from generation of energy to extraction of targeted materials at very high efficiency. The ribosome, histones and chromatin, the Golgi apparatus, the interior structure of the mitochondrion, the photosynthetic reaction center, and the fabulous ATPases that power the cell are all nanostructures, which work quite efficiently.[5] Ancient Indian medicinal system, *Ayurveda* has been using gold in different formulations for curing acute diseases such as rheumatoid Arthritics.[6] With present day understanding of nanoscience, one can unambiguously get enlightened that these formulations contained gold nanoparticles (Fig. 1.1). Thus, the fusion of ancient wisdom and present understanding of nanoscience can imparts more light on future development of medical sciences.

The area of research in the field of nanotechnology is as diverse as physics, chemistry, material science, microbiology, biochemistry and also molecular biology. The interface of nanotechnology in combination with biotechnology and biomedical engineering is emerging by the use of nanoscale structures in diagnosis, gene sequencing, and drug delivery. Nanotechnology holds promise for enabling us to learn

more about the detailed operation of individual cells and neurons, which could help us to re-engineer living systems.[7]

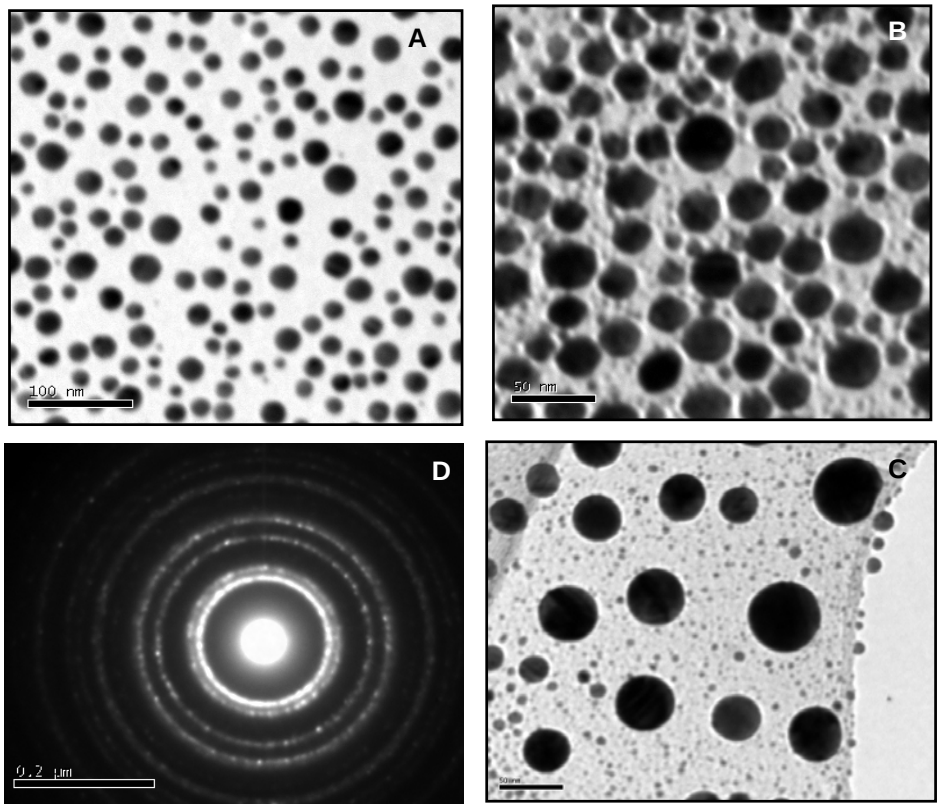

Figure 1.1. TEM micrographs (A-C) and SAD (D) recorded from Fig. 1.1C of gold powder (commercially available as *Swarna Bhasma* manufactured and supplied by Shree Vaidyanath, Ayurved Bhawan, Nagpur, India). These figures (A-C) clearly show the spherical gold nanoparticles as evident from Fig. D, which is characteristic of fcc gold. This gold powder (in Sanskrit *Swarna* meaning gold) is commonly used as one of the potent traditional formulations in different *Ayurvedic* food supplements and medicines.

1.1.2. Emergence of Nanotechnology

The first so-called scientific study of nanoparticles took place way back in 1831, when Michael Faraday investigated the ruby red colloids of gold and made public that the color was due to the small size of the metal particles. Gold and silver have found their way into glasses for over 2000 years, usually as nanoparticles. They have most

frequently been employed as colorants, particularly for church windows. Until 1959, nobody had thought of using atoms and molecules for fabricating devices. It was first revisioned by Nobel Laureate Physicist Richard Feynman at a lecture entitled “There is plenty of room at the bottom”. It was much later in 1974 that Norio Taniguchi, a researcher at the University of Tokyo, Japan used the term “nanotechnology” while engineering the materials precisely at the nanometer level. The primary driving force for miniaturization at that time came from the electronics industry, which aimed to develop tools to create smaller electronic devices on silicon chips of 40–70 nm dimensions. The use of this term, “nanotechnology” has been growing to mean a whole range of tiny technologies, such as material sciences, where designing of new materials for wide-ranging applications are concerned; to electronics, where memories, computers, components and semiconductors are concerned; to biotechnology, where diagnostics and new drug delivery systems are concerned.[8]

1.1.3. Consequences of Miniaturization

Every substance regardless of composition exhibits new properties when the size is reduced to less than 100 nm. The electronic structure of a nanocrystal critically depends on its size. For small particles, the electronic energy levels are not continuous as in bulk materials, but discrete. This arises primarily due to confinement of electrons within particles of dimension smaller than the bulk electron delocalization length; this process is termed as quantum confinement.[9] Noble metal and semiconductor nanoparticles are unique examples of this principle (Fig. 1.2).[10] The average electronic energy level spacing of successive quantum levels, also known as Kubo gap, (Kubo gap (δ) = $4E_f/3n$, where E_f is the Fermi energy of the bulk material and n is total number of valence electrons in the nanocrystal), can be tuned to make a system either metallic and

non-metallic. For example, for an individual silver nanoparticle of 3 nm diameter containing approximately 10^3 silver atoms, the value of δ would be 5–10 meV. Since the

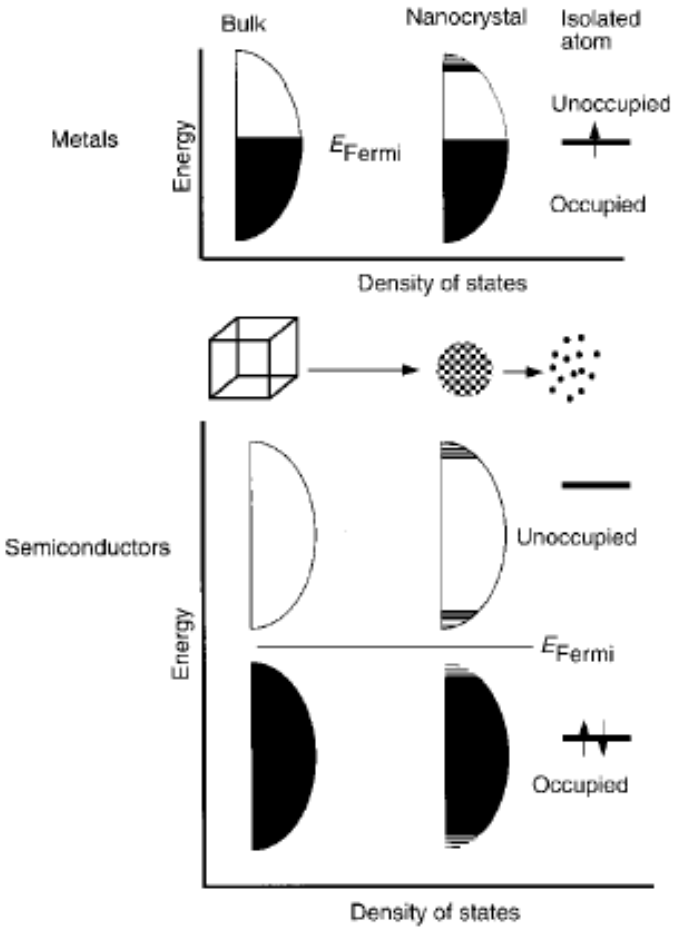

Figure 1.2. Density of states for metal and semiconductor nanocrystals. In each case, the density of states is discrete at the band edges. The Fermi level is in the center of a band in a metal, and so kT may exceed the electronic energy level spacing even at room temperatures and small sizes. In contrast, in semiconductors, the Fermi level lies between two bands, so that the relevant level spacing remains large even at small sizes. The HOMO–LUMO gap increases in semiconductor crystal of smaller size. [Source: Ref. 10]

thermal energy at room temperature, $kT \cong 25$ meV (k is Boltzmann's constant), the 3 nm particle would be metallic ($kT>\delta$). However, at low temperatures, the level spacings specially in small particles, may become comparable to kT, rendering them

nonmetallic.[11] Thus, the properties such as electrical conductivity and magnetic susceptibility exhibit quantum size effects due to the presence of the Kubo gap in individual nanoparticles.[12]

Thus, the properties of traditional materials change at nano level due to the quantum effect and the behavior of surfaces start to dominate the behavior of bulk materials. The optical, electrical, mechanical, magnetic, and chemical properties can be systematically manipulated by adjusting the size, composition, and shape of the nanoscale materials. Nanomaterials have tremendous potential applications in catalysis,[13] photocatalysis,[14] optoelectronics,[15] single-electron transistors, light emitters,[16] nonlinear optical devices,[17] hyperthermia treatment for malignant cells,[18] magnetic memory storage devices, magnetic resonance imaging enhancement,[19] cell labeling,[20] cell tracking,[21] *in vivo* imaging,[22] and DNA detection.[23] The wide range of applications shown by nanomaterials is mainly due to (i) large surface area and (ii) small size. Electron transport, manifested in phenomena like Coloumb blockade,[24] as well as the catalytic and thermodynamic properties of structures can be tailored when one can rationally design materials on this length scale. Therefore, analytical tools and synthetic methods allow one to control composition and design on this nanometer range and will undoubtedly yield important advances in almost all fields of science.

1.2. VARIOUS METHODS FOR SYNTHESIS OF NANOPARTICLES

Nanoparticles are being viewed as fundamental building blocks of nanotechnology. They are the starting point for preparing many nanostructured materials and devices. Their synthesis is an important component of rapidly growing research efforts in nanoscale science and engineering. The nanoparticles of a wide range of

materials can be prepared by a number of methods. In synthesis and assembly strategies of nanoparticles or nanomaterials, precursors from liquids, solid or gas phase are used. They employ both chemical and physical deposition approach. They rely on either chemical reactivity or physical compaction to integrate nanostructure building blocks. Generally the manufacturing techniques fall under two categories: 'bottom-up' and 'top-down' approach. The bottom-up approach refers to the build up of a material from the bottom, i.e. atom-by-atom, molecule-by-molecule or cluster-by-cluster. The colloidal dispersion is a good example of bottom up approach in the synthesis of nanoparticles. Nanolithography and nanomanipulation techniques are also a bottom-up approach. These techniques have been widely used in the formation of structural composite nanomaterials. Top-down approach involves starting with a block bulk material and designing or milling it down to desire shape. This technique is similar to the approach used by the semiconductor industry in forming devices, utilizing pattern formation (such as electron beam lithography). Both approaches play very important roles in modern industry and most likely in nanotechnology as well. There are advantages and disadvantages in both approaches. The main challenge for top- down approach is the creation of increasingly small structure with sufficient accuracy whereas in bottom-up approach, the main challenge is to make structure large enough and of sufficient quality to be of useful as materials.[25] Bottom-up approach promises a better chance to obtain nanostructures with less defects, more homogeneous chemical composition, and better short and long range ordering. This is because the bottom-up approach is driven mainly by the reduction of Gibbs free energy, so that nanostructures and materials such produced are in a state closer to a thermodynamic equilibrium state. On the contrary, top-down approach most likely introduces internal stress, in addition to surface defects. The

different methods for the synthesis of nanoparticles will be discussed under the following categories:

1.2.1. Synthesis of Nanoparticles by Sol Process

In this approach, the reagents (metal ion solution) are rapidly added into a reaction vessel containing a hot coordinating solvent such as alkyl phosphate, alkyl phosphite, pyridine, alkylamine, furan etc. The quick addition of reagents to the reaction vessel raises the precursor concentration above the nucleation threshold and also the solution becomes supersaturated due to high reaction temperature. As a result, a short nucleation brust occurs and consequently the concentration of these species in solution drops below the critical concentration for nucleation. If the time of nanocluster growth during the nucleation period is short compared to the subsequent growth processes, the nanoclusters can become more uniform and monodispersed.[26]

An alternative synthetic approach involves mixing of the reagents in a vessel at a low temperature to prevent any appreciable reaction.[26, 27] A controlled rise of the solution temperature accelerates the chemical reaction and produces the required supersaturation, which is then relieved by a burst of nucleation and the particles start growing. In either approach, the size distribution of the nanocluster sample is limited primarily by the short time interval in which the initial crystallites form and begin to grow.

In general, nanocluster size increases with increase in reaction time as more material is added to nanocluster surfaces and also with increasing temperature as the rate of addition of material to the existing nuclei increases.[26, 27] The systematic adjustment of the reaction parameters, such as reaction time, temperature, concentration, and the selection of reagents and surfactants, can be used to control the size, shape, and quality of nanoclusters.[26, 27]

There are number of reports in literature on synthesis the nanoparticles using this approach. A wide range of nanoparticles have been successfully synthesized by this method such as CdSe,[26, 27, 28] CdS,[26b, 29] CdTe,[28a, 30] ZnSe,[31] ZnO,[32] InP,[33] InAs,[34] PbSe,[35] bimetallic nanoclusters such as AuAg, FePt,[36] CoPt,[37] core/shell nanoclusters such as CdSe/ZnS,[38] CdSe/CdS,[39] metal oxides nanoclusters such as Fe_3O_4,[40] TiO_2,[41] $BaTiO_3$.[42] Peng et al. demonstrated the one-pot synthesis of high quality cadmium chalcogenides nanoclusters by heating a mixture of CdO as the cadmium precursor, trioctylphosphine oxide and tetradecylphosphonic acid at 300–320 °C and then injecting the tellurium solution into the reaction mixture.[30b] Recently, Alivisatos et al. reported the synthesis of nanorods, as well as arrow-, tetrapod- and branched tetrapod-shaped nanocrystals of CdSe by growing the nanoparticles in a mixture of hexylphosphonic acid and trioctylphosphine oxide at around 300 °C.[28e]

1.2.2. Synthesis of Nanoparticles using Micelle

The use of reversed micelles in the synthesis of metal nanoparticles has well been documented in literature.[43] Strong reducing agents such as $NaBH_4$, N_2H_4, and sometimes hydrogen gas were used. Recently, Pilani et al. has shown that synthesis in reverse micelles combined with precipitation can lead to highly monodispersed metal and semiconducting nanoparticles and their spontaneous formation of 2D or 3D networks. They demonstrated the organization of silver particles in 2D and 3D supperlattices using N_2H_4 as a reducing agent.[44] Baglioni et al. reported the synthesis of Cu_3Au alloy nanocluster by chemical reduction of the cations in water with isooctane as microemulsion.[45] A wide variety of nanoparticles have been synthesized using this process. The nanoparticles of Pt, Rh, Pd, Ir,[46] Ag,[47] Au,[48] Cu,[49] Co,[50] Ni, FeNi,[51] CoNi,[52] etc. have been effectively synthesized.

Metal oxide nanoparticles can also be prepared inside reverse micelles by the hydrolysis procedure where metal alkoxide dissolved in oil reacts with water inside the droplets. Joselevich and Willner[53] reported the synthesis of ultrasmall TiO_2 particles in situ in a water/oil microemulsion composed of water, cetyldimethylbenzylammonium chloride (CDBA) and benzene by controlled hydrolysis of $TiCl_4$. Shah et al.[54] demonstrated the use of water/triton X-100/hexanol/cyclohexane microemulsions for the preparation of TiO_2 nanoparticles in the size range of 20–40 nm. Chang and Fogler[55] reported the synthesis of silica particles from the hydrolysis of tetraethylorthosilicate (TEOS) in nonionic water/oil (W/O) microemulsion. Metal oxide nanoparticles such as ZrO_2,[56] TiO_2,[53, , 57] SiO_2,[55, 58] and Fe_2O_3[59] have been prepared in this fashion. Metal sulfate,[60] metal sulfides,[61] metal carbonates,[62] and silver halides[63] can be produced by the precipitation reaction between reactants in reverse micelles. It has observed that the water content in the micelles greatly affects the shape of the nanoparticles. Nanowires such as $BaCO_3$ and $BaSO_4$ have been synthesized using reverse micelles with different water contents.

1.2.3. Synthesis of Nanoparticles by Sol-Gel Process

The sol-gel method is based on inorganic polymerization reactions. The sol-gel process includes four steps: hydrolysis, polycondensation, drying, and thermal decomposition. The size of the sol particles depends on the solution composition, pH, and temperature. By controlling these factors, one can tune the size of the particles. This method has been used to synthesize metal oxide nanostructures, such as TiO_2,[64] UO_2,[65] TnO_2, ZrO_2,[66] CeO_2,[67] SnO_2,[68] SiO_2,[69] CuO,[70] SnO_2,[71] ZnO,[72] Al_2O_3,[73] Sc_2O_3,[74] $ZnTiO_3$,[75] $SrTiO_3$,[76] $BaZrO_3$,[77] $CaSnO_3$[78] and other nanostructures.

1.2.4. Synthesis of Nanoparticles by Chemical Precipitation

The kinetics of nucleation and particle growth in homogeneous solutions can be adjusted by the controlled release of the anions and cations. Careful control of the kinetics of the precipitation can result in monodisperse nanoparticles. Thus, it is essential to control the factors that determine the precipitation process, such as the pH and the concentration of the reactants and ions. Organic molecules are used to control the release of the reagents and ions in the solution during the precipitation process. The particle size is influenced by the reactant concentration, pH, and temperature. By engineering these factors, nanoparticles with narrow size distributions can be synthesized. $Zr(OH)_4$,[79] $BaTiO_3$,[80] CdS,[81] HgTe,[82] HgTe,[83] and CdTe[84], AuAg nanoparticles have been produced by this approach. Sordelet and Akinc reported the utilization of urea to control the nucleation process in the synthesis of Y_2O_3:Eu nanoparticles.[85] Henglein et al. demonstrated the preparation of CdS nanocrystals with a relatively narrow size distribution of 4–6 nm by precipitating Cd^{2+} ions with the addition of stoichiometric amount of H_2S at higher pH. Yamamura et al. described the preparation of barium titanate nanoparticles by addition of ethanolic oxalic acid solution to barium titanium mixed aqueous solution at room temperature.[80a] Although the method of using precipitation to prepare nanoparticles is very straightforward and simple, very complicated nanostructures can also be constructed using this method such as CdS/HgS/CdS,[86] $CdS/(HgS)_2/CdS$[87] and HgTe/CdS[88] quantum well systems and other core/shell structures.

1.2.5. Synthesis of Nanoparticles by Hydrothermal Method

Hydrothermal synthesis is a common method to synthesize zeolite/molecular sieve crystals. This method exploits the solubility of almost all inorganic substances in

water at elevated temperatures and pressures and subsequent crystallization of the dissolved material from the fluid. Water at elevated temperatures plays an essential role in the precursor material transformation because the vapor pressure is much higher and the structure of water at elevated temperatures is different from that at room temperature. The properties of the reactants, including their solubility and reactivity, also change at high temperatures. The changes mentioned above provide more parameters to produce different high-quality nanoparticles and nanotubes, which are not possible at low temperatures. During the synthesis of nanocrystals, parameters such as pressure, temperature, reaction time, and the respective precursor-product system can be tuned to maintain quite high rate of simultaneous nucleation and narrow particle size distribution. Different types of nanoparticles such as TiO_2,[89] $LaCrO_3$,[90] ZrO_2,[91] $BaTiO_3$,[92] $SrTiO_3$,[93] $Y_2Si_2O_7$,[94] Sb_2S_3,[95] CrN,[96] SnS_2,[97] PbS,[98] Ni_2P[99] and SnS_2 nanotubes,[100] Bi_2S_3 nanorods[101] and SiC nanowires[102] have been successfully synthesized using this methodology.

Different types of nanostructures have also been obtained by solvothermal synthesis using supercritical fluids as solvents. Min ji et al.[103] described a method to synthesize metallic silver nanoparticles having diameter from 5–15 nm in supercritical CO_2 using water in CO_2 microemulsion. Ag,[103, 104] Cu,[104b, 105] Ni,[106] Co, Pt, Ge,[107] Au,[108] PdS,[109] ZnS[110] and CdS,[110, 111] Ge,[112] GaAs[113] and also nanowire, and carbon nanotube[114] have also been synthesized.

In addition, a new approach, named solventless synthesis, has recently been developed,[115] and various shapes of nanostructures have been synthesized, including Cu_2S nanoparticles,[115a,b] nanorods,[115a,b] nanodisks,[115a,b] nanoplates,[115a,b] NiS nanorods, and triangular nanoprisms.[116]

1.2.6. Synthesis of Nanoparticles by Pyrolysis

Pyrolysis is a chemical process in which chemical precursors decompose into solid compound and unwanted waste evaporates away. Upon completion, the desired new substance is obtained. Generally, the pyrolytic synthesis of compounds leads to powders with a wide size distribution in the micrometer regime. To get a uniform nanosized material, some modifications or revisions of the pyrolytic preparation procedure and reaction conditions are need to be changed such as slowing of the reaction rate or decomposition of the precursor in the inert solvent. Pyrolysis can be used to prepare different kinds of nanoparticles including metals, metal oxides, semiconductors, and composite materials such as Ag,[117] Au,[118] ZrO_2,[119] Al_2O_3,[120] SnO_2, TiO_2,[121] GaN,[122] ZnS,[123] $YBa_2Cu_3O_{7-x}$,[124] Ni,[125] and carbon nanotubes.[126]

The pyrolysis of organic precursors seems to provide a direct and effective method of producing nanotubes of various kinds such as the one-step synthesis of aligned carbon nanotubes and Y-junction nanotubes. Carbon nanotubes produced from organometallic precursors can be used to further prepare gallium nitride nanowires, silicon nitride nanotubes, and boron nitride nanotubes.[127]

1.2.7. Synthesis of Nanoparticles using Chemical Vapor Deposition

In chemical vapor deposition (CVD) technique, the vaporized precursors are introduced into a CVD reactor and adsorb onto a substance held at an elevated temperature. These adsorbed molecules will either thermally decompose or react with other gases/ vapors to form crystals. The CVD process consists of three steps: (a) mass transport of reactants to the growth surface through a boundary layer by diffusion, (b) chemical reactions on the growth surface, and (c) removal of the gas-phase reaction byproducts from the growth surface.

There are many good examples of the application of this method in the recent literature. Ostraat et al.[128] have demonstrated a two-stage reactor for producing oxide-coated silicon nanoparticles that have been incorporated into high-density non-volatile memory devices. This is one of relatively few examples of a working microelectronic device in which vapor-phase synthesized nanoparticles perform an active function. In other recent examples of this approach, Magnusson et al.[129] produced tungsten nanoparticles by decomposition of tungsten hexacarbonyl and Nasibulin et al.[130] produced copper and copper oxide nanoparticles from copper acetylacetonate.

Another key feature of chemical vapor synthesis is that it allows formation of doped or multi-component nanoparticle by use of multiple precursors. Schmechel et al.[131] prepared nanocrystalline europium doped yttria (Y_2O_3:Eu^{3+}) from organometallic yttrium and europium precursors. Senter et al.[132] incorporated erbiumin to silicon nanoparticles using disilane and an organometallic erbium compound as precursors. Srdic et al.[133] prepared zirconia particles doped with alumina. It is also possible to make composite nanoparticles where one material is encapsulated within another. A particularly promising approach to this is the sodium metal/metal halide chemistry used by Ehrman et al.[134] In this approach, a halide, such as $SiCl_4$, is reacted with sodium vapor in a heated furnace to produce NaCl-encapsulated particles. For example, $SiCl_4$ reacts with sodium to produce NaCl-encapsulated Si particles. The salt-encapsulation can potentially be used to prevent agglomeration of particles, and the salt can then be washed away in a post-processing step.

A wide variety of nanoparticles can be synthesized using other techniques, which fall under the vapor phase process viz, inert gas condensation,[135] pulsed laser ablation,[136] ion sputtering,[137] thermal plasma synthesis,[138] flame synthesis,[139] etc.

1.2.8. Synthesis of Nanoparticles using Bio-based Protocol

The utilization of microorganisms such as bacteria[140] and yeast[141] in the synthesis of nanoparticles is a relatively recent phenomenon. The microorganisms minimize the toxicity by reduction of the metal ions or by formation of insoluble complexes with metal ions (e.g. metal sulfides) in the form of colloidal particles. An amalgamation of curiosity, environmental compulsions, and understanding that nature has evolved the processes for synthesis of inorganic materials on nano- and micro-length scale have created great interest among material scientists for the utilization of microorganisms in the synthesis of nanomaterials. It is well known that many unicellular organisms such as bacteria and algae are capable of synthesizing inorganic materials, both intra- and extracellularly.[142] Some of the examples include magnetotactic bacteria, which synthesize magnetite nanoparticles,[143] diatoms and radiolarians that synthesize siliceous materials[144] and S-layer bacteria that produce gypsum and calcium carbonate as surface layers.[145] These bioinorganic materials can be extremely complex both in structure and function, and also exhibit exquisite hierarchical ordering from the nanometer to macroscopic length scale, which has not even remotely been achieved in the laboratory based syntheses.

The accumulation of inorganic particles in microbes has been reported by Zumberg, Sigleo and Nagy (gold in Precambrian algal blooms),[146] Hosea and coworkers (gold in algal cells),[147] Beveridge and coworkers (gold in bacteria),[148] Aiking and coworkers (CdS in bacteria),[140a] Reese and coworkers (CdS in yeast),[149] Temple and Leroux (ZnS in sulfate-reducing bacteria)[150] and Blakemore, Maratea and Wolfe (magnetite in bacteria).[151] More recent and detailed investigations into the use of microbes in the synthesis of nanoparticles of different chemical compositions and shape

include bacteria for silver,[152] gold,[152d, 153] CdS,[154] ZnS (sphalerite),[155] magnetite,[143, 156] iron sulfide,[157] yeast for PbS[158] and CdS[159] and algae for gold.[160] Very recently, the synthesis of nanoparticles of variable morphology using leaves of different plants, sprouts, roots and stems of live alfalfa plants have been demonstrated.[161, 162]

Tanja Klaus and co-workers showed that the metal-resistant bacterium, *Pseudomonas stutzeri* AG259 (originally isolated from a silver mine), when challenged with high concentrations of silver ions during culturing resulted in the intracellular formation of silver nanoparticles, ranging in size from few nm to 200 nm.[152a, b] Most of the nanoparticles were found to be composed of elemental silver, while occasionally the formation of Ag_2S was observed. Biofilms of metal nanoparticles embedded in a biological matrix may have important applications in the synthesis of eco-friendly and economically viable cermet materials for optically functional thin film coatings. Jorger, Klaus and Granqvist showed that heat treatment of the Ag nano-bacteria biomass yielded hard coatings of a cermet, which was resistant to mechanical scratching with a knife and whose optical properties could be tailored by varying the silver loading factor.[152c] The cermet material was composed primarily of graphitic carbon and up to 5 % by weight (of the dry biomass) of silver. Recently, Nair and Pradeep have demonstrated that exposure of large concentration of metal ions to bacteria may also be used to grow nanoparticles.[152d] They showed that *Lactobacillus* strains present in buttermilk, when exposed to silver and gold ions, resulted in the production of nanoparticles within the bacterial cell.[152d] They also concluded that the nucleation of the gold and silver nanoparticles occurs on the cell surface through sugars and enzymes in the cell wall, following which the metal nuclei are transported into the cell where they aggregate and grow to larger-sized particles. Holmes and co-workers have demonstrated that on

exposure of the bacterium, *Klebsiella aerogenes* to Cd^{2+} ions resulted in the intracellular formation of CdS nanopaticles in the size range 20–200 nm.[154b] They also showed that the composition of the nanoparticles formed was a strong function of buffered growth medium for the bacterium. In an interesting extension of the bacteria-based methodology for the growth of magnetic nanoparticles, Roh and coworkers showed that metals such as Co, Cr, and Ni may be substituted into magnetite crystals biosynthesized in the thermophilic iron-reducing bacterium *Thermoanaerobacter ethanolicus*.[143c] This procedure led to the formation of octahedral-shaped magnetite nanoparticles in large quantities that co-existed with a poorly crystalline magnetite phase near the surface of the cells. In a classical study, Dameron and co-workers for the first time have demonstrated that the yeasts such as *Schizosaccharomyces pombe* and *Candida glabrata* produced intracellular CdS nanoparticles when challenged with cadmium salt in solution.[149b] Yeast cells exposed to Cd^{2+} ions produce metal-chelating peptides (glutathiones), and this is accompanied by an increase in the intracellular sulfide concentration and the formation of nanocrystalline CdS. The biogenic CdS quantum dots are capped and stabilized by the peptides, glutathione and its derivative phytochelatins with the general structure $(\gamma\text{-glu-cys})_n\text{Gly}$. Based on an extensive screening programme, Kowshik and co-workers have identified the yeast, *Turolopsis* sp., is capable of intracellular synthesis of PbS nanoparticles when exposed to aqueous Pb^{2+} ions. These crystallites were recovered from the biomass by freeze thawing and analyzed by a variety of techniques. The CdS nanocystals in the size range of 1–1.5 nm synthesized intracellularly in *Schizosaccharomyces pombe* yeast cells exhibit ideal diode characteristics. In an interesting study, Yacaman and coworkers have demonstrated the growth of gold and silver nanoparticles in sprouts, roots and stems of live alfalfa plants.

Very recently, Sastry and coworkers have demonstrated the synthesis of gold nanotriangles by using the extract of lemongrass.[162a] They also showed that, by simple variation of the experimental conditions, it is possible to vary the size of the gold nanotriangles, which show interesting absorption in the near-infrared (NIR) region of the electromagnetic spectrum. [162b]

1.3. PHYSICOCHEMICAL CHARACTERIZATION

The nanomaterials can be characterized by various techniques, which provide important information for the understanding of different physicochemical features. The most extensively used techniques can be categorized into the following:

(a) X-ray diffraction (XRD),

(b) Scanning electron microscopy (SEM),

(c) Transmission electron microscopy (TEM).

(d) Optical Spectroscopy

  (i) Ultraviolet-visible (UV-Vis) spectroscopy,

  (ii) Fluorescence spectroscopy,

  (iii)Fourier transform infrared (FTIR) spectroscopy,

(e) X-ray photoelectron spectroscopy (XPS),

(f) Atomic absorption spectroscopy (AAS).

1.3.1. X-Ray Diffraction

X-ray diffraction is a very important technique that has long been used to determine the crystal structure of solids, including lattice constants and geometry, identification of unknown materials, orientation of single crystals, defects, etc.[163] The X-ray diffraction patterns are obtained by measurement of the angles at which an X-ray

beam is diffracted by the crystalline phases in the specimen. Bragg's equation relates the distance between two *hkl* planes (*d*) and the angle of diffraction (2θ) as: $n\lambda = 2d\sin\theta$, where, λ = wavelength of X-rays, *n* = an integer known as the order of reflection (*h*, *k* and *l* represent Miller indices of the respective planes).[164] From the diffraction patterns, the uniqueness of nanocrystal structure, phase purity, degree of crystallinity and unit cell parameters of the nanocrystalline materials can be determined. X-ray diffraction technique is nondestructive and does not require elaborate sample preparation, which partly explains the wide use of XRD methods in material characterization.

X-ray diffraction broadening analysis has been widely used to determine the crystal size of nanoscale materials. The average size of the nanoparticles can be estimated using the Debye–Scherrer equation: $D = k\lambda / \beta\cos\theta$, where *D* = thickness of the nanocrystal, *k* is a constant, λ = wavelength of X-rays, β = width at half maxima of (111) reflection at Bragg's angle 2θ.[165]

1.3.2. Scanning Electron Microscopy

Scanning electron microscopy (SEM) is one of the most widely used techniques for characterization of nanomaterials and nanostructures. The resolution of the SEM approaches a few nanometers, and the instruments can operate at magnifications that are easily adjusted from ~10 to over 300,000. This technique provides not only topographical information like optical microscopes do, but also information of chemical composition near the surface. A scanning electron microscope can generate an electron beam scanning back and forth over a solid sample. The interaction between the beam and the sample produces different types of signals providing detailed information about the surface structure and morphology of the sample. When an electron from the beam

encounters a nucleus in the sample, the resultant coulombic attraction leads to a deflection in the electron's path, known as Rutherford elastic scattering. A fraction of these electrons will be completely backscattered, reemerging from the incident surface of the sample. Since the scattering angle depends on the atomic number of the nucleus, the primary electrons arriving at a given detector position can be used to produce images containing topological and compositional information.[166] The high-energy incident electrons can also interact with the loosely bound conduction band electrons in the sample. However, the amount of energy given to these secondary electrons as a result of the interactions is small, and so they have a very limited range in the sample. Hence, only those secondary electrons that are produced within a very short distance from the surface are able to escape from the sample. As a result, high-resolution topographical images can be obtained in this detection mode.[167]

1.3.3. Transmission Electron Microscopy

Transmission electron microscopy (TEM) is typically used for high resolution imaging of thin films of a solid sample for nanostructural and compositional analysis. The technique involves: (i) irradiation of a very thin sample by a high-energy electron beam, which is diffracted by the lattices of a crystalline or semicrystalline material and propagated along different directions, (ii) imaging and angular distribution analysis of the forward-scattered electrons (unlike SEM where backscattered electrons are detected), and (iii) energy analysis of the emitted X-rays.[168] The topographic information obtained by TEM in the vicinity of atomic resolution can be utilized for structural characterization and identification of various phases of nanomaterials, *viz.*, hexagonal, cubic or lamellar.[169] One shortcoming of TEM is that the electron scattering information in a TEM image originates from a three-dimensional sample, but is projected onto a two-

dimensional detector. Therefore, structural information along the electron beam direction is superimposed at the image plane.

Selected area diffraction (SAD) offers a unique advantage to determine the crystal structure of individual nanomaterials, such as nanocrystals and nanorods, and the crystal structures of different parts of the sample. In SAD, the condenser lens is defocused to produce parallel illumination at the specimen and a selected-area aperture is used to limit the diffracting volume. SAD patterns are often used to determine the Bravais lattices and lattice parameters of crystalline materials by the same procedure used in XRD.[170]

In addition to the capability of structural characterization and chemical analyses, TEM has been also explored for the other applications in nanotechnology. Examples include the determination of melting points of nanocrystals, in which, an electron beam is used to heat up the nanocrystals and the melting points are determined by the disappearance of electron diffraction.[171] Another example is the measurement of mechanical and electrical properties of individual nanowires and nanotubes.[172]

1.3.4. Optical Spectroscopy

Optical spectroscopy has been widely used for the characterization of nanomaterials and the techniques can be generally categorized into two groups: absorption (UV-Vis) and emission (fluorescence) and vibrational (infrared) spectroscopy. The former determines the electronic structures of atoms, ions, molecules or crystals through exciting electrons from the ground to excited states (absorption) and relaxing from the excited to ground states (emission). The vibrational technique involves the interactions of photons with species in a sample that results in energy transfer to or

from the sample via vibrational excitation or de-excitation. The vibrational frequencies provide the information of chemical bonds in the detecting samples.

1.3.4.1. UV-Vis Spectroscopy

It deals with the study of electronic transitions between orbitals or bands of atoms, ions or molecules in gaseous, liquid and solid state.[173] The metallic nanoparticles are known to exhibit different characteristic colors. Mie was the first to explain the origin of this color theoretically in 1908 by solving Maxwell's equation for the absorption and scattering of electromagnetic radiation by small metallic particles.[174] This absorption of electromagnetic radiation by metallic nanoparticles originates from the coherent oscillation of the valence band electrons induced by an interaction with the electromagnetic field.[175] These resonances are known as surface plasmons, which occur only in the case of nanoparticles and not in the case of bulk metallic particles.[176] Hence, UV-Vis can be utilized to study the unique optical properties of nanoparticles.[177]

1.3.4.2. Fluorescence Spectroscopy

In this technique, light of some wavelength is directed onto a specimen, prompting the transition of electron from the ground to excited state, which then undergoes a non-radiative internal relaxation and the excited electron moves to a more stable excited level. After a characteristic lifetime in the excited state, the electron returns to the ground state by emitting the characteristic wavelength in the form of light. This emitted energy can be used to provide qualitative and sometime quantitative information about chemical composition, structure, impurities, kinetic process and energy transfer.

1.3.4.3. Fourier Transform Infrared Spectroscopy

Fourier transform infrared (FTIR) spectroscopy deals with the vibration of chemical bonds in a molecule at various frequencies depending on the elements and types of bonds. After absorbing electromagnetic radiation the frequency of vibration of a bond increases leading to transition between ground state and several excited states. These absorption frequencies represent excitations of vibrations of the chemical bonds and thus are specific to the type of bond and the group of atoms involved in the vibration. The energy corresponding to these frequencies correspond to the infrared region (4000–400 cm^{-1}) of the electromagnetic spectrum. The term Fourier transform (FT) refers to a recent development in the manner in which the data are collected and converted from an interference pattern to an infrared absorption spectrum that is like a molecular "fingerprint".[178] The FTIR measurement can be utilized to study the presence of protein molecule in the solution, as the FTIR spectra in the 1400–1700 cm^{-1} region provides information about the presence of –CO- and –NH- groups.[179]

1.3.5. X-Ray Photoelectron Spectroscopy

X-ray photoelectron spectroscopy (XPS) is widely used for probing the electronic structure of atoms, molecules and condensed matter. When an X-ray photon of energy $h\nu$ is incident on a solid matter, the kinetic energy (E_k) and the binding energy (E_b) of the ejected photoelectrons can be related as follows: $E_k = h\nu - E_b$.

This kinetic energy distribution of the photoelectrons is fabricated by a series of discrete bands, which symbolizes for the electronic structure of the sample.[180] The core level binding energies of all the elements (other than H and He) in all different oxidation states are unique, which provides instant detection of the chemical composition of the

sample after a full range scan.[181] However, to account for the multiplet splitting and satellites accompanying the photoemission peaks, the photoelectron spectra should be interpreted in terms of many-electron states of the final ionized state of the sample, rather than the occupied one-electron states of the neutral species.[182]

1.3.6. Atomic Absorption Spectrometry

The principle of atomic absorption is based on energy absorbed during transitions between electronic energy levels of an atom. When some sort of energy is provided to an atom in ground state by a source such as a flame (temperature ranging from 2100–2800 °C), outer-shell electrons are promoted to a higher energy excited state. The radiation absorbed as a result of this transition between electronic levels can be used for quantitative analysis of metals and metalloids present in solid matrices, which have to be dissolved by appropriate solvents before analysis. The basis of quantitative analysis depends on measurement of radiation intensity and the assumption that radiation absorbed is proportional to atomic concentration. Analogy of relative intensity values for reference standards is used to determine elemental concentrations.[183]

1.4. PROPERTIES OF NANOMATERIALS

The reduction of materials' dimension has pronounced effects on the physical properties that may be significantly different from the corresponding bulk material. Some of the physical properties exhibited by nanomaterials are due to (i) large surface atom, (ii) large surface energy, (iii) spatial confinement, and (iv) reduced imperfections. The few properties of nanomaterials are discussed in the following:

1.4.1. Optical Property

For last few decades, metallic nanoparticles have fascinated researchers due to their colorful colloidal solutions. Mie was the first to explain the red color of gold nanoparticle in 1908 by solving Maxwell's equation for an electromagnetic light wave interacting with small metallic spheres. The color exhibited by metallic nanoparticles is due to the coherent excitation of all the "free" electrons within the conduction band, leading to an in-phase oscillation and is known is surface plasmon resonance. Thus, the color of metallic nanoparticles may change with their size due to surface plasmon resonance.

Unique optical property of nanomaterials may also be due to quantum size effect, which arises primarily because of confinement of electrons within particles of dimension smaller than the bulk electron delocalization length. This effect is more pronounced for semiconductor nanoparticle, where the band gap increases with a decreasing size. The same quantum size effect is also shown by metal nanoparticles, when the particle size is >2 nm.

1.4.2. Magnetic Property

Magnetic properties of nanostructured materials are distinctly different from that of bulk materials. Ferromagnetic particles become unstable when the particle size reduces below a certain size as the increase in surface energy provides a sufficient energy for domains to spontaneously switch polarization directions and become paramagnetic. But this transformed paramagnetism behaves differently from the conventional paramagnetism and thus is referred to as superparamagnetism.[184] In other words, ferromagnetism of bulk materials disappears and get transferred to superparamagnetism in the nanoscale due to the high surface energy.

1.4.3. Mechanical Property

The mechanical properties of nanomaterials increase with the decrease in size. Most of the studies have been focused on the mechanical properties of one dimensional structure such as nanowire. The enhanced mechanical strength of nanowires or nanorods is ascribed to the high internal perfection of the nanowires. Generally, imperfections such as dislocations, micro-twins, impurities, etc. in crystals are highly energetic and should be eliminated from the perfect crystal structures. The smaller the cross-section of nanowires, the less is the probability of finding in it any imperfections as nanoscale dimension makes the elimination of such imperfections possible.

1.4.4. Thermal Property

Metal and semiconductor nanoparticles are found to have significantly lower melting point or phase transition temperature as compared to their bulk counterparts. The lowering of the melting points is observed when the particle size is >100 nm and is attributed to increase in surface energy with a reduction of size. The decrease in the phase transition temperature can be ascribed to the changes in the ratio of surface energy to volume energy as a function of size.

1.5. APPLICATION OF NANOMATERIALS

Nanotechnology offers an extremely broad range of potential applications from electronics, optical communications and biological systems to new smart materials. The wide range of applications shown by nanostructures and nanomaterials are due to (i) the unusual physical properties exhibited by nanosized materials, e.g. gold nanoparticles used as an inorganic dye for coloration of glass, (ii) the large surface area, such as gold nanoparticles supported on metal oxide are used as low temperature catalyst and

nanoparticles for various sensors, and (iii) small size. For many applications, new materials and new properties are introduced. For example, various organic molecules are incorporated into electronic devices.[185] Some of the applications of nanostructures and nanomaterials are highlighted in the following:

1.5.1. Molecular Electronic and Nanoelectronics

The last few years have been witnessing a tremendous progress in the molecular electronic and nanoelectronics. [186] In molecular electronics, single molecules are designed to control electron transport, which offers the promise of exploring the vast variety of molecular functions for electronic devices. The control over electronic energy levels at the surface of conventional semiconductors and metals is achieved by assembling on the solid surfaces and molecules can be designed into a working circuit. If molecules are biologically active, then bioelectronic devices could be developed.[185, 187]

Many nanoelectronic devices have been developed which includes tunneling junctions,[188] electrically configurable switches,[186f] carbon nanotube transistors,[189] single molecular transistors[190] etc. Various techniques have been used in the fabrication of nanoelectronics such as focused ion beam (FIB),[191] electron beam lithography[192] and imprint lithography.[193]

Gold nanoparticles have been extensively used in nanoelectronics and molecular electronics using its surface property and uniform size. For example, gold nanoparticles function as a carrier by attaching various functional organic molecules or biocomponents.[194] Gold nanoparticles can also be used as a mediator to connect different functionalities together in the construction of nanoscale electronics for the applications of sensors and detectors.[195]

1.5.2. Nanorobots

Promising applications of nanotechnology in medical science, also referred to as nanomedicine, have fascinated a lot. One of the attractive applications of nanomedicine is the creation of nanoscale devices for improved therapy and diagnostics. Such nanoscale devices are known as nanorobot.[196] These nanorobots have the potential to serve as vehicles for delivery of therapeutic agents and detectors against early disease and perhaps may repair metabolic or genetic defects.

1.5.3. Biological Application

One of the important biological applications of colloidal nanocrystals is molecular recognition.[197] Certain biological molecules can recognize and bind to other molecules with extremely high selectivity and specificity. For molecular recognition application, antibodies and oligonucleotides are widely used as receptors. If, for example, a virus enters an organism, antibodies will recognize the virus as a hostile intruder, or antigen, and bind to it in such a way that the virus can be destroyed by other parts of the immune system.[197b]

Antibodies and oligonucleitides are typically attached to the surface of nanocrystals via (i) thiol-gold bonds to gold nanoparticles,[198] (ii) covalents linkage to silanized nanocrystals with bifunctional crosslinker molecules,[199] and (iii) a biotin-avidin linkage, where avidin is adsorbed on the particle surface.[200] Nanocrystals thus conjugated or attached to a receptor molecules can be directed to bind to positions where ligand molecules are present, which ‘fit’ the molecular recognition of the receptor.[201] This facilitates a set of applications including molecular labeling.[201,202] For example, the change in color of gold nanoparticles from ruby-red to blue due to aggregation has been

exploited for the development of very sensitive colorimetric methods of DNA analysis.[203]

Other potential biological applications of nanostructure and nanomaterials include the use of colloidal semiconductor nanocrystals as fluorescent probes to label cells[204] and chemical libraries[205] and the use of nanostructured materials as artificial bones.[204a]

1.5.4. Catalytic Application

Any material to show good catalytic activity must possess high surface area. Nanomaterials have tremendous implications in catalysis since the surface area of nanomaterials markedly increases with the reduction of their size. For example, a nanocrystal of 10 nm diameter will have ~15 % of its atoms on the surface while nanocrystal of 1 nm diameter will have ~100 %. Thus, a small nanocrystal with a higher surface area would be more catalytically active. Furthermore, the change in electronic properties arising due to quantum confinement in small nanocyrstals will also bestow unusual catalytic properties on these particles.[206] Yates et al. demonstrated that the decrease in catalytic activity per unit surface area of nickel with the increase in particle size in the hydrogenation reaction of ethane.[207] In a series of papers, Corrolleur, Gault and their co-workers demonstrated that the effect of particle size on mechanisms and product distributions of hydrogenolysis reactions over platinum catalysts.[208] There have been quite a few interesting examples of nanostructured metal oxides and sulfides exhibiting unusual catalytic properties.[209] Ying et al. reported the use of cerium oxide nanoparticles in the selective reduction of SO_2 by CO with excellent poisoning resistance towards H_2O and CO_2.[210] Very recently, Liu et al. developed a highly efficient catalyst system for CO oxidation with Au-Ag alloy nanoparticles supported on the mesoporous

MCM-41 and observed that the size effect is no longer a critical factor and Ag is believed to play a key role in the activation of oxygen.[211]

Surface science investigations[212] and theoretical calculations[213] have proved that the smooth surface of gold is catalytically inactive for both hydrogenation and oxidation reactions. It is due to the absence of no characteristic dissociative absorption of H_2 and O_2 over the smooth surface of gold at a temperature below 473 K. However, in a series of papers, Bond et al. and Haruta et al. demonstrated the nano-effect of gold particle in heterogeneous catalysis.[214] They have reported that when nanosized gold (>10 nm) deposited on certain metal oxides exhibits surprisingly high catalytic activity in hydrogenation reaction and oxidation of carbon monoxide. Bond and sermon demonstrated the hydrogenation of linear alkenes over Au/SiO_2 catalyst.[214a,b] Haruta et al. showed that the gold nanoparticles with clean surface if deposited on partly reactive oxides, such as Fe_2O_3, Co_2O_3, NiO, MnO_2, γ-alumina and titania was found to be extremely reactive in the oxidation of carbon monoxide even at a temperature of –70 °C.[215] The enhanced catalytic activities are due to combined effect of gold particle size and the selection of appropriate transition metal oxide supports. Parravano and his coworkers dispersed small gold particles over MgO and Al_2O_3 for oxygen and hydrogen transfer reactions.[216] Recently, Mukherjee et al. reported the catalytic activity of gold nanoparticles supported on fumed silica in the hydrogenation of cyclohexane.[217] Suo et al. reported the liquid phase oxidation of cyclohexane over Au/ZSM-5 and Au/MCM-41.[218] Thiol-stabilized gold nanoparticles have also been exploited for catalysis applications. Examples include asymmetric dihydroxylation reactions,[219] carboxylic ester cleavage,[220] electrocatalytic reductions by anthraquinone functionalized gold particles[221]

and particle-bound ring opening metathesis polymerization.[222] Thus, these observations clearly suggest that the smaller gold particles can exhibit appreciable catalytic activity.

1.6. SCOPE AND OBJECTIVES OF THE THESIS

One of the important areas of nanotechnology is the development of reliable processes for the synthesis of nanomaterials over a range of sizes (with good monodispersity) and chemical composition. Hence, the current research is directed towards the development of different experimental protocols for the synthesis of nanomaterials of variable sizes and shapes. Chemically a number of reports prevail in literature that is eco-unfriendly and expensive. Thus, there is a need to develop eco-friendly processes that do not employ toxic chemicals in the synthesis protocols. This has fuelled the researchers to look at the biological systems. Recently, the utilization of prokaryotic cell (such as bacteria, algae) has emerged as novel methods for the synthesis of nanomaterials. Although, several reports of the use of microbes has been addressed for nanoparticle synthesis but the exposure of different inorganic salts to these prokaryotic cells resulted in the synthesis of nanoparticles intracellularly. However, such biotransformation-based nanoparticle synthesis strategies would have greater commercial viability if the nanoparticles could be synthesized extracellularly directly in the aqueous medium. Towards this objective, the thesis will focus on the extracellular synthesis of nanoparticles using such bio-based protocols. Prokaryotic and eukaryotic organisms such as actinomycetes and fungi respectively, for the first time, have been used for the extracellular synthesis of nanoparticles.[223]

Very recently, a number of fungal strains for the biotransformation of Baeyer-Villiger type reaction were screened in our laboratory. Mandal et al. demonstrated the

fungus, *Fusarium oxysporum*, to be a new biocatalyst for the biotransformation of carbonyl compounds, both cyclic aliphatic and aromatic compounds.[224] Observing the redox nature of the fungus, *Fusarium oxysporum*, in the Baeyer-Villiger type reaction, the same microorganism has been found to reduce the inorganic salts extracellularly. It has been observed that the exposure of aqueous solutions of metal salts and a mixture of metal salts to *Fusarium oxysporum* resulted in extracellular formation of nanoparticles of dimensions 5–50 nm and alloy nanoparticles of dimensions 8–14 nm, respectively. In-depth characterization of these nanoparticles will be highlighted to understand the high stability of nanoparticles and the probable pathways of their formation.

The main challenges frequently encountered by the researchers of nanoparticle synthesis are (i) controlling the particle size/shape and (ii) achieving the monodispersity. The synthesis of nanoparticles with controlled monodispersity is a recent demand by the material developers for the advancement of nanotechnology. Various chemical methods to control size and the distribution of the nanoparticles involve micelle, Langmuir-Blodgett, and organometallic techniques. As chemical protocols for the synthesis of nanoparticles are focusing on controlled monodispersity, a number of actinomycetes have been screened for the similar objective. It has been identified that the alkalothermophilic (extremophilic) actinomycete, *Thermomonospora* sp., and alkalotolerant actinomycete, *Rhodococcus* sp., are the exciting candidate for the synthesis of metal nanoparticles with good monodispersity.[225]

The semiconductor nanoparticles have generated great interest during the past decades due to their quantum confinement effects and size dependent photoemission characteristics. These semiconductor nanocrystals have been applied to many different technological areas including biological labeling and diagnostics,[20-23] single-electron

transistors and light-emitting diodes. Both prokaryotic (bacteria) and eukaryotic organisms (such as yeast) have been found to produce semiconductor nanoparticles intracellularly.[154, 158, 159] However, the synthesis of metal sulfide nanoparticles will be more viable if it could be accomplished extracellularly. Here too, eukaryotic organisms such as fungi were found to be a good candidate for the synthesis of metal sulfide nanoparticles extracellularly.[223d] The fungus, *Fusarium oxysporum*, when exposed to aqueous solution of metal sulfate, leads to the formation of extremely stable metal sulfide nanoparticles in solution.

Metallic gold when deposited on selected metal oxides as ultrafine particles of nanometer size range (~2–3 nm) is found to be very active in many important reactions for chemical industry and environmental protection. Industrial application of anyone these methods can either be hazardous or eco-unfriendly. The gold nanoparticle synthesized extracellularly by fungus, *Fusarium oxysporum*, supported on SiO_2 has been exploited to study the catalytic activity in the aerial oxidation of cyclohexane to adipic acid.

The specific problems chosen are:

- Biosynthesis of metal (gold and silver) and bimetallic alloy (gold silver) nanoparticles using fungus, *Fusarium oxysporum*.
- Biosynthesis of metal (gold and silver) nanoparticles with better size and controlled monodispersity using actinomycetes.
- Biosynthesis of technologically important semiconductor metal (cadmium, lead, zinc, manganese and nickel) sulfide nanoparticles using fungus, *Fusarium oxysporum*, by a purely enzymatic process.

- To study the catalytic activity of aerial oxidation of cyclohexane to adipic acid using supported gold nanoparticles synthesized using fungi.

1.7. OUTLINE OF THE THESIS

The **THESIS** will be presented in **SIX (6)** chapters, a brief summary of which is given below.

Chapter 1. Introduction and Literature Survey

Chapter 1 presents a general introduction about various physicochemical aspects of nanomaterials. The different characteristic properties of nanomaterials, their chemically synthesized protocols, characterization techniques, and their applications are discussed in brief. Based on these reviews, the scope and objective of the present work have been outlined.

Chapter 2. Biosynthesis of metal and bimetallic alloy nanoparticles using fungus, *Fusarium oxysporum*

Chapter 2 presents a novel biological process towards metal and bimetallic alloy nanoparticles. Gold and silver nanoparticles in the size range of 5–50 nm and bimetallic Au-Ag alloy nanoparticles of dimensions 6–14 nm of different compositions have been synthesized using fungus, *Fusarium oxysporum*. The probable mechanism of the metal and bimetallic alloy nanoparticles has been discussed.

Chapter 3. Biosynthesis of metal nanoparticles using actinomycetes

Chapter 3 deals with microorganism actinomycetes for the synthesis of metal nanoparticles of better size/shape and controlled monodispersity. The exposure of

actinomycete, *Thermomonospora* sp., to metal ions solution resulted in the reduction of metal ions and formation of fairly monodispersed metal nanoparticles extracellularly. However, the use of actinomycete, *Rhodoccocus* sp., leads to the formation of metal nanoparticles intracellularly with good dispersity. The probable mechanism of the extra- and intracellular growth of metal nanoparticles by *Thermomonospora* sp. and *Rhodoccocus* sp. respectively has been discussed.

Chapter 4. Biosynthesis of metal sulfide nanoparticles using fungus, *Fusarium oxysporum*

Chapter 4 focuses on a novel method for the synthesis of technologically important semiconductor metal sulfide nanoparticles using fungus, *Fusarium oxysporum*, by a purely enzymatic pathway. When *Fusarium oxysporum* was challenged with aqueous solution of metal sulfate (where, metal = cadmium, lead, zinc and nickel), highly stable quantum dots of metal sulfide nanocrystals can be formed extracellularly by a purely enzymatic process. The metal sulfide quantum dots are formed by reaction of M^{2+} ions (metal ions) with sulfide ions that are formed by the enzymatic reduction of sulfate ions where the enzymes are released *in situ* by *Fusarium oxysporum*.

Chapter 5. Aerial oxidation of cyclohexane to adipic acid

Chapter 5 deals with the study of catalytic activity shown by gold nanoparticles in the aerial oxidation of cyclohexane to adipic acid using extracellularly synthesized gold nanoparticles by *Fusarium oxysporum* supported on amorphous (fumed) SiO_2. A comparative study between the catalytic activities of supported gold nanoparticles synthesized chemically and biologically using fungi will also be discussed.

Chapter 6. Summary and Conclusions

The summary of the results obtained and the conclusions drawn are presented in this chapter. The scope for future work is also discussed.

1.8. REFERENCES

1. A. Dowling, *Nanoscience and Nanotechnology: Opportunities and Uncertainties,* A Report by The Royal Society & The Royal Academy of Engineering, London, July 2004.
2. (a) D. H. Bamford, *Curr. Biol.* **2000**, *10*, R558. (b) G. Cao, *Nanotructures and Nanomaterials: Synthesis, Properties and Applications*, Imperial College Press, London, 2004.
3. (a) C. N. R. Rao, A. Muller, A. K. Cheetham (Eds.), *The Chemistry of Nanomaterials: Synthesis, Properties and Applications*, Wiley-VCH, Weinheim, 2004, Vol. 1. (b) C. A. Mirkin, *Small* **2005**, *1*, 14.
4. J. Z. Zhang, R. H. O'Neil, T. W. Roberti, *J. Phys. Chem.* **1994**, *98*, 3859.
5. D. S. Goodsell, *Bionanotechnology: Lessons from Nature*, Wiley-Liss, Hoboken, New York, 2004.
6. B. Dash, B. K. Sharma (eds.), *Charak Samhita*, Chaukhamba Sanskrit Series, Varanasi, 2001.
7. (a) C. R. Lowe, *Curr. Opin. Struc. Biol.* **2000**, *10*, 428. (b) N. Tsapis, D. Bennett, B. Jackson, D. A. Weitz, D. A. Edwards, *PNAS*, **2002**, *19*, 12001. (c) G. M. Whitesides, *Nature Biotechnol.* **2003**, *21*, 1161.
8. J. S. A. Bhatt, *Curr. Sci* . **2003**, *85*, 147.
9. (a) H. Weller, *Angew. Chem. Int. Ed. Engl.* **1993**, *32*, 41. (b) V. L. Colvin, M. C. Schlamp, A. P. Alivisatos, *Nature* **1994**, *370*, 354. (c) L. E. Brus, *J. Chem. Phys.* **1984**, *80*, 4403. (d) A. Henglein, *J. Phys. Chem.* **1993**, *97*, 5457.
10. C. N. R. Rao, G. U. Kulkarni, P. J. Thomas, P. P. Edwards, *Chem. Eur. J.* **2002**, *8*, 29.
11. P. P. Edwards, R. L. Johnston, C. N. R. Rao in *Metal Clusters in Chemistry*, P. Braunstein, G. Oro, P. R. Raithby (Eds.), Wiley-VCH, Weinheim, 1998.
12. H. N. Aiyer, V. Vijayakrishnan, G. N. Subanna, C. N. R. Rao, *Surf. Sci.* **1994**, *313*, 392.
13. (a) G. Schmid, *Chem. Rev.* **1992**, *92*, 1709. (b) A. J. Hoffman, G. Mills, H. Yee, M. R. Hoffman, *J. Phys. Chem.* **1992**, *96*, 5546.
14. P. A. Brugger, P. Cuendet, M. Graetzel, *J. Am. Chem. Soc.* **1981**, *103*, 2923.

15. Y. Wang, N. Herron, *J. Phys. Chem.* **1991**, *95*, 525.

16. (a) D. L. Klein, R. Roth, A. K. L. Lim, A. P. Alivisatos, P. L. McEven, *Nature* **1997**, *389*, 699. (b) H. Weller, *Angew. Chem. Int. Ed. Engl.* **1998**, *37*, 1658.

17. Y. Wang, *Acc. Chem. Res.* **1991**, *24*, 133.

18. (a) J. Shi, S. Gider, K. Babcock, D. D. Awschalom, *Science* **1996**, *271*, 937. (b) Q. A. Pankhurst, J. Connolly, S. K. Jones, J. Dobson, *J. Phys. D: Appl. Phys.* **2003**, *36*, R167. (c) O. V. Salata, *J. Nanobiotech.* **2004**, *2*, 1. (d) P. P. Tartaj, M. D. P. Morales, S. Veintemillas-Verdaguer, T. Gonzalez-Carreno, C. J. Serna, *J. Phys. D: Appl. Phys.* **2003**, *36*, R182. (e) C. C. Berry, A. S. G. Curtis, *J. Phys. D: Appl. Phys.* **2003**, *36*, R198. (f) S. Shivshankar, A. Rai, B. Ankamwar, A. Singh, A. Ahmad, M. Sastry, *Nature Mater.* **2004**, *3*, 482.

19. S. Mornet, S. Vasseur, F. Grasset, E. Duguet, *J. Mater. Chem.* **2004**, *14*, 2161.

20. X. Wu, H. Liu, J. Liu, K. N. Haley, J. A. Treadway, J. P. Larson, N. Ge, F. Peale, M. P. Bruchez, *Nature Biotechnol.* **2003**, *21*, 41.

21. W. J. Parak, R. Boudreau, M. L. Gros, D. Gerion, D. Zanchet, C. M. Micheel, S. C. Williams, A. P. Alivisatos, C. Larabell, *Adv. Mater.* **2002**, *14*, 882.

22. B. Dubertret, P. Skourides, D. J. Norris, V. Noireaux, A. H. Brivanlou, A. Libchaber, *Science* **2002**, *298*, 1759.

23. (a) J. R. Taylor, M. M. Fang, S. Nie, *Anal. Chem.* **2000**, *72*, 1979. (b) H. Xu, M. Y. Sha, E. Y. Wong, J. Uphoff, Y. Xu, J. A. Treadway, A. Truong, E. O'Brien, S. Asquith, M. Stubbins, N. K. Spurr, E. H. Lai, W. Mahoney, *Nucl. Acids Res.* **2003**, *31*, e 43.

24. D. L. Feldheim, C. D. Keating, *Chem. Soc. Rev.* **1998**, *27*, 1.

25. J. H. Fendler, (Ed.) *Nanoparticles and Nanostructured films: Preparation, Characterization and Applications*, John Wiley & Son, 1998.

26. (a) B. Murray, D. J. Norris, M. G. Bawendi, *J. Am. Chem. Soc.* **1993**, *115*, 8706. (b) Z. A. Peng, X. Peng, *J. Am. Chem. Soc.* **2001**, *123*, 183. (c) L. Qu, Z. A. Peng, X. Peng, *Nano Lett.* **2001**, *1*, 333.

27. C. B. Murray, C. R. Kagan, M. G. Bawendi, *Annu. Rev. Mater. Sci.* **2000**, *30*, 545.

28. (a) L. Qu, W. W. Yu, X. Peng, *Nano Lett.* **2004**, *4*, 465. (b) X. Wang, L. Qu, J. Zhang, X. Peng, M. Xiao, *Nano Lett.* **2003**, *3*, 1103. (c) W. W. Yu, L. Qu, W. Guo, X. Peng, *Chem. Mater.* **2003**, *15*, 2854. (d) X. Chen, A. Y. Nazzal, M. Xiao, Z. A. Peng, X. Peng, *J. Lumin.* **2002**, *97*, 205. (e) X. Peng, T. E. Wilson, A. P. Alivisatos, P. G. Schultz, *Angew. Chem., Int. Ed. Engl.* **1997**, *36*, 145. (f) Z. A. Peng, X. Peng, *J. Am. Chem. Soc.* **2002**, *124*, 3343. (g) B. K. H. Yen, N. E. Stott, K. F. Jensen, M. G. Bawendi, *Adv. Mater.* **2003**, *15*, 1858. (h) M. Liberato, C. S. Erik, A. P. Alivisatos, *J. Am. Chem. Soc.* **2000**, *122*, 12700.

29. (a) W. W. Yu, L. Qu, W. Guo, X. Peng, *Chem. Mater.* **2003**, *15*, 2854. (b) W. W. Yu, X. Peng, *Angew. Chem., Int. Ed. Engl.* **2002**, *41*, 2368.

30. (a) D. V. Talapin, A. L. Rogach, I. Mekis, S. Haubold, A. Kornowski, M. Haase, H. Weller, *Colloids Surf., A* **2002**, *202*, 145. (b) W. W. Yu, X. Peng, *Angew. Chem., Int. Ed. Engl.* **2002**, *41*, 2368. (c) W. W. Yu, Y. A. Wang, X. Peng, *Chem. Mater.* **2003**, *15*, 4300. (d) D. V. Talapin, S. Haubold, A. L. Rogach, A. Kornowski, M. Haase, H. Weller, *J. Phys. Chem. B* **2001**, *105*, 2260. (e) N. Gaponik, D. V. Talapin, A. L. Rogach, K. Hoppe, E. V. Shevchenko, A. Kornowski, A. Eychmueller, H. Weller, *J. Phys. Chem. B* **2002**, *106*, 7177.

31. M. A. Hines, P. Guyot-Sionnest, *J. Phys. Chem. B* **1998**, *102*, 3655.

32. M. Shim, P. Guyot-Sionnest, *J. Am. Chem. Soc.* **2001**, *123*, 11651.

33. D. Battaglia, X. Peng, *Nano Lett.* **2002**, *2*, 1027.

34. X. Peng, J. Wickham, A. P. Alivisatos, *J. Am. Chem. Soc.* **1998**, *120*, 5343.

35. (a) J. S. Steckel, S. Coe-sullivan, V. Bulovic, M. G. Bawendi, *Adv.Mater.* **2003**, *15*, 1862. (b) B. L. Wehrenberg, C. Wang, P. Guyot-Sionnest, *J. Phys. Chem. B* **2002**, *106*, 10634. (c) C. B. Murray, S. Sun, W. Gaschler, H. Doyle, T. A. Betley, C. R. Kagan, *IBM J. Res. Rev.* **2001**, *45*, 47.

36. (a) S. Sun, C. B. Murray, D. Weller, L. Folks, A. Moser, *Science* **2000**, *287*, 1989. (b) S. Sun, S. Anders, T. Thomson, J. E. E. Baglin, M. F. Toney, H. F. Hamann, C. B. Murray, B. D. Terris, *J. Phys. Chem. B* **2003**, *107*, 5419. (c) W. L. Zhou, J. He, J. Fang, T. A. Huynh, T. J. Kennedy, K. L. Stokes, C. J. O'Connor, *J. Appl. Phys.* **2003**, *93*, 7340.

37. (a) E. V. Shevchenko, D. V. Talapin, H. Schnablegger, A. Kornowski, O. Festin, P. Svedlindh, M. Haase, H. Weller, *J. Am. Chem. Soc.* **2003**, *125*, 9090. (b) E. V. Shevchenko, D. V. Talapin, A. L. Rogach, A. Kornowski, M. Haase, H. Weller, *J. Am. Chem. Soc*. **2002**, *124*, 11480.

38. (a) A. R. Kortan, R. Hull, R. L. Opila, M. G. Bawendi, M. L. Steigerwald, P. J. Carroll, L. Brus, E. Louis, *J. Am. Chem. Soc.* **1990**, *112*, 1327. (b) M. A. Hines, P. Guyot-Sionnest, *J. Phys. Chem.* **1996**, *100*, 468. (c) B. O. Dabbousi, J. Rodriguez-Viejo, F. V. Mikulec, J. R. Heine, H. Mattoussi, R. Ober, K. F. Jensen, M. G. Bawendi, *J. Phys. Chem. B* **1997**, *101*, 9463. (d) D. V. Talapin, A. L. Rogach, A. Kornowski, M. Haase, H. Weller, *Nano Lett.* **2001**, *1*, 207.

39. (a) D. V. Talapin, R. Koeppe, S. Goetzinger, A. Kornowski, J. M. Lupton, A. L. Rogach, O. Benson, J. Feldmann, H. Weller, *Nano Lett.* **2003**, *3*, 1677. (b) I. Mekis, D. V. Talapin, A. Kornowski, M. Haase, H. Weller, *J. Phys. Chem. B* **2003**, *107*, 7454. (c) X. Peng, M. C. Schlamp, A. V. Kadavanich, A. P. Alivisatos, *J. Am. Chem. Soc.* **1997**, *119*, 7019. (d) X. Chen, Y. Lou, C. Burda, *Int. J. Nanotech.* **2004**, *1*, 105. (e) X. Chen, Y. Lou, A. C. Samia, C. Burda, *Nano Lett.* **2003**, *3*,799.

40. H. Zeng, J. Li, Z. L. Wang, J. P. Liu, S. Sun, *Nano Lett.* **2004**, *4*, 187.

41. P. D. Cozzoli, A. Kornowski, H. Weller, *J. Am. Chem. Soc.* **2003**, *125*, 14539.

42. S. O'Brien, L. Brus, C. B. Murray, *J. Am. Chem. Soc.* **2001**, *123*, 12085.

43. M. Boutonnet, A. N. Khan-Lodhi, T. Towey, *Structure and Reactivity in Reversed Micelles*, M. P. Pileni, (Ed.) Elsevier:Amsterdam, The Netherlands, 1989, p 198.

44. A. Taleb, C. Petit, M. P. Pileni, *Chem. Mater.* **1997**, *9*, 950.

45. C. Sangregorio, M. Galeotti, U. Bardi, P. Baglioni, *Langmuir* **1996**, *12*, 5800.

46. M. Boutonnet, J. Kizling, P. Stenius, G. Maire, *Colloids Surf.* **1983**, *5*, 209.

47. J. Turkevich, P. C. Stevenson, J. Hillier, *Discuss. Faraday Soc.* **1951**, *11*, 55.

48. (a) P. Barnickel, A. Wokaun, *Mol. Phys.* **1990**, *69*, 1. (b) Z. J. Chen, X. M. Qu, F. Q. Fang, L. Jiang, *Colloids Surf. B* **1996**, *7*, 173.

49. (a) I. Lisiecki, M. P. Pileni, *J. Am. Chem. Soc.* **1993**, *115*, 3887. (b) M. Pileni, I. Lisiecki, *Colloids Surf.* **1993**, *80*, 63. (c) M. P. Pileni, I. Lisiecki, L. Motte, C.

Petit, J. Cizeron, N. Moumen, P. Lixon, *Prog. Colloid Polym. Sci.* **1993**, *93*, 1. (d) C. Petit, P. Lixon, M. P. Pileni, *J. Phys. Chem.* **1993**, *97*, 12974. (e) I. Lisiecki, M. P. Pileni, *J. Phys. Chem.* **1995**, *99*, 5077.

50. (a) C. Petit, A. Taleb, M. P. Pileni, *J. Phys. Chem. B* **1999**, *103*, 1805. (b) J. P. Chen, K. M. Lee, C. M. Sorensen, K. J. Klabunde, G. C. Hadjipanayis, *J. Appl. Phys.* **1994**, *75*, 5876. (c) J. Eastoe, B. Warne, *Curr. Opin. Colloid Interface Sci.* **1996**, *1*, 800.
51. J. A. Lopez-Perez, M. A. Lopez-Quintela, J. Mira, J. Rivas, S. W. Charles, *J. Phys. Chem. B* **1997**, *101*, 8045.
52. J. B. Nagy, *Colloids Surf.* **1989**, *35*, 201.
53. E. Joselevich, I. Willner, *J. Phys. Chem.* **1994**, *98*, 7628.
54. V. Chhabra, V. Pillai, B. K. Mishra, A. Morrone, D. O. Shah, *Langmuir* **1995**, *11*, 3307.
55. C. L. Chang, H. S. Fogler, *Langmuir* **1997**, *13*, 3295.
56. T. Kawai, A. Fujino, K. Kon-No, *Colloids Surf. A* **1996**, *100*, 245.
57. (a) S. Y. Chang, L. Liu, S. A. Asher, *J. Am. Chem. Soc.* **1994**, *116*, 6739.
58. (a) K. Osseo-Asare, F. J. Arriagada, *J. Colloids Surf.* **1990**, *50*, 321. (b) W. Wang, X. Fu, J. Tang, L. Jiang, *Colloids Surf. A* **1993**, *81*, 177. (c) F. J. Arriagada, K. Osseo-Asare, *J. Colloid Interface Sci.* **1995**, *170*, 8. (d) L. M. Gan, K. Zhang, C. H. Chew, *Colloids Surf. A* **1996**, *110*, 199. (e) J. Esquena, T. F. Tadros, K. Kostarelos, C. Solans, *Langmuir* **1997**, *13*, 6400.
59. J. A. Lopez-Perez, M. A. Lopez-Quintela, J. Mira, Rivas, S. W. Charles, *J. Phys. Chem. B* **1997**, *101*, 8045.
60. L. M. Qi, J. Ma, H. Chen, Z. Zhao, *J. Phys. Chem. B* **1997**, *101*, 3460.
61. L. Motte, F. Billoudet, E. Lacaze, M. P. Pileni, *Adv. Mater.* **1996**, *8*, 1018.
62. (a) K. Kandori, K. Kon-No, A. Kitahara, *J. Colloid Interface Sci.* **1987**, *122*, 78. (b) K. Kandori, K. Kon-No, A. Kitahara, *J. Dispersion Sci. Technol.* **1988**, *9*, 61.
63. (a) M. Dvolaitzky, R. Ober, C. Taupin, R. Anthore, X. Auvray, C. Petipas, C. *J.* Williams, *Dispersion Sci. Technol.* **1983**, *4*, 29. (b) C. H. Chew, L. M.; Gan, D. O. Shah, *J. Dispersion Sci. Technol.* **1990**, *11*, 593. (c) P. Monnoyer, A. Fonseca,

J. B. Nagy, *Colloid Surf. A.* **1996**, *100*, 233. (d) R. P. Bagwe, K. C. Khilar, *Langmuir* **1997**, *13*, 6432.

64. (a) Y. Li, T. White, S. H. Lim, *Rev. Adv. Mater. Sci.* **2003**, *5*, 211. (b) G. Coln, M. C. Hidalgo, J. A. Navo, *Catal. Today* **2002**, *76*, 91. (c) N. Uekawa, J. Kajiwara, K. Kakegawa, Y. J. Sasaki, *Colloid Interface Sci.* **2002**, *250*, 285. (d) A. J. Maira, K. L. Yeung, J. Soria, J. M. Coronado, C. Belver, C. Y. Lee, V. Augugliaro, *Appl. Catal. B* **2001**, *29*, 327. (e) B. Li, X. Wang, M. Yan, L. Li, *Mater. Chem. Phys.* **2003**, *78*, 184. (f) H. Parala, A. Devi, R. Bhakta, R. A. Fischer, *J. Mater. Chem.* **2002**, *12*, 1625.
65. W. Lackey, *J. Nucl. Technol.* **1980**, *49*, 321.
66. J. L. Woodhead, *Sci. Ceram.* **1983**, *12*, 179.
67. (a) A. Chatterjee, D. Chakravorty, *J. Mater. Sci.* **1992**, *27*, 4115. (b) J. Gao, Y. Qi, W. Yang, X. Guo, S. Li, X. Li, *Mater. Chem. Phys.* **2003**, *82*, 602.
68. K. Kiss, J. Magder, M. S. Vukasovich, R. J. Lockhart, *J. Am. Ceram. Soc.* **1966**, *49*, 291.
69. J. Shen, Z. Zhang, G. Wu, *J. Chem. Eng. Jpn.* **2003**, *36*, 1270.
70. A. Viano, S. R. Mishra, R. Lloyd, J. Losby, T. Gheyi, *J. Non-Cryst. Solids* **2003**, *325*, 16.
71. A. Jitianu, Y. Altindag, M. Zaharescu, M. Wark, *J. Sol-Gel Sci. Technol.* **2003**, *26*, 483.
72. D. Mondelaers, G. Vanhoyland, H. Van den Rul, J. D'Haen, M. K. Van Bael, J. Mullens, L. C. Van Poucke, *Mater. Res. Bull.* **2002**, *37*, 901.
73. (a) W. M. Zeng, L. Gao, J. K. Guo, *Nanostruct. Mater.* **1998**, *10*, 543. (b) L. C. Pathak, T. B. Singh, A. K. Verma, P. Ramachandrarao, *J. Metall. Mater. Sci.* **2000**, *42*, 93.
74. D. Grosso, P. A. Sermon, *J. Mater. Chem.* **2000**, *10*, 359.
75. Y. S. Chang, Y. H. Chang, I. G. Chen, G. J. Chen, Y. L. Chai, *J. Cryst. Growth* **2002**, *243*, 319.
76. X. Wang, Z. Zhang, S. Zhou, *Mater. Sci. Eng. B* **2001**, *86*, 29.
77. M. Veith, S. Mathur, N. Lecerf, V. Huch, T. Decker, H. P. Beck, W. Eiser, R. Haberkorn, *J. Sol-Gel Sci. Technol.* **2000**, *17*, 145.

78. N. Sharma, K. M. Shaju, G. V. S. Rao, B. V. R. Chowdari, *Electrochem. Commun.* **2002**, *4*, 947.

79. Y. X. Huang, C. Guo, *J. Powder Technol.* **1992**, *72*, 101.

80. (a) H.Yamamura, S. Shirasaki, Y. Moriyoshi, M. Tanada, *Ceram. Int.* **1985**, *11*, 72. (b) H. S. Potdar, S. B. Deshpande, S. K. Date, *Mater. Chem. Phys.* **1999**, *58*, 121.

81. L. Spanhel, M. Haase, H. Weller, A. Henglein, *J. Am. Chem. Soc.* **1987**, *109*, 5649.

82. M. T. Harrison, S. V. Kershaw, M. G. Burt, A. Rogach, A. Eychmuller, H. Weller, *J. Mater. Chem.* **1999**, *9*, 2721.

83. A. L. Rogach, A. Kornowski, M. Gao, A. Eychmueller, H.Weller, *J. Phys. Chem. B* **1999**, *103*, 3065.

84. M. Gao, B. Richter, S. Kirstein, H. Moehwald, *J. Phys. Chem. B* **1998**, *102*, 8360.

85. D. Sordelet and M. Akinc, *J. Colloid Interf. Sci.* **1988**, *122*, 47.

86. (a) A. Mews, A. Eychmueller, M. Giersig, D. Schooss, H. Weller, *J. Phys. Chem.* **1994**, *98*, 934. (b) A. Mews, A. V. Kadavanich, U. Banin, A. P. Alivisatos, *Phys. Rev. B* **1996**, *53*, R13242. (c) H. E. Porteanu, E. Lifshitz, M. Pflughoefft, A. Eychmuller, H. Weller, *Phys. Status Solidi B* **2001**, *226*, 219. (d) V. F. Kamalov, R. Little, S. L. Logunov, M. A. El-Sayed, *J. Phys. Chem.* **1996**, *100*, 6381. (e) D. Schooss, A. Mews, A. Eychmoeller, H. Weller, *Phys. Rev. B* **1994**, *49*, 17072/1. (f) A. Eychmueller, T. Vossmeyer, A. Mews, H. Weller, *J. Lumin.* **1994**, *58*, 223. (g) M. Braun, C. Burda, M. A. El-Sayed, *J. Phys. Chem. A* **2001**, *105*, 5548. (h) M. Braun, S. Link, C. Burda, M. A. El-Sayed, *Phys. Rev. B* **2002**, *66*, 205312. (i) M. Braun, S. Link, C. Burda, M. A. El-Sayed, *Chem. Phys. Lett.* **2002**, *361*, 446. (j) H. Borchert, D. V. Talapin, N. Gaponik, C. McGinley, S. Adam, A. Lobo, T. Moeller, H. Weller, *J. Phys. Chem. B* **2003**, *107*, 7486.

87. M. Braun, C. Burda, M. Mohamed, M. A. El-Sayed, *Phys. Rev. B* **2001**, *64*, 035317/1.

88. (a) M. T. Harrison, S. V. Kershaw, A. L. Rogach, A. Kornowski A. Eychmuller, H. Weller, *Adv. Mater.* **2000**, *12*, 123. (b) S. V. Kershaw, M. Burt, M. Harrison, A. Rogach, H. Weller, A. Eychmuller, *Appl. Phys. Lett.* **1999**, *75*, 1694.

89. J. Yang, S. Mei, J. M. F. Ferreira, *Mater. Sci. Eng. C* **2001**, *15*, 183.

90. (a) M. Yoshimura, S. Somiya, *Am. Ceram. Soc. Bull.* **1980**, *59*, 246. (b) S. Hirano, S. Somiya, *J. Am. Ceram. Soc.* **1976**, *59*, 534.

91. A. A. Burukhin, B. R. Churagulov, N. N. Oleynikov, *High Press. Res.* **2001**, *20*, 255.

92. S. W. Lu, B. I. Lee, Z. L. Wang, J. K. Guo, *J. Cryst. Growth* **2000**, *219*, 269.

93. C. C. Chen, X. Jiao, D. Chen, Y. Zhao, *Mater. Res. Bull.* **2001**, *36*, 2119.

94. I. Maclaren, P. A. Trusty, C. B. Ponton *Acta Mater.* **1999**, *47*, 779.

95. S. H. Yu, L. Shu, Y. S. Wu, Y. T. Qian, Y. Xie, L. Yang, *Mater.Res. Bull.* **1998**, *33*, 1207.

96. X. F. Qian, X. M. Zhang, C. Wang, K. B. Tang, Y. Xie, Y. T. Qian, *Mater. Res. Bull.* **1999**, *34*, 433.

97. X. F. Qian, X. M. Zhang, C. Wang, W. Z. Wang, Y. Xie, Y. T. Qian, *J. Phys. Chem. Solids* **1999**, *60*, 415.

98. C. Wang, W. X. Zhang, X. F. Qian, X. M. Zhang, Y. Xie, Y. T. Qian, *Mater. Lett.* **1999**, *40*, 255.

99. X. F. Qian, X. M. Zhang, C. Wang, W. Z. Wang, Y. T. Qian, *Mater. Res. Bull.* **1998**, *33*, 669.

100. D. Chen, G. Z. Shen, K. B. Tang, Y. K. Liu, Y. T. Qian, *Appl. Phys. A* **2003**, *77*, 747.

101. M. W. Shao, M. S. Mo, Y. Cui, G. Chen, Y. T. Qian *J. Cryst. Growth* **2001**, *233*, 799.

102. J. Q. Hu, Q. Y. Lu, K. B. Tang, B. Deng, R. R. Jiang, Y. T. Qian, W. C. Yu, G. E. Zhou, X. M. Liu, J. X. Wu, *J. Phys. Chem. B* **2000**, *104*, 5251.

103. M. Ji, X. Chen, C. M. Wai, J. L. Fulton, *J. Am. Chem. Soc.* **1999**, *121*, 2631.

104. (a) H. Ohde, F. Hunt, C. M. Wai, *Chem. Mater.* **2001**, *13*, 4130. (b) M. C. McLeod, R. S. McHenry, E. J. Beckman, C. B. Roberts, *J. Phys. Chem. B* **2003**, *107*, 2693.

105. (a) K. J. Ziegler, R. C. Doty, K. P. Johnston, B. A. Korgel, *J. Am. Chem. Soc.* **2001**, *123*, 7797. (b) J. P. Cason, C. B. Roberts, *J. Phys. Chem. B* **2000**, *104*, 1217. (c) J. P. Cason, M. E. Miller, J. B. Thompson, C. B. Roberts, *J. Phys.*

Chem. B **2001**, *105*, 2297. (d) J. P. Cason, K. Khambaswadkar, C. B. Roberts, *Ind. Eng. Chem. Res.* **2000**, *39*, 4749.

106. Y. P. Sun, H. W. Rollins, R. Guduru, *Chem. Mater.* **1999**, *11*, 7.
107. (a) P. S. Shah, T. Hanrath, K. P. Johnston, B. A. Korgel, *J. Phys. Chem. B* **2004**, *108*, 9574. (b) X. Lu, K. J. Ziegler, A. Ghezelbash, K. P. Johnston, B. A. Korgel, *Nano Lett.* **2004**, *4*, 969.
108. Y. P. Sun, R. Guduru, F. Lin, T. Whiteside, *Ind. Eng. Chem. Res.* **2000**, *39*, 4663.
109. P. S. Shah, B. J. Novick, H. S. Hwang, K. T. Lim, R. G. Carbonell, K. P. Johnston, B. A. Korgel, *Nano Lett.* **2003**, *3*, 1671.
110. H. Ohde, M. Ohde, F. Bailey, H. Kim, C. M. Wai, *Nano Lett.* **2002**, *2*, 721.
111. (a) J. D. Holmes, P. A. Bhargava, B. A. Korgel, K. P. Johnston, *Langmuir* **1999**, *15*, 6613. (b) Y. P. Sun, H. W. Rollins, *Chem. Phys. Lett.* **1998**, *288*, 585.
112. (a) T. Hanrath, B. A. Korgel, *J. Am. Chem. Soc.* **2002**, *124*, 1424. (b) T. Hanrath, B. Korgel, A. *Adv. Mater.* **2003**, *15*, 437.
113. F. M. Davidson, A. D. Schricker, R. J. Wiacek, B. A. Korgel, *Adv. Mater.* **2004**, *16*, 646.
114. D. C. Lee, F. V. Mikulec, B. A. Korgel, *J. Am. Chem. Soc.* **2004**, *126*, 4951.
115. (a) T. H. Larsen, M. Sigman, A. Ghezelbash, R. C. Doty, B. A. Korgel, *J. Am. Chem. Soc.* **2003**, *125*, 5638. (b) M. Sigman, A. Ghexelbash, T. Hanrath, A. E. Saunders, F. Lee, B. A. Korgel, *J. Am. Chem. Soc.* **2003**, *125*, 16050.
116. A. Ghexelbash, M. Sigman, B. A. Korgel, *Nano Lett.* **2004**, *4*, 537.
117. W. Cai, L. Zhang, *J. Phys. Condensed Matter* **1997**, *9*, 7257.
118. L. Maya, M. Paranthaman, T. Thundat, M. L. Bauer, *J. Vac. Sci. Technol. B* **1996**, *14*, 15.
119. W. Li, L. Gao, J. K. Guo, *Nanostruct. Mater.* **1998**, *10*, 1043.
120. D. Indackers, C. Janzen, B. Rellinghaus, *Nanostruct. Mater.* **1998**, *10*, 247.
121. L. E. Depero, P. Bonzi, M. Musci, C. Casale, *J. Solid State Chem.* **1994**, *111*, 247.
122. Y. Yang, V. J. Leppert, S. H. Risbud, B. Twamley, P. P. Power, H. W. H. Lee, *Appl. Phys. Lett.* **1999**, *74*, 2262.
123. K. Okuyama, I. W. Lenggoro, N. Tagami, *J. Mater. Sci.* **1997**, *32*, 1229.

124. J. R. Binder, H. Wedemeyer, *Adv. Mater.* **1997**, *9*, 1049.

125. A. Valentini, N. L. V. Carreno, L. F. D. Probst, E. R. Leite, E. Longo, *Microporous Mesoporous Mater.* **2004**, *68*, 151.

126. (a) S. Jou, C. K. Hsu, *Mater. Science Eng. B* **2004**, *106*, 275. (b) F. Dumitrache, I. Morjan, R. Alexandrescu, R. E. Morjan, I. Voicu, I. Sandu, I. Soare, M. Ploscaru, C. Fleaca, V. Ciupina, G. Prodan, B. Rand, R. Brydson, A. Woodword, *Diamond Relat. Mater.* **2004**, *13*, 362. (c) R. Sen, A. Govindaraj, C. N. R. Rao, *Chem. Phys. Lett.* **1997**, *267*, 276. (d) R. Sen, A. Govindaraj, C. N. R. Rao, *Chem. Mater.* **1997**, *9*, 2078. (e) B. C. Satishkumar, A. Govindaraj, R. Sen, C. N. R. Rao, *Chem. Phys. Lett.* **1998**, *293*, 47. (f) B. C. Satishkumar, A. Govindaraj, C. N. R. Rao, *Chem. Phys. Lett.* **1999**, *307*, 158. (g) C. N. R. Rao, R. Sen, B. C. Satishkumar, A. Govindaraj, *Chem. Commun.* **1998**, 1525. (h) B. C. Satishkumar, P. J. Thomas, A. Govindaraj, C. N. R. Rao, *Appl. Phys. Lett.* **2000**, *77*, 2530. (i) F. L. Deepak, A. Govindaraj, C. N. R. Rao, *Chem. Phys. Lett.* **2001**, *345*, 5. (j) C. N. R. Rao, A. Govindaraj, R. Sen, B. C. SatishKumar, *Mater. Res. Innovations* **1998**, *2*, 128.

127. (a) C. N. R. Rao, A.Govindaraj, *Acc. Chem. Res.* **2002**, *35*, 998. (b) G. Gundiah, G. V. Madhav, A. Govindaraj, C. N. R. Rao, *J. Mater. Chem.* **2002**, *12*, 1606. (c) F. L. Deepak, C. P. Vinod, K. Mukhopadhyay, A. Govindaraj, C. N. R. Rao, *Chem. Phys. Lett.* **2002**, *353*, 345.

128. M. L. Ostraat, J. W. De Blauwe, M. L. Green, L. D. Bell, H. A. Atwater, R. C. Flagan, *J. Electrochem. Soc.* **2001**, *148*, G265.

129. M. H. Magnusson, K. Deppert, J. O. Malm, *J. Mater. Res.* **2000**, *15*, 1564.

130. A. G. Nasibulin, O. Richard, E. I. Kauppinen, D. P. Brown, J. K. Jokiniemi, I. S. Altman, *Aerosol. Sci. Technol.* **2002**, *36*, 899.

131. R. Schmechel, M. Kennedy, H. von Seggern, *J. Appl. Phys.* **2001**, *89*, 1679.

132. R. A. Senter, Y. Chen, J. L. Coffer, L. R. Tessler, *Nano Lett.* **2001**, *1*, 383.

133. V. V. Srdic, M. Winterer, A. Moller, G. Miehe, H. Hahn, *J. Am. Ceram. Soc.* **2001**, *84*, 2771.

134. S. H. Ehrman, M. I. Aquino-Class, M. R. Zachariah, *J. Mater. Res.* **1999**, *14*, 1664.

135. (a) K. Wegner, B. Walker, S. Tsantilis, S. E. Pratsinis, *Chem. Eng. Sci.* **2002**, *57*, 1753. (b) A. Maisels, F. E. Kruis, H. Fissan, B. Rellinghaus, H. Zahres, *Appl. Phys. Lett.* **2000**, *77*, 4431. (c) T. Ohno, *J. Nanoparticle Res.* **2002**, *4*, 255. (d) K. Nakaso, M. Shimada, K. Okuyama, K. Deppert, *J. Aerosol. Sci.* **2002**, *33*, 1061. (e) K. K. Nanda, F. E. Kruis, H. Fissan, H. Acet, *J. Appl. Phys.* **2002**, *91*, 2315.

136. (a) W. Marine, L. Patrone, B. Luk'yanchuk, M. Sentis, *Appl. Surf. Sci.* **2000**, *154-155*, 345. (b) Y. Nakata, J. Muramoto, T. Okada, M. Maeda, *J. Appl. Phys.* **2002**, *91*, 1640. (c) S. R. Shinde, S. D. Kulkarni, A. G. Banpurkar, R. Nawathey-Dixit, S. K. Date, S. B. Ogale, *J. Appl. Phys.* **2000**, *88*, 1566. (d) A. Harano, K. Shimada, T. Okubo, M. Sadakata, *J. Nanoparticle Res.* **2002**, *4*, 215.

137. F. K. Urban, A. Hosseini-Tehrani, P. Griffiths, A. Khabari, Y. W. Kim, I. Petrov, *J. Vac. Sci. Technol. B* **2002**, *20*, 995.

138. J. Heberlein, O. Postel, S. L. Girshick, *Surf. Coat Technol.* **2001**, *142-144*, 265.

139. (a) C. Janzen, P. Roth, *Combust Flame* **2001**, *125*, 1150. (b) D. Lee, M. Choi, *J. Aerosol Sci.* **2002**, *33*, 1. (c) K. Wegner, W. J. Stark, S. E. Pratsinis, *Mater. Lett.* **2002**, *55*, 318. (d) H. K. Kammler, S. E. Pratsinis, P. W. Morrison, *Combust Flame* **2002**, *128*, 369.

140. (a) H. Aiking, k. Kok, H. Van Heerikhuizen, J. V. Riet, *Appl. Environ. Microbiol.* **1982**, *44*, 938. (b) J. R. Stephen, S. J. Maenaughton, *Curr. Opin. Biotechnol.* **1999**, *10*, 230.

141. R. K. Mehra, D. R. Winge, *J. Cell. Biochem.* **1991**, *45*, 30.

142. K. Simkiss and K. M. Wilbur *Biomineralization*, Academic Press, New York 1989.

143. (a) R. B. Frankel, R. P. Blakemore (Eds.) *Iron Biominerals*, Plenum Press, New York, 1991. (b) A. P. Philipse, D. Maas, *Langmuir* **2002**, *18*, 9977. (c) Y. Roh, R. J. Lauf, A. D. McMillan, C. Zhang, C. J. Rawn, J. Bai, T. J. Phelps, *Solid State Commun.* **2001**, *118*, 529.

144. (a) N. Kroger, R. Deutzmann, M. Sumper, *Science* **1999**, *286*, 1129. (b) J. Parkinson, R. Gordon, *Trends Biotechnol.* **1999**, *17*, 190. (c) S. Mann, *Nature* **1993**, *365*, 499. (d) S. Oliver, A. Kupermann, N. Coombs, A. Lough, G. A. Ozin,

Nature **1995**, *378*, 47. (e) N. Kroger, R. Deutzmann, M. Sumper, *Science* **1999**, *286*, 1129.

145. (a) S. Schultz-Lam, G. Harauz, T. J. Beveridge, *J. Bacteriol*. **1992**, *174*, 7971. (b) D. Pum, U. B. Sleytr, *Trends Biotechnol.* 1999, *17*, 8. (c) U. B. Sleytr, P. Messner, D. Pum, M. Sara, *Angew. Chem. Int. Ed. Engl.* **1999**, *38*, 1034.
146. J. E. Zumberg, A. C. Sieglo, B. Nagy, *Miner. Ci. Eng.* **1978**, *10*, 223.
147. M. Hosea, B. Greene, R. McPherson, M. Heinzl, M. D. Alexander, D. W. Darnall, *Inorg. Chim. Acta.* **1986**, *123*, 161.
148. T. J. Beveridge, R. J. Doyle, *Metal ions* and bacteria, J. Wiley Sons, New York, 1989.
149. (a) R. N. Reese, D. R. Winge, *J. Biol. Chem.* **1988**, *263*, 12832. (b) C. T. Dameron, R. N. Reese, R. K. Mehra, A. R. Kortan, P. J. Carroll, M. L. Steigerwald, L. E. Brus, D. R. Winge, *Nature* **1989**, *338*, 596.
150. K. L. Temple, N. LeRoux, *Econ. Geol.* **1964**, *59*, 647.
151. R. P. Blakemore, D. Maratea, R. S. Wolfe, *J. Bacteriol.* **1979**, *140*, 720.
152. (a) T. Klaus, R. Joerger, E. Olsson, C. G. Granqvist, *Proc. Natl. Acad. Sci. USA* **1999**, *96*, 13611. (b) T. Klaus-Joerger, R. Joerger, E. Olsson, C. G. Granqvist, *Trends Biotechnol.* **2001**, *19*, 15. (c) R. Joerger, T. Klaus, C. G. Granqvist, *Adv. Mater*. **2000**, *12*, 407. (d) B. Nair, T. Pradeep, *Crys. Growth Des.* **2002**, *2*, 293.
153. (a) G. Southam, T. J. Beveridge, Geochimica et Cosmochimica Acta **1996**, *60*, 4369. (b) T. J. Beveridge, R. G. E. Murray, *J. Bacteriol.* **1980**, *141*, 876. (c) D. Fortin, T. J. Beveridge, *In Biomineralization. From Biology to Biotechnology and Medical Applications*, E. Baeuerien (Ed.), Wiley-VCH, Weinheim, 2000, p. 7.
154. (a) D. P. Cunningham, L. L. Lundie, *Appl. Environ. Microbiol.* **1993**, *59*, 7. (b) J. D. Holmes, P. R. Smith, R. Evans-Gowing, D. J. Richardson, D. A. Russell, J. R. Sodeau, *Arch. Microbiol.* **1995**, *163*, 143. (c) P. R. Smith, J. D. Holmes, D. J. Richardson, D. A. Russell, J. R. Sodeau, *J. Chem. Soc., Faraday Trans.* **1998**, *94*, 1235.
155. M. Labrenz, G. K. Druschel, T. Thomsen-Ebert, B. Gilbert, S. A. Welch, K. M. Kemner, G. A. Logan, R. E. Summons, G. De Stasio, P. L. Bond, B. Lai, S. D. Kelly, J. F. Banfield, *Science* **2000**, *290*, 1744.

156. D. R. Lovley, J. F. Stolz, G. L. Nord, E. J. P. Phillips, *Nature* **1987**, *330*, 252.

157. (a) J. H. P. Watson, D. C. Ellwood, A. K. Sper, J. Charnock, *J. Magn. Magn. Mater.* **1999**, *203*, 69. (b) J. H. P. Watson, B. A. Cressey, A. P. Roberts, D. C. Ellwoood, J. M. Charnock, *J. Magn. Magn. Mater.* **2000**, *214*, 13.

158. M. Kowshik, W. Vogel, J. Urban, S. K. Kulkarni, K. M. Paknikar, *Adv. Mater.* **2002**, *14*, 815.

159. M. Kowshik, N. Deshmukh, W. Vogel, J. Urban, S. K. Kulkarni, K. M. Paknikar, *Biotechnol. Bioengineer.* **2002**, *78*, 583.

160. M. G. Robinson, L. N. Brown, D. Beverley, *Biofouling*, **1997**, *11*, 59.

161. (a) J. L. Gardea-Torresdey, J. G. Parsons, E. Gomez, J. Peralta-Videa, H. E. Troiani, P. Santiago, M. J. Yacaman, *Nano Lett.* 2001, *2*, 397. (b) J. L. Gardea-Torresdey, E. Gomez, J. R. Peralta-Videa, J. G. Parsons, H. Troiani, M. Jose-Yacaman, *Langmuir* **2003**, *19*, 1357.

162. (a) S. S. Shankar, A. Rai, B. Ankamwar, A. Singh, A. Ahmad, M. Sastry, *Nat. Mater.* **2004**, *3*, 482. (b) S. S. Shankar, A. Rai, A. Ahmad, M. Sastry, *Chem. Mater.* **2005**, *17*, 566. (c) S. S. Shankar, A. Ahmad, R. Pasricha, M. Sastry, *J. Mater. Chem.* **2003**, *13*, 1822. (d) S. S. Shankar, A. Ahmad, M. Sastry, *Biotechnol. Prog.* **2003,** *19*, 1627.

163. Z. L. Wang, in: *Characterization of Nanophase Materials*, Ed: Z. L. Wang, Wiley-VCH, Weinheim, 2000, Ch 2.

164. W. H. Bragg, W. L. Bragg, *The Crystalline State*, McMillan, New York, 1949, Vol. 1.

165. (a) R. C. Rau, in: *Advances in X-ray Analysis*, Ed: W. M. Mueller, Sir Isaac Pitman and Sons Ltd., London, 1962, *Vol. 5*, pp. 104–116. (b) L. S. Birks, H. Friedman, *J. Appl. Phys.* **1946**, *17*, 687.

166. G. Lawes, *Scanning Electron Microscopy and X-ray Microanalysis*, John Wiley and Sons Ltd., Chichester, 1987.

167. D. E. Newbury, D. C. Joy, P. Echlin, C. E. Fiori, J. I. Goldstein, *Advanced Scanning Electron Microscopy and X-ray Microanalysis*, Plenum Press, New York, 1986.

168. J. R. Fryer, *Chemical Applications of Transmission Electron Microscopy*, Academic Press, San Diego, 1979.

169. Z. L. Wang, in: *Characterization of Nanophase Materials*, Ed: Z. L. Wang, Wiley-VCH, Weinheim, 2000, Ch 3, pp. 37–80.

170. B. D. Cullity, S. R. Stock, *Elements of X-ray Diffraction*, 3rd edition, Prentice Hall, Upper Saddle River, New York, 2001.

171. A. N. Goldstein, C. M. Echer, A. P. Alivisatos, *Science* **1992**, *256*, 1425.

172. (a) Z. L. Wang, *Adv. Mater.* **2000**, *12*, 1295. (b) P. Poncharal, Z. I. Wang, D. Ugarte, W. A. De Heer, *Science* **1999**, *283*, 1516. (c) Z. l. Wang, P. Poncharal, W. A. De Heer, *J. Phys. Chem. Solids* **2000**, *61*, 1025.

173. C. K. Jorgensen, *Absorption Spectra and Chemical Bonding in Complexes*, Pergamon, New York, 1962.

174. G. Mie, *Ann. Physik* **1908**, *25*, 377.

175. M. Faraday, *Philos. Trans.* **1857**, *147*, 145.

176. G. C. Papavassiliou, *Prog. Solid State Chem.* **1980**, *12*, 185.

177. (a) S. Link, M. A. El-Sayed, *J. Phys. Chem. B* **1999**, *103*, 4212. (b) C. Burda, T. Green, C. Landes, S. Link, R. Little, J. Petroski, M. A. El-Sayed, in: *Characterization of Nanophase Materials*, Ed: Z. L. Wang, Wiley-VCH, Weinheim, 2000, Chapter 7, pp. 197–241.

178. P. R. Griffiths, J. A. De Haseth, *Fourier Transform Infrared Spectrometry*, John Wiley and Sons Inc., New York, 1986.

179. C. N. Banwell, E. M. McCash, *Fundamentals of Molecular Spectroscopy*, McGraw-Hill, United Kingdom, 1996, Ch. 3, p. 55.

180. C. S. Fadley, in: *Electron Spectroscopy: Theory, Techniques and Applications*, Eds: C. R. Brundle, A. D. Baker, Academic Press, New York, 1978, Vol. 2, pp. 1–156.

181. W. N. Delgass, T. R. Hughes, C. S. Fadley, *Catal. Rev.* **1970**, *4*, 179.

182. W. F. Egelhoff Jr., *Surf. Sci. Rep.* **1987**, *6*, 253.

183. J. W. Robinson, *Atomic Absorption Spectroscopy*, Marcel Dekker, New York, 1975.

184. (a) J. Frankel, J. Dorfman, *Nature* **1930**, *126*, 274. (b) J. P. Bucher, D. C. Douglass, L. A. Bloomfield, *Phys. Rev. Lett.* **1991**, *70*, 2283.

185. A. Vilan, D. Cahen, *Trends Biotech.* **2002**, *22*, 20.

186. (a) R. F. Service, *Science* **2001**, *293*, 782. (b) G. Y. Tseng, J. Ellenbogen, *Science* **2001**, *294*, 1293. (c) J. H. Schon, H. Meng, Z. Bao, *Nature* **2001**, *413*, 713. (d) J. H. Schon, H. Meng, Z. Bao, *Science* **2001**, *294*, 2138. (e) A. Bachtold, P. Hadley, T. Nakanishi, C. Dekker, *Science* **2001**, *294*, 1317. (f) J. Chen, M. A. Reed, A. M. Rawlett, J. M. Tour, *Science* **1999**, *286*, 1550. (g) Y. Huang, X. F. Duan, Q. Wei, C. M. Lieber, *Science* **2001**, *291*, 630. (h) D. L. Klein, R. Roth, A. K. L. Lim, A. P. Alivisatos, P. L. McEuen, *Nature* **1997**, *389*, 699.

187. D. L. Klein, R. Roth, A. K. L. Lim, A. P. Alivisatos, P. L. McEuen, *Nature* **1997**, *389*, 699.

188. (a) M. A. Reed, C. Zhou, C. J. Muller, T. P. Burgin, J. M. Tour, *Science* **1997**, *278*, 252. (b) X. D. Cui, A. Primak, X. Zarate, J. Tomfohr, O. F. Sankey, A. L. Moore, T. A. Moore, D. Gust, G. Harris, S. M. Landsay, *Science* **2001**, *294*, 571. (c) R. Compano, *Nanotechnology* **2001**, *12*, 85.

189. (a) S. J. Tans, A. R. M. Verschueren, C. Dekker, *Nature* **1998**, *393*, 49. (b) S. J. Wind, J. Appenzeller, R. Martel, V, Derycke, P. Avouris, *Appl. Phys. Lett.* **2002**, *80*, 3817.

190. (a) W. Liang, M. P. Shores, M. Bockrath, J. R. Long, H. Park, *Nature* **2002**, *417*, 725. (b) J. Park, A. N. Pasupathy, J. I. Goldsmith, C. Chang, Y. Yaish, J. R. Petta, M. Rinkoski, J. P. Sethna, H. D. Abruna, P. L. McEuen, D. C. Ralph, *Nature* **2002**, *417*, 722.

191. (a) S. J. Kim, Yu I. Latyshev, T. Yamashita, *Appl. Phys. Lett.* **1999**, *74*, 1156. (b) R. W. Mosley, W. E. Booji, E. J. Tarte, M. G. Blamire, *Appl. Phys. Lett.* **1999**, *75*, 262. (c) C. Bell, G. Burnell, D. J. Kang, R. H. Hadfield, M. J. Kappers, M. G. Blamire, *Nanotechnology* **2003**, *14*, 630.

192. (a) N. A. Melosh, A. Boukai, F. Diana, B. Gerardot, A. Badolato, P. M. Petroff, J. M. Heath, *Science* **2003**, *300*, 112. (b) C. Vieu, F. Carcenac, A. Pepin, Y. Chen, M. Mejias, A. Lebib, L. Manin-Ferlazzo, L. Couraud, H. Launois, *Appl. Surf. Sci.* **2000**, *164*, 111.

193. Y. Chen, G. Y. Jung, D. A. A. Ohlberg, X. Li, D. R. Stewart, J. O. Jeppesen, K. A. Nielsen, J. F. Stoddart, R. S. Williams, *Nanotechno.* **2003**, *14*, 462.

194. D. L. Feldheim, C. D. Keating, *Chem. Soc. Rev.* **1998**, *27*, 1.

195. (a) T. Sato, H. Ahmad, D. Brown, B. F. G. Johnson, *J. Appl. Phys.* **1997**, *82*, 1007. (b) S. H. M. Persson, L. Olofsson, L. Hedberg, *Appl. Phys. Lett.* **1999**, *74*, 2546. (c) M. Brust, C. J. Kiely, *Colloids Surf.* **2002**, *A202*, 175.

196. C. A. Haberzettl, *Nanotechnology* **2002**, *R9*, 13.

197. (a) J. Fritz, M. K. Baller, H. P. Lang, H. Rothuizen, P. Vettiger, E. Meyer, H. J. Guntherodt, C. Gerber, J. K. Gimzewski *Science* **2000**, *288*, 316. (b) L. Stryer, *Biochemistry*, 4th edition, Freeman, New York, 1995. (c) J. Liu, J. Alvarez, A. E. Kaifer, *Adv. Mater.* **2000**, *12*, 1381. (d) M. Ludwig, W. Dettmann, H. E. Gaub, *J. Biophys.* **1997**, *72*, 445. (e) J. Spinke, M. Liley, H. J. Guder, L. Angermaier, W. Knoll *Langmuir* **1993**, *9*, 1821.

198. (a) A. P. Alivisatos, K. P. Johnsson, X. Peng, T. E. Wilson, C. J. Loweth, M. P. Bruchez, P. G. Schultz, *Nature* **1996**, *382*, 609. (b) R. Elghanian, J. J. Storhoff, R. C. Mucic, R. L. Letsinger, C. A. Mirkin, *Science* **1997**, *277*, 1078.

199. (a) W. J. Parak, D. Gerion, D. Zanchet, A. S. Woerz, T. Pellegrino, C. Michael, S. C. Williams, M. Seitz, R. E. Bruehl, Z. Bryant, C. Bustamante, C. R. Bertozzi, A. P. Alivisatos, *Chem. Mater.* **2002**, *14*, 2113. (b) M. J. Bruchez, M. Moronne, P. Gin, S. Weiss, A. P. Alivisatos, *Science* **1998**, *281*, 2013. (c) W. C. W. Chan, S. Nie, *Science* **1998**, *281*, 2016.

200. (a) W. L. Shaiu, D. D. Larson, J. Vesenka, E. Henderson, *Nucl. Acids. Res.* **1993**, *21*, 99. (b) E. L. Florin, V. T. Moy, H. E. Gaub, *Science* **1994**, *264*, 415.

201. W. J. Parak, D. Gerion, T. Pellegrino, D. Zanchet, C. Michael, S. C. Williams, R. Boudreau, M. A. Le Gros, C. A. Larabell, A. P. Alivisatos, *Nanotechnology* **2003**, *14*, R15.

202. (a) C. M. Niemeyer, *Angew. Chem. Int. Ed. Engl.* **2001**, *40*, 4128. (b) C. A. Mirikin, *J. Nanoparticle Res.* **2000**, *2*, 121. (c) A. A. Taton, *Trends Biotechnol.* **2002**, *20*, 277.

203. J. J. Storhoff, R. Elghanian, R. C. Mucic, C. A. Mirkin, R. L. Letsinger, *J. Am. Chem. Soc.* **1998**, *120*, 1959.

204. (a) T. A. Taton, *Nature* **2001**, *412*, 491. (b) M. J. Bruchez, M. Moronne, P. Gin, S. Weiss, A. P. Alivisatos, *Science* **1998**, *281*, 2013. (c) S. Pathak, S. K. Choi, N. Arnheim, M. E. Thompson, *J. Am. Chem. Soc.* **2001**, *123*, 4103. (d) E. Klarreich, *Nature* **2001**, *413*, 450. (e) P. S. Weiss, *Nature* **2001**, *413*, 585. (f) S. J. Rosenthal, I. Tomlinson, E. M. Adkins, S. Schroeter, S. Adams, L. Swafford, J. McBride, Y. Wang, L. J. DeFelice, R. D. Blakely, *J. Am. Chem. Soc.* **2002**, *124*, 4586. (g) J. K. Jaiswal, H. Mattoussi, J. M. Mauro, S. M. Simon, *Nature Biotechnol.* **2003**, *21*, 47. (h) B. Dubertret, P. Skourides, D. J. Norris, V. Noireaux, A. H. Brivanlou, A. Libchaber, *Science* **2002**, *298*, 1759. (i) M. E. Akerman, W. C. W. Chan, P. Laakkonen, S. N. Bhatia, E. Ruoslahti, *Proc. Natl Acad. Sci. USA* **2002**, *99*, 12617.

205. (a) M. Han, X. Gao, J. Z. Su, S. Nie, *Nature Biotechnol.* **2001**, *19*, 631. (b) S. J. Rosenthal, *Nature Biotechnol.* **2001**, *19*, 621.

206. C. R. Henry, *Appl. Surf. Sci*. **2000**, *164*, 252.

207. D. J. C. Yates, J. H. Sinfelt, *J. Catal.* **1967**, *8*, 348.

208. (a) F. G. Gault, *Adv. Catal.* **1981**, *30*, 1. (b) C. Corrolleur, F. G. Gault, D. Juttard, G. Maire, J. M. Muller, *J. Catal.* **1972**, *27*, 466. (c) C. Corrolleur, S. Corrolleur, F. G. Gault, *J. Catal.* **1972**, *24*, 385. (d) C. Corrolleur, D. Tomanova, F. G. Gault, *J. Catal.* **1972**, *24*, 201.

209. (a) N. Sun, K. J. Klabunde, *J. Catal.* **1999**, *185*, 506. (b) N. Sun, K. J. Klabunde, *J. Am. Chem. Soc.* **1999**, *121*, 5587. (c) T. R. Thurston, J. P. Wilcoxon, *J. Phys. Chem.* **1999**, *103*, 11. (d) A. Tschope, J. Y. Ying, *Nanostruct. Mater.* **1994**, *4*, 617.

210. A. Tschope, J. Y. Ying, *Nanostruct. Mater.* **1994**, *4*, 617.

211. J. -H. Liu, A. -Q. Wang, Y. -S. Chi, H. -P. Lin, C. -Y. Mou, *J. Phys. Chem. B* **2005**, *109*, 40.

212. (a) M. Iwamoto, *Stud. Surf. Sci. Catal.* **2000**, *130*, 23. (b) A. G. Sault, R. J. Madix, C. T. Campbell, *Surf. Sci.* **1986**, *169*, 347.

213. B. Hammer, J. K. Norskov, *Nature* **1995**, *376*, 238.

214. (a) G. C. Bond, P. A. Sermon, *Gold Bull.* **1973**, *6*, 102. (b) G. C. Bond, P. A. Sermon, *J. Chem. Soc., Chem. Commun.* **1973**, 444. (c) M. Haruta, N. Yamada,

T. Kobayashi, S. Iijima, *J. Catal.* **1989**, *115*, 301. (d) M. Haruta, S. Tsubota, T. Kobayashi, H. Kageyama, M. J. Genet, B. Delmon, *J. Catal.* **1993**, *144*, 175. (e) G. C. Bond, D. T. Thompson, *Catal. Rev. Sci. Eng.* **1999**, *41*, 319. (f) M. Haruta, *Catal. Today* **1997**, *36*, 153. (g) M. Haruta, M. Date, *Appl. Catal. A: General* **2001**, *222*, 427. (h) M. Okumura, M. Haruta, *Chem. Lett.* **2000**, 396.

215. M. Haruta, *Cat. Tech.* **2002**, *6*, 102.

216. (a) D. Y. Cha and G. Parravano, *J. Catal.* **1970**, *18*, 2000. (b) S. Galvano and G. Parravano, *J. Catal.* **1978**, *55*, 178.

217. P. Mukherjee, C. R. Patra, A. Ghosh, R. Kumar, M. Sastry, *Chem. Mater.* **2002**, *14*, 1678.

218. R. Zhao, D. Ji, G. Lv, G. Qian, L. Yan, X, Wang, J. Suo, *Chem. Commun.* **2004**, 904. (b) G. Lu, R. Zhao, G. Qian, Y. Qi X, Wang, J. Suo, *Catal. Lett.* **2004**, *97*, 115.

219. H. Li, Y. Y. Luk, M. Mrksich, *Langmuir* **1999**, *15*, 4957.

220. L. Pasquato, F. Rancan, P. Scrimin, F. Mincin, C. Frigeri, *Chem. Commun.* **2000**, 2253.

221. J. J. Pietron, R. W. Murray, *J. Phys. Chem. B* **1999**, *103*, 4440.

222. M. Bartz, J. Kuther, R. Seshadri, W. Tremel, *Angew. Chem. Int. Ed. Engl.* **1998**, *37*, 2466.

223. (a) P. Mukherjee, S. Senapati, D. Mandal, A. Ahmad, M. I. Khan, R. Kumar, M. Sastry, *ChemBioChem* **2002,** *3***,** 461. (b) A. Ahmad, P. Mukherjee, S. Senapati, D. Mandal, M. I. Khan, R. Kumar, M. Sastry, *Colloids Surf.* B **2003**, *28***,** 313. (c) S. Senapati, A. Ahmad, M. I. Khan, M. Sastry, R. Kumar, *Small* **2005**, *1*, 517. (d) A. Ahmad, P. Mukherjee, D. Mandal, S. Senapati, M. I. Khan, R, Kumar, M. Sastry, *J. Am. Chem. Soc.* **2002**, *124*, 12108.

224. D. Mandal, A. Ahmad, M. I. Khan, R. Kumar, *J. Mol. Catal. A: Chem.* **2002**, *181*, 237.

225. (a) A. Ahmad, S. Senapati, M. I. Khan, R. Kumar, M. Sastry, *Langmuir* **2003**, *19*, 3550. (b) A. Ahmad, S. Senapati, M. I. Khan, R. Kumar, R. Ramani, V. Srinivas, M. Sastry, *Nanotechnology* **2003**, *14*, 824.

2.1. INTRODUCTION

The use of nanostructured materials is gaining importance in recent years because of their expected impact in biomedical sciences, optoelectronics, magnetics, catalysis, etc.[1] However, the preparation of such nanostructured materials poses several unique challenges. Several different manufacturing techniques are in use, that usually employs atomistic, molecular and particulate processing in a vacuum or in a liquid medium. Most of the techniques are environmental unfriendly and expensive. Consequently, researchers in the field of nanoscale material synthesis and assembly have been eagerly looking at biological systems. Recently, the utilization of biological systems has emerged as a novel method for the synthesis of nanoparticles. Some of the examples of the use of microbes in the synthesis of nanoparticles of different chemical compositions include bacteria for gold,[2] silver,[3] cadmium sulfide,[4] zinc sulfide,[5] magnetite,[6] iron sulfide,[7] yeast for lead sulfide[8] and cadmium sulfide[9] and algae for gold.[10] Mandal et al. have recently embarked on a programme of biotransformation of Baeyer-Villiger type reaction in our laboratory. A number of fungal strains were screened in this effort and it has been observed that *Fusarium oxysporum* is an exciting biocatalyst for the biotransformation of carbonyl compounds, both cyclic aliphatic and aromatic compounds.[11] Observing the redox nature of fungus, *Fusarium oxysporum*, in the Baeyer-Villiger type reaction, the scope of biotransformation was further explored for the reduction of metal ions, and it was observed that the fungus, *Fusarium oxysporum*, when challenged with aqueous solution of $AuCl_4^-$ and Ag^+ ions leads to their reduction and formation of gold and silver nanoparticles respectively, extracellularly in the size range of 5–50 nm dimensions.[12] However, *Fusarium oxysporum* when exposed simultaneously with an aqueous mixture

of 1 mM gold and silver salts results in the extracellular synthesis of bimetallic Au-Ag alloy nanoparticles of varying mole fractions.[13]

2.2. EXPERIMENTAL

The fungus, *Fusarium oxysporum*, was obtained from National Collection of Industrial Microorganisms (NCIM), NCL, Pune and maintained on potato-dextrose agar slants at 25 °C. Stock cultures were maintained by subculturing at monthly intervals. The fungus was grown at pH 7.0 and 25 °C for 5–6 days; the slants were preserved at 15 °C. From an actively growing stock culture, subcultures were made on fresh slants and after 5–6 days incubation at pH 7.0 and 25 °C, were used as the starting material for synthesis of nanoparticles.

For the synthesis of nanoparticles, the fungus was grown in 500 mL Erlenmeyer flasks each containing MGYP media (100 mL), composed of malt extract (0.3 %), glucose (1.0 %), yeast extract (0.3 %) and peptone (0.5 %) at 25–28 °C under shaking at 200 rpm for 96 h. The mycelial mass were then separated from the culture broth by centrifugation (5000 rpm) at 10 °C for 20 min and the settled mycelia were washed thrice with sterile distilled water. Some of the harvested mycelial mass (20 g) was then used for the synthesis of gold, silver nanoparticles and gold silver alloy nanoparticles.

2.2.1. Biosynthesis of Gold and Silver Nanoparticles

In a typical synthesis of gold and silver nanoparticles, 20 g of fungus, *Fusarium oxysporum*, wet biomass was exposed to an aqueous solution of 1 mM chloroauric acid ($HAuCl_4$) and silver nitrate ($AgNO_3$) respectively, and the whole mixture was put into a shaker at 28 °C (200 rpm).

2.2.2. Biosynthesis of Gold Silver Alloy Nanoparticles

In a typical experiment, 30 g, 40 g, 50 g and 60 g of *Fusarium oxysporum* wet biomass was taken in four conical flasks each containing 100 mL of distilled water. A carefully weighed quantity of $HAuCl_4$ and $AgNO_3$ was added to each of the conical flask to yield an overall concentration of $AuCl_4^-$ and Ag^+ ions of 1 mM in the aqueous solution. The whole mixture was thereafter put into a shaker at 28 °C (200 rpm) for 96 h.

2.2.3. Instruments for Characterization

The reduction of metal ions was routinely monitored by visual inspection of the solution as well as by measuring the UV-Vis spectra of the solution by periodic sampling of aliquots (2 mL) of the aqueous component. The UV-Vis spectroscopy measurements were recorded on a Shimadzu dual-beam spectrophotometer (model UV-1601 PC) operated at a resolution of 1 nm. The fluorescence measurements were carried out on a Perkin-Elmer LS 50B luminescence spectrophotometer.

The films of nanoparticles were made on Si(111) substrates by drop-coating the metal nanoparticle solution to study FTIR, XRD and XPS. Fourier transform infrared spectroscopic (FTIR) studies were performed on a Shimadzu FTIR-8201 PC instrument in the diffuse reflectance mode at a resolution of 4 cm^{-1}. X-ray diffraction (XRD) patterns were recorded in the transmission mode on a Philips PW 1830 instrument operating at 40 kV and a current of 30 mA with Cu K_α radiation (λ = 1.5404 Å). The XPS measurements were carried out on a VG MicroTech ESCA 3000 spectrometer equipped with a multichanneltron hemispherical electron energy analyzer at a pressure no higher than 1×10^{-9} Torr. The electrons were excited with unmonochromatized Mg K_α X-rays (energy) 1253.6 eV, and the spectra were collected in the constant analyzer

energy mode at pass energy of 50 eV. This leads to an overall resolution of *ca.* 1 eV for the measurements. The core level spectra were background corrected using the Shirley algorithm[14] and the chemically distinct species resolved using a nonlinear least squares procedure. The core level binding energies (BEs) were aligned with the adventitious carbon binding energy of 285 eV.

The nanoparticle films were also formed on carbon coated copper grids (40 μm × 40 μm mesh size) and transmission electron microscopy (TEM) images were scanned on a JEOL 1200EX instrument operated at an accelerated voltage of 120 kV.

2.3. CHARACTERIZATION

2.3.1. Extracellular Synthesis of Gold Nanoparticles

2.3.1.1. Visual Inspection

Two conical flasks with *Fusarium oxysporum* biomass before (A) and after (B) reaction with 1 mM $HAuCl_4$ solution for 48 h are shown in Figure 2.1.

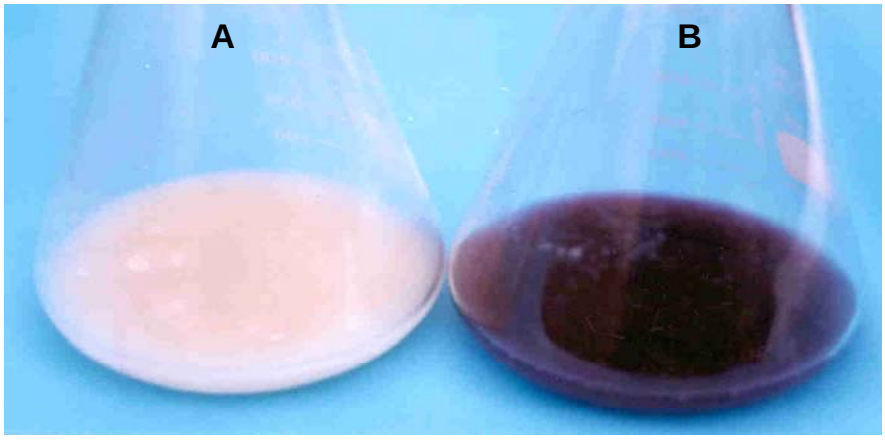

Figure 2.1. Picture of conical flasks containing *Fusarium oxysporum* biomass before (A) and after (B) exposure to $AuCl_4^-$ ions for 48 h.

The pale yellow color of the biomass before reaction with $AuCl_4^-$ ions can clearly be observed (A) which changes to dark purple on completion of the reaction (B). The appearance of the purple color clearly indicates the formation of gold nanoparticles in the reaction mixture and is due to excitation of surface plasmon resonance in the nanoparticles.[15]

2.3.1.2. UV-Vis spectroscopy

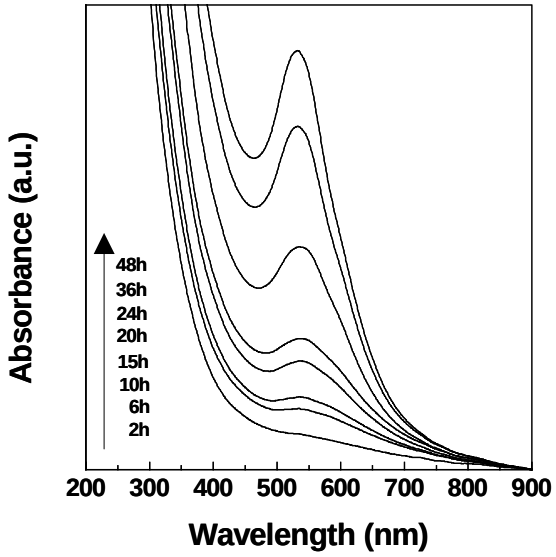

Figure 2.2. UV-Vis spectra recorded with respect to time after the reaction of 1mM $HAuCl_4$ solution with 20 g *Fusarium oxysporum* wet biomass for 48 h.

The UV-Vis measurement of the reaction mixture at different interval of time is plotted in Figure 2.2. The spectra show a well-defined surface plasmon band centered at around 545 nm, which is the characteristic of gold nanoparticles and clearly indicates the formation of nanoparticles in solution.[15] Various studies have established that the surface plasmon resonance band of gold appears around this value for colloidal gold in the size range of 30 nm. The exact position of absorbance depends on a number of factors such as the dielectric constant of the medium, size of the particle etc. The gold nanoparticles

solution was found to be extremely stable, with no evidence of flocculation of the particles even a month after the reaction. The resonance is sharp and indicates no aggregation of gold nanoparticles in solution.

2.3.1.3. X-ray Diffraction

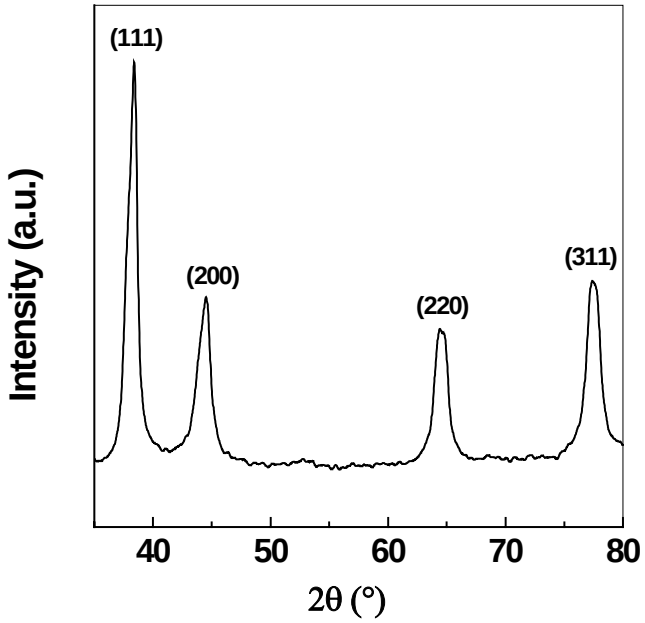

Figure 2.3. XRD pattern recorded from the thin film prepared by drop coating the gold nanoparticle solution on a Si(111) wafer. The principal Bragg reflections are identified.

The evidence of formation of elemental gold extracellularly is provided by X-ray diffraction (XRD) analysis of the thin film prepared by drop coating the gold nanoparticle solution on Si(111) substrate and is shown in Figure 2.3. The intense peaks due to (111), (200), (220) and (311) Bragg reflection at $2\theta = 38°$, 45°, 67° and 78° respectively, were the only features observed corresponding to bulk fcc gold.[16] An estimate of the mean size of the gold nanoparticles formed in the reaction mixture was made by using the Debye–Scherrer equation by determining the width of the (111) Bragg

reflection.[17] The average size of the gold nanoparticles was thus determined to be about 25 nm.

2.3.1.4. X-ray Photoelectron Spectroscopy

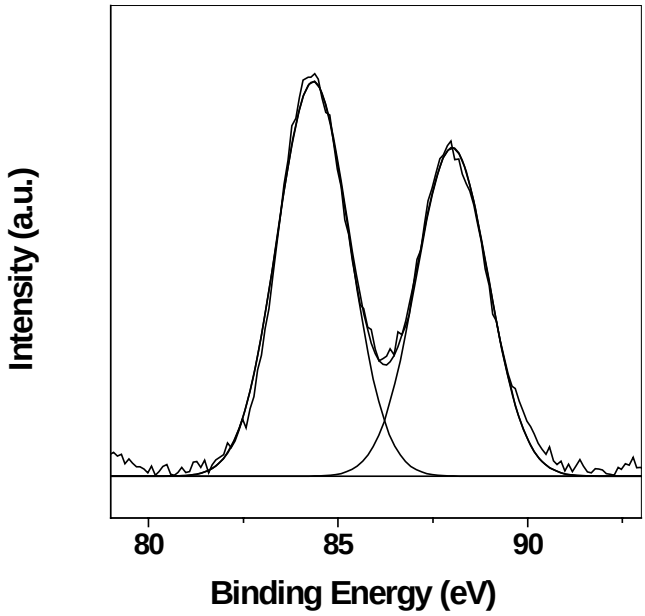

Figure 2.4. Au 4f core level spectra recorded from the drop coated gold nanoparticle solution on a Si(111) substrate. The two spin-orbit components are shown in the Figure.

The chemical analysis of the gold nanoparticle solution was performed using X-ray photoelectron spectroscopy (XPS) to confirm the reduction of chloroaurate ions. The sample of gold nanoparticle was solution casted in the form of a film onto a Si(111) substrate and is shown in Figure 2.4. The Au 4f spectrum from the gold-fungal reaction mixture could be decomposed into two spin-orbit components 1 and 2 (spin-orbit splitting ~ 3.8 eV). The Au $4f_{7/2}$ and $4f_{5/2}$ peaks occurred at a binding energy (BE) of 84.3 eV and 88.1 eV respectively and are characteristic of metallic Au. [18] The absence of a higher binding energy Au 4f component clearly reveals that all the chloroaurate ions are fully reduced by the fungus, *Fusarium oxysporum*. Thus, it can be concluded from

the XPS measurements that all the gold ions used in the nanoparticle synthesis are reduced and in the metallic form.

2.3.1.5. Fourier Transform Infrared Spectroscopy

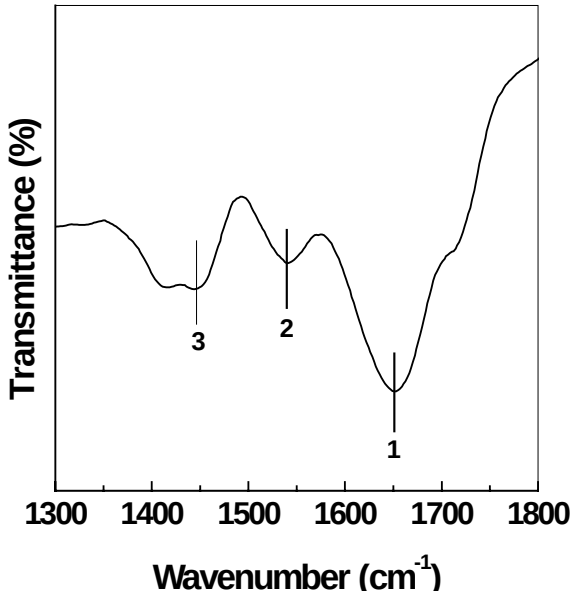

Figure 2.5. FTIR spectrum recorded from a drop-coated film of an aqueous solution incubated with *Fusarium oxysporum* and treated with $AuCl_4^-$ ions for 48 h.

To confirm the presence of protein molecules in the reaction mixture and to determine the effect of chloroauric acid on the structure of protein molecules, the FTIR measurement was performed. The sample was prepared by drop-coating the gold nanoparticle–fungus reaction solution on Si(111) substrate and the spectrum is shown in Figure 2.5. The spectrum shows the three bands at 1650 cm^{-1} (1), 1540 cm^{-1} (2) and 1450 cm^{-1} (3), which confirm the presence of proteins in the reaction mixture. The bands at 1650 and 1540 cm^{-1} are identified as the amide I and II bands and arise due to carbonyl stretch and –N-H stretch vibrations in the amide linkages of the proteins, respectively.[19] The positions of these bands are close to that reported for native proteins

and are in excellent agreement with that observed in gold colloid-pepsin bioconjugates. The FTIR results thus also indicate that the secondary structure of the proteins is not affected as a consequence of reaction with $AuCl_4^-$ ions or binding with the gold nanoparticles. The band at *ca.* 1450 cm^{-1} is assigned to methylene scissoring vibrations from the proteins in the solution.

2.3.1.6. Transmission Electron Microscopy

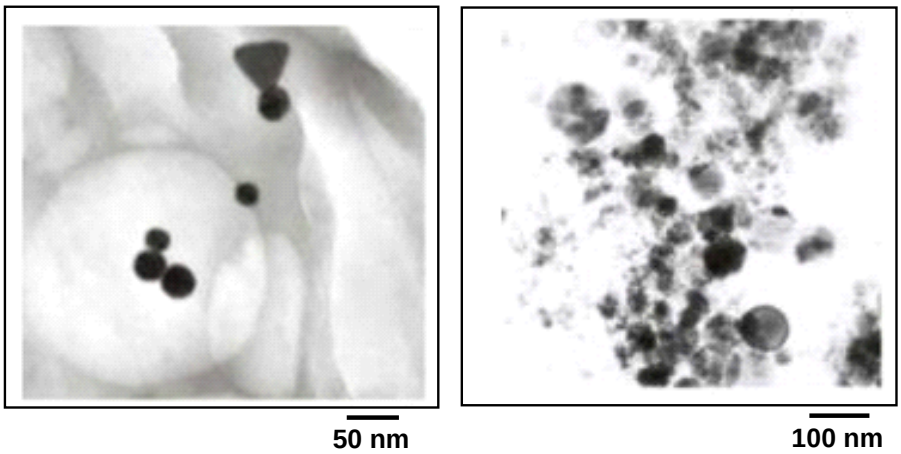

Figure 2.6. TEM micrographs recorded from two different regions of a drop–coated film of an aqueous solution incubated with *Fusarium oxysporum* and treated with $AuCl_4^-$ ions for 48 h.

The two TEM pictures recorded from the gold nanoparticle film deposited on a carbon coated TEM grid are shown in Figure 2.6. In the left picture, well-separated gold particles having spherical and triangular morphology are seen. The right picture shows aggregates of gold nanoparticles. Even though there is large–scale association of the particles, individual, discrete gold nanoparticles can clearly be discerned in this micrograph. The gold nanoparticles are thus undoubtedly stabilized by the proteins that prevent their sintering, a result in agreement with the UV-Vis spectroscopy

measurements which showed the gold solutions to be exceptionally stable. Optical microscopy analysis of number of such pictures yielded nanoparticles of 8–40 nm. The TEM results indicate that it is indeed possible to synthesize gold particles of nanoscale dimensions and tolerable monodispersity by using the fungus, *Fusarium oxysporum*. The gold nanoparticles synthesized with *Fusarium oxysporum* are much smaller and more monodisperse than those synthesized intracellularly with bacteria.[2a,3b]

2.3.2. Extracellular Synthesis of Silver Nanoparticles

2.3.2.1. Visual Inspection

Figure 2.7A shows a conical flask of the fungal cells after removal from the culture medium and before immersion in 1 mM $AgNO_3$ solution (1). The pale yellow color of the fungal cells can clearly be observed in the Figure. A picture of the conical flask containing the fungal cells after immersion in 1 mM $AgNO_3$ solution for 72 h is shown in Figure 2.7B. It can be observed that the pale yellow color of the reaction mixture changed to the brownish color after 72 h of reaction. The appearance of a yellowish-brown color in solution containing the biomass is a clear indication of the formation of silver nanoparticles in the reaction mixture and the color of the solution is due to the excitation of surface plasmon vibrations in the silver nanoparticles.

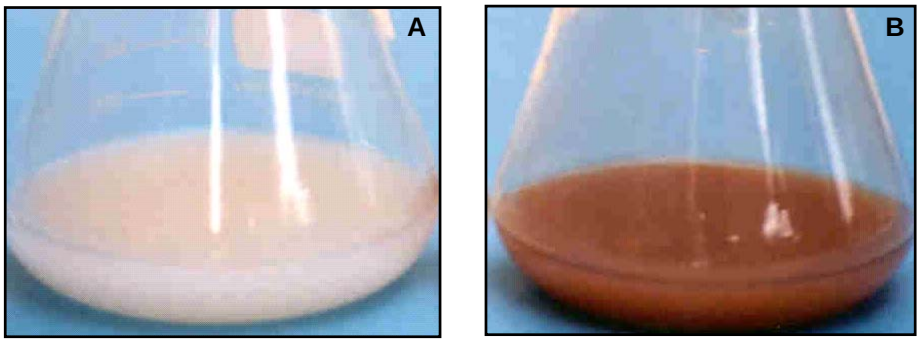

Figure 2.7. Picture of conical flasks containing *Fusarium oxysporum* biomass before (A) and after (B) exposure to Ag^+ ions for 72 h.

2.3.2.2. UV-Vis Spectroscopy

The UV-Vis spectra recorded from the *Fusarium oxysporum* reaction vessel at different reaction times are plotted in Figure 2.8. The time at which the aliquots were removed for measurement is indicated next to the respective curves. The strong surface plasmon resonance centered at *ca*. 413 nm, characteristic of colloidal silver. The spectra clearly show the increase in intensity of silver solution with time, indicating the formation of increased number of silver nanoparticles in the solution. Quite interestingly, the solution was extremely stable even after a month of reaction, with no evidence of aggregation of particles.

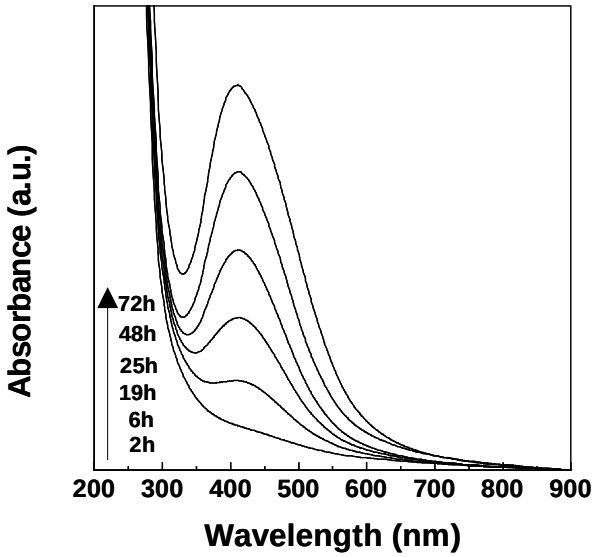

Figure 2.8. UV-Vis spectra recorded with respect to time after the reaction of 1 mM $AgNO_3$ solution with 20 g *Fusarium oxysporum* wet biomass for 72 h.

2.3.2.3. Transmission Electron Microscopy

A representative TEM picture recorded from the silver nanoparticle film deposited on a carbon coated copper TEM grid is shown in Fig. 2.9. This picture shows individual silver particles as well as a number of aggregates. The morphology of the

nanoparticles is highly variable, with spherical and occasionally triangular nanoparticles observed in the micrograph. Under observation of such images in an optical microscope, these assemblies were found to be aggregates of silver nanoparticles in the size range 5–50 nm. The nanoparticles were not in direct contact even within the aggregates, indicating stabilization of the nanoparticles by a capping agent. As discussed earlier, the silver nanoparticle solution, synthesized by the reaction of Ag^+ ions with *Fusarium oxysporum*, is exceptionally stable and the stability is likely to be due to capping with proteins secreted by the fungus. The separation between the silver nanoparticles seen in the TEM image could be due to capping by proteins and would explain the UV-Vis spectroscopy measurements, which is characteristic of well-dispersed silver nanoparticles. The silver particles are crystalline, as can be seen from the selected area diffraction pattern recorded from one of the nanoparticles in the aggregates (Fig. 2.9B).

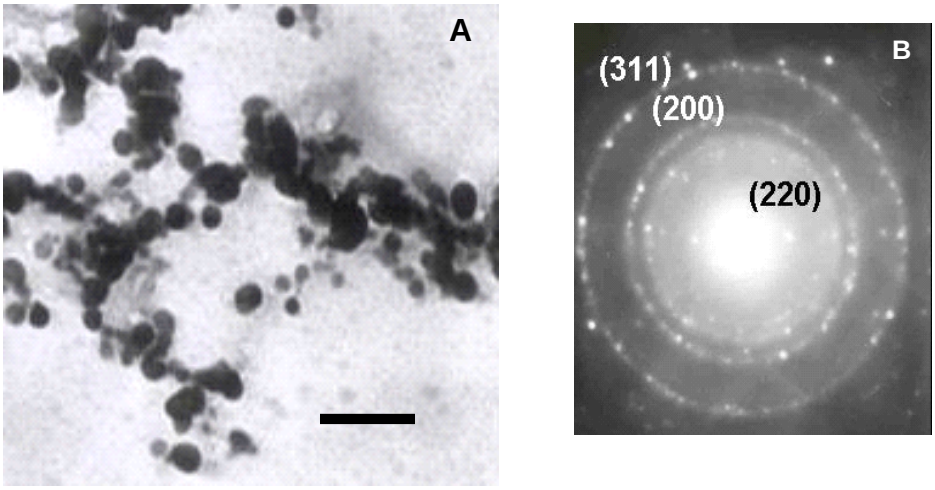

Figure 2.9. (A) TEM micrograph recorded from a drop-coated film of an aqueous solution incubated with *Fusarium oxysporum* and reacted with Ag^+ ions for 72 h. The scale bar corresponds to 100 nm. (B) Selected area of electron diffraction pattern recorded from one of the silver nanoparticles shown in Figure (A). The diffraction rings have been indexed with reference to fcc silver.

2.3.2.4. X-ray Diffraction

The extracellular formation of silver nanoparticles is provided by X-ray diffraction (XRD) analysis of the silver nano solution and is shown in Figure 2.10. The sample of nanoparticles was solution casted in the form of a thin film onto a Si(111) substrate. The presence of sharp reflections due to (111), (200), (220) and (311) agree well with those reported for fcc silver. The inset of Fig. 2.10 shows the (111) Bragg reflection of silver, along with a Lorentzian fit to the reflection. An estimate of the size of the nanoparticles was made from the line broadening of the (111) reflection using the Debye–Scherrer formula. It is found to be *ca.* 11 nm, which is in fairly good agreement with the nanoparticle size estimated by the TEM analysis (Fig. 2.9A).

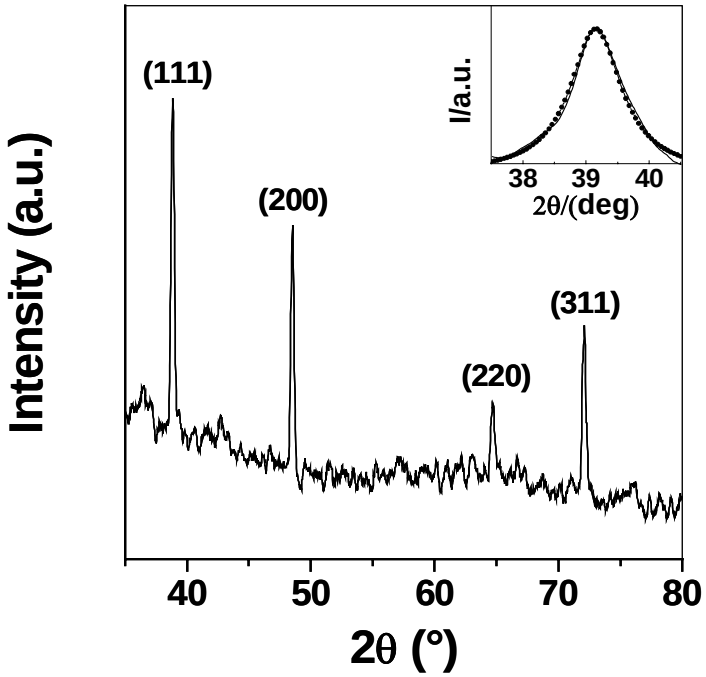

Figure 2.10. XRD pattern recorded from the thin film prepared by drop coating the silver nanoparticle solution on a Si(111) wafer. The principal Bragg reflections are identified. The inset shows the (111) Bragg reflection for a silver nanoparticle film grown by reaction of Ag^{+} ions with *Fusarium oxysporum*. The solid line is a Lorentzian fit to the data and has been used to estimate the silver nanoparticles size.

2.3.2.5. X-ray Photoelectron Spectroscopy (XPS) Measurements

The additional support of reduction of Ag^+ ions to elemental silver by *Fusarium oxysporum* is provided by X-ray photoelectron spectroscopy (XPS) analysis and is shown in Figure 2.11. The sample was prepared by drop-coating the silver nanoparticles-fungal biomass reaction mixture on Si(111) substrate. The Ag 3d spectrum could be decomposed into a single spin-orbit pair (spin-orbit splitting ~ 5.9). The Ag $3d_{5/2}$ and $3d_{3/2}$ peaks occurred at a binding energy (BE) of 368.1 eV and 374 eV respectively and are assigned to the metallic Ag. The absence of a higher binding energy Ag 3d component clearly indicates that all the silver ions are fully reduced by the fungus, *Fusarium oxysporum*, and are in the metallic form.

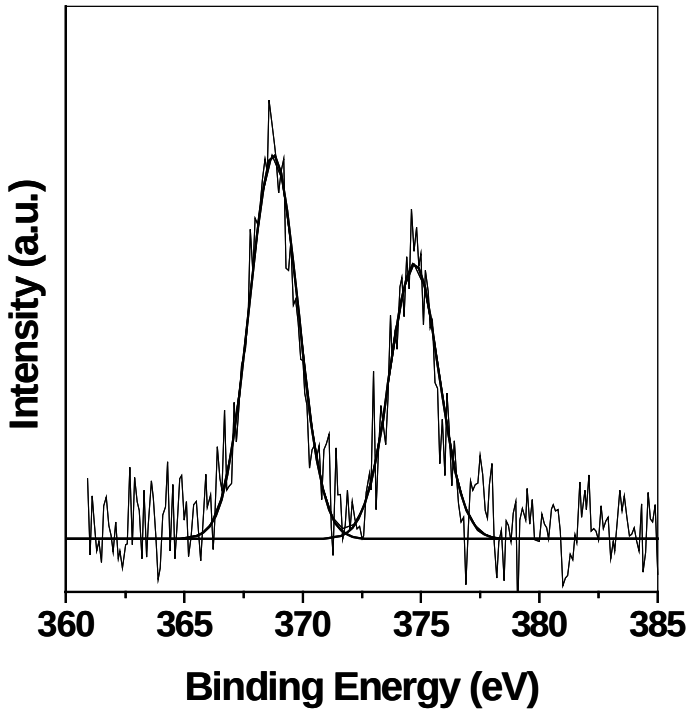

Figure 2.11. Ag 3d core level spectra recorded from a drop coated silver nanoparticle solution on Si(111) substrate. A single spin-orbit pair is shown in the Figure.

2.3.2.6. Fourier Transform Infrared Spectroscopy

The amide linkages between amino acid residues in polypeptides and proteins give rise to well known signatures in the infrared region of the electromagnetic spectrum. The positions of the amide I and II bands in the FTIR spectra of proteins are a sensitive indicator of conformational changes in the protein-secondary structure.[20] The Figure shows the FTIR spectrum recorded from a drop-coated film of the silver nanoparticle-fungus reaction mixture on Si(111) substrate. The spectrum shows the presence of three bands (Fig. 2.12). The bands at 1650 (1) and 1540 (2) cm^{-1} are due to –C=O and –N-H stretch vibrations present in the amide linkages of the proteins, respectively. The positions of these bands are close to that reported in literature for native proteins. Thus, the FTIR measurement indicates that the secondary structure of proteins is not affected because of its interaction with Ag^{+} ions or nanoparticles. The band at ca. 1450 (3) cm^{-1} is due to methylene scissoring vibrations present in the proteins.

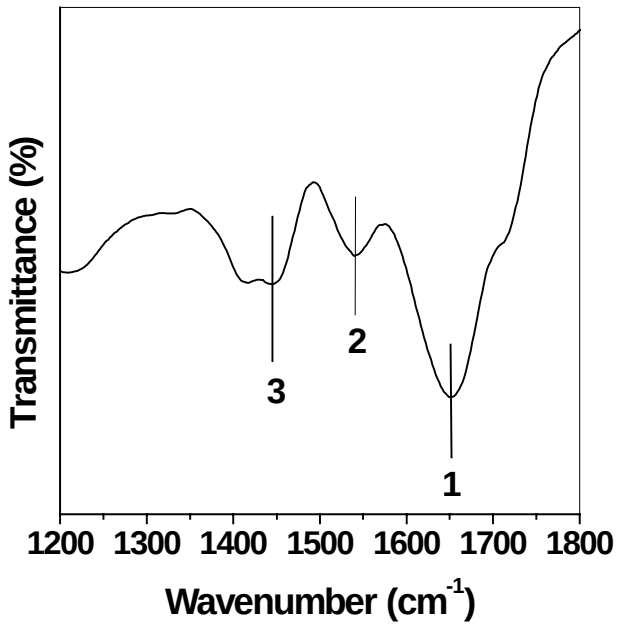

Figure 2.12. FTIR spectrum recorded from a drop-coated film of an aqueous solution incubated with *Fusarium oxysporum* and reacted with Ag^{+} ions for 72 h. The amide bands are identified in the Figure.

2.3.3. Probable Mechanism of Formation of Gold and Silver Nanoparticles

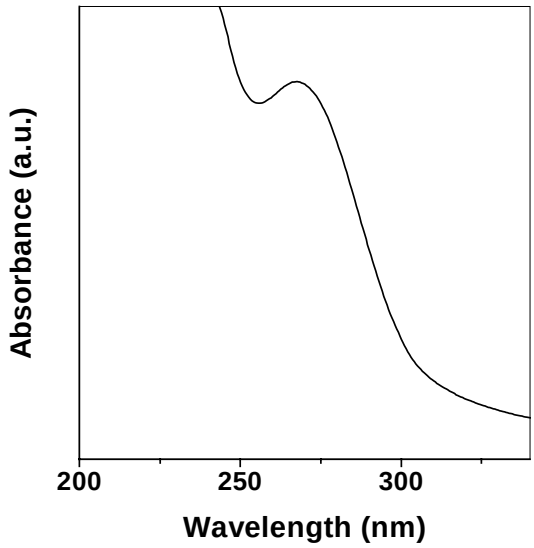

Fugure 2.13. The UV-Vis absorption spectrum in the low wavelength region recorded from the reaction medium of silver nanoparticles 72 h after commencement of the reaction.

The Figure 2.13 shows the UV-Vis spectrum in low wavelength region recorded from the reaction medium of silver nanoparticles 72 h after reaction. The presence of the absorption edge at *ca.* 270 nm is due to the electronic excitations in tryptophan and tyrosine residues present in the proteins moiety.[21] This observation clearly indicates the release of proteins into solution by *Fusarium oxysporum* and that are responsible for the reduction of the metal ions present in the solution. In order to demonstrate that the reduction of the gold or silver ions does indeed take place extracellularly, possibly through the release of reducing agents by the fungus into solution, a control experiment was performed. 20 g of *Fusarium oxysporum* biomass was immersed in 100 mL of water for 72 h, and then the aqueous extract was separated by filtration. To this aqueous extract, 1mM $HAuCl_4$ or 1 mM $AgNO_3$ solution was added. It was observed that this initially colorless aqueous solution gradually changed to purple color (for gold solution) and to pale yellowish-brown (for silver solution) within 24 h of reaction. It clearly

suggests that the reduction of the ions occurs extracellularly through reducing agents released into the solution by *Fusarium oxysporum*. While the above experiments clearly establish that the reduction of the $AuCl_4^-$ and Ag^+ ions occurs extracellularly, it would be important to identify the reducing agents responsible for this. A preliminary gel electrophoresis study shows the presence of a minimum of four high molecular weight proteins released by the biomass in solution. The protein extract for gel electrophoresis was obtained by suspending the *Fusarium oxysporum* mycelial biomass for 72 h and was concentrated by ultrafiltration through a YM–3 ultrafiltration membrane and then dialyzed against distilled water by using a 3K cut-off dialysis bag. This process removes the low molecular weight components in the extract such as co-factors. The protein mixture obtained after dialysis failed to reduce Au^{+3} and Ag^+ ions. However, on addition of stoichiometric amounts of NADH to the protein extract, the reduction of ions occurs quite readily. This clearly suggests that the reduction of Au^{+3} and Ag^+ ions by NADH dependent reductases in the extract and the subsequent formation of nanoparticles. It may be mentioned here that in bacteria, an NADH-dependent iron (III) reductase has been observed in the outer membrane of *Geabacter sulfurreducens*,[22] while a periplasmic iron (III) reductase has been isolated from *Magnetospirillum magnetotacticum*.[23] We would like to point out here that this reductase is specific to *Fusarium oxysporum*–prolonged reaction of $AuCl_4^-$ or Ag^+ ions with another fungus, *Fusarium moniliforme*, did not result in the formation of gold or silver nanoparticles, neither intracellularly nor extracellularly. The long term stability of the nanoparticles solution mentioned earlier may be due to the stabilization of the gold or silver particles by the proteins. Metal nanoparticles have been reported to interact strongly with enzymes such as cytochrome c,[24] and a similar binding mechanism may be operative in this study.

2.3.4. Effect of Biomass Concentration

The effect of biomass concentration on the extracellular synthesis of gold and silver nanoparticles was studied by exposing 5 g, 10 g, 20 g and 30 g of wet biomass of *Fusarium oxysporum* to 1 mM aqueous solution of $HAuCl_4$ and $AgNO_3$ respectively. The Figure 2.14A shows UV-Vis spectra of the reaction mixtures of gold nanoparticles by exposing 5 g, 10 g, 20 g and 30 g respectively of wet biomass of *Fusarium oxysporum* to aqueous solution of 1 mM $HAuCl_4$. The pH of the reaction mixture at the beginning was 3.3. It can be observed that when an aqueous solution of 1 mM $HAuCl_4$ exposed to 5 g to 10 g of wet biomass of *Fusarium oxysporum*, the absorbance of surface plasmon

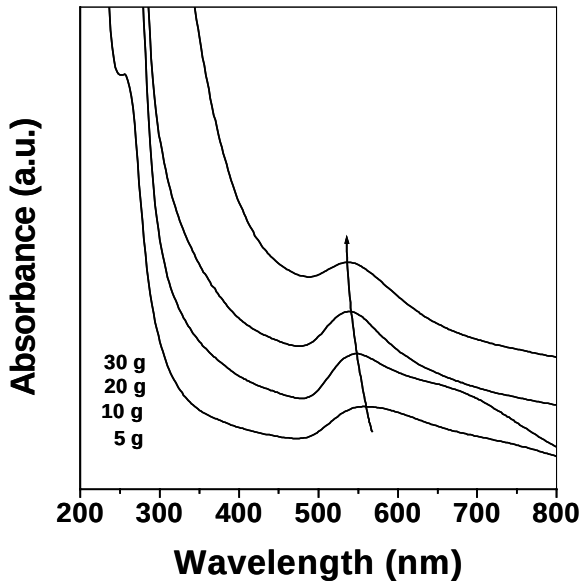

Figure 2.14. UV-Vis spectra of the reaction mixtures of gold nanoparticles by exposing 5 g, 10 g, 20 g and 30 g respectively of wet biomass of *Fusarium oxysporum* to aqueous solution of 1 mM $HAuCl_4$. The spectra have been shifted vertically for clarity.

resonance of reaction mixtures show an apparent broadening and red shift at 550 nm indicating the aggregation of gold nanoparticles whereas when the amount of biomass is increased to 20 g to 30 g, no broadening or red shift of absorbance is observed. This

indicates that when less amount of wet biomass of *Fusarium oxysporum* (5–10 g) exposed to an aqueous solution of 1 mM $HAuCl_4$ at pH = 3.3, which is generally a harsh condition for survival of fungus, *Fusarium oxysporum*, it releases enzyme in solution in faster rate than the capping protein (which is necessary to prevent the aggregation of gold nanoparticles). The secreted enzyme then reduces the Au^{+3} ions to Au^0 and aggregates due to the absence of required amount of capping proteins. Further, support of formation of aggregated particles, when low amount of biomass is used, is provided by TEM analysis (Fig. 2.15).

The Figure 2.15 (A-D) shows the TEM images recorded from gold nanoparticle solution synthesized using different amount of biomass 5 g, 10 g, 20 g and 30 g respectively. It can be observed in Figure 2.15 (A and B) that when the gold nanoparticles are synthesized using 5 g and 10 g fungal biomass, the aggregated nanoparticles of bigger sizes are formed. Although the few smaller particles are also observed in the TEM images, but the concentration of bigger particles are much higher. On careful inspection of the micrographs reveals that the particles are not well separated within the aggregates, indicating the presence of less amount of capping protein in the reaction mixtures. But when the slightly increased amount of biomass 20 g and 30 g is used, well separated and polydispersed particles are observed [Fig. 2.15 (C and D)].

However, when the same reaction was performed with 1 mM $AgNO_3$ solution at pH = 6.7, no broadening or red shift of absorbance maxima is observed (Fig. 2.16). This observation is completely converse to that observed for gold nanoparticles.

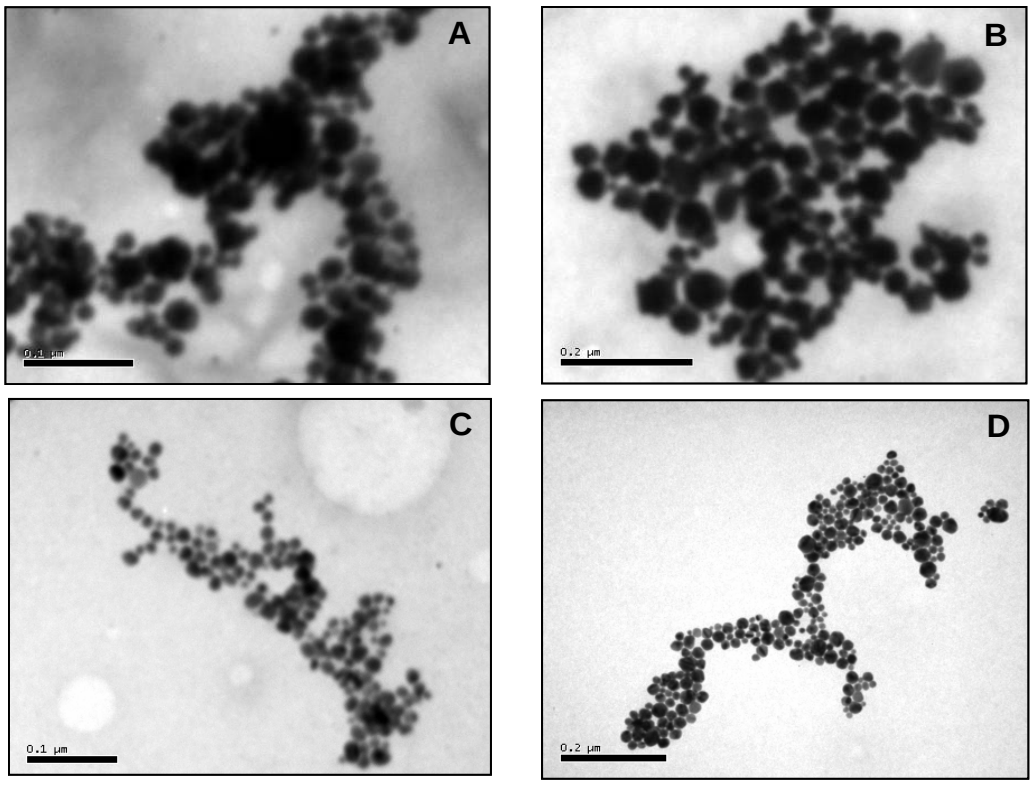

Figure 2.15. (A-D) TEM micrographs recorded from gold nanoparticle solutions synthesized by exposing 5 g, 10 g, 20 g and 30 g wet biomass of *Fusarium oxysporum* to aqueous solution of 1 mM $HAuCl_4$.

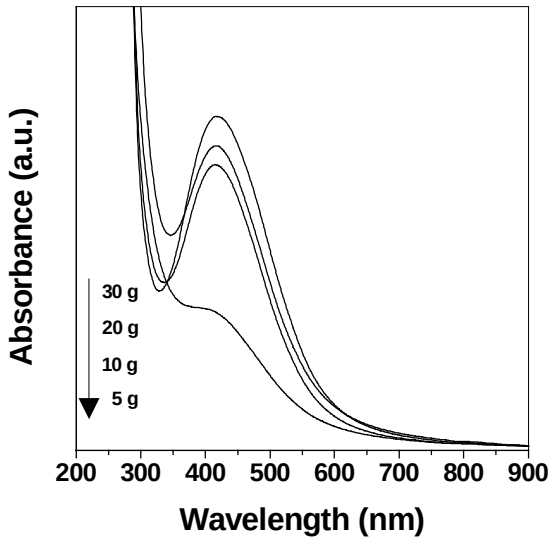

Figure 2.16. UV-Vis spectra of the reaction mixtures of silver nanoparticles by exposing 5 g, 10 g, 20 g and 30 g respectively of wet biomass of *Fusarium oxysporum* to aqueous solution of 1 mM $AgNO_3$.

It can be inferred from above observations that either metal ion or the pH of the reaction mixture has a role to play. In order to determine the role of pH, a set of experiments were designed in which the reduction of $HAuCl_4$ was carried out at pH 6.7 and of $AgNO_3$ at pH 3.3 keeping all other parameters constant. In both the cases, there was no deviation from the results obtained earlier (Fig. 2.14 and 2.16).

Thus, it can be concluded that the synthesis of gold and silver nanoparticles using fungus, *Fusarium oxysporum*, is independent of pH of the reaction mixture. Since all other factors are common for both the reactions, the difference in the observation can be attributed to the difference in metal ions themselves. Thus, this phenomenon can be an indicator to the differential toxicity of metal ions towards fungus, *Fusarium oxysporum*. The higher toxicity of gold ion for *Fusarium oxysporum* may trigger the release of higher amount of reducing agent in the solution to convert Au^{3+} to Au^0 for its survival in that environment, whereas the release of capping proteins may remain unaffected by the toxicity of gold ion. This may explain the higher aggregation of gold nanoparticles at lower amount of biomass, which is not observed for silver nanoparticles.

2.3.5. Effect of pH on Stability of Nanoparticle Solution

The effect of pH on the stability of gold and silver nanoparticle solution synthesized extracellularly by exposing 20 g of wet biomass of *Fusarium oxysporum* to 1 mM aqueous solution of $HAuCl_4$ and $AgNO_3$ respectively and is shown in Figure 2.17. It can be clearly seen from the UV-Vis spectra that the absorption maxima are uniform in the pH range from 7.5 to >12.0 for both gold and silver nanoparticle solutions indicating the extreme stability of nanoparticles at higher pH [Fig. 2.17 (A and B)]. But at lower pH (6.5 to < 2.0), the broadening of absorbance with a little red shift of absorption maxima

is observed for both gold and silver nanoparticles solution indicating the aggregation of particles [Fig. 2.18 (A and B)]. This observation can be attributed to the capping proteins secreted by the fungus, *Fusarium oxysporum*, in solution are very much stable at higher pH and the capping protein retains its characteristics as can be seen from FTIR measurement (Figure 2.19A) and hence the nanoparticle solutions remain stable at higher pH. But at lower pH, at around pH =3.4, the protein structure gets affected and the protein gets denatured and loses its activity (Figure 2.19B), thus aggregation of nanoparticle is observed. Thus, it can be concluded from above observation that the proteins secreted by *Fusarium oxysporum* in solution for the capping of both gold and silver nanoparticles are stable at basic pH but not in acidic pH which can be attributed to the stability of capping protein.

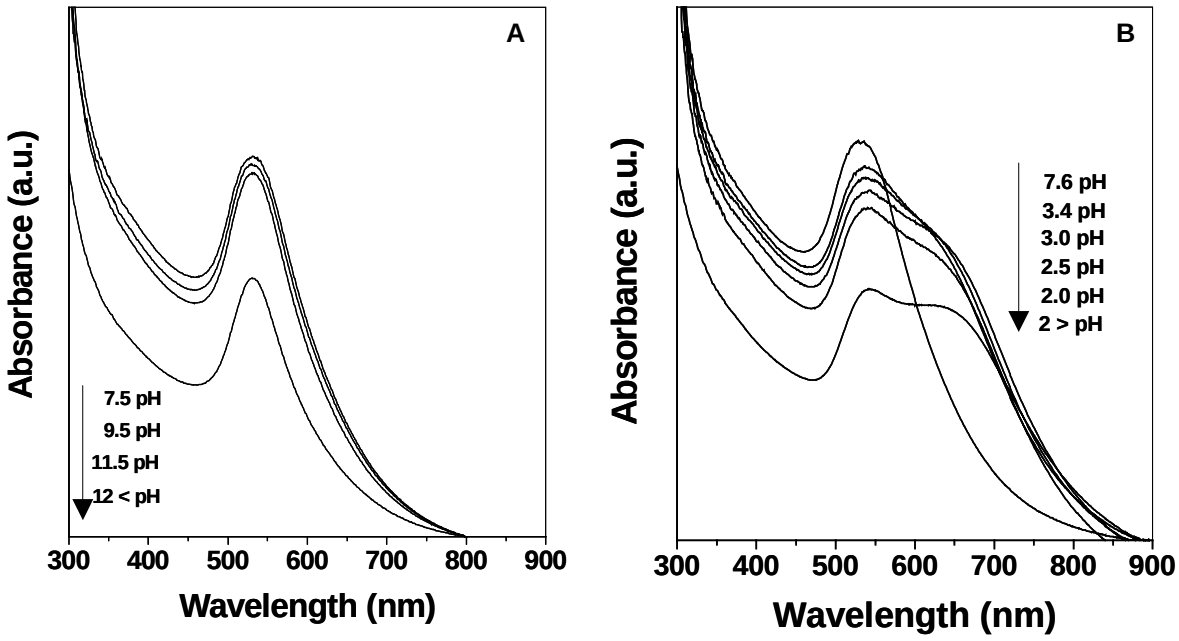

Figure 2.17. UV-Vis spectra of gold nanoparticle–fungus reaction mixture after 48 h of reaction at higher pH (A) and at lower pH (B).

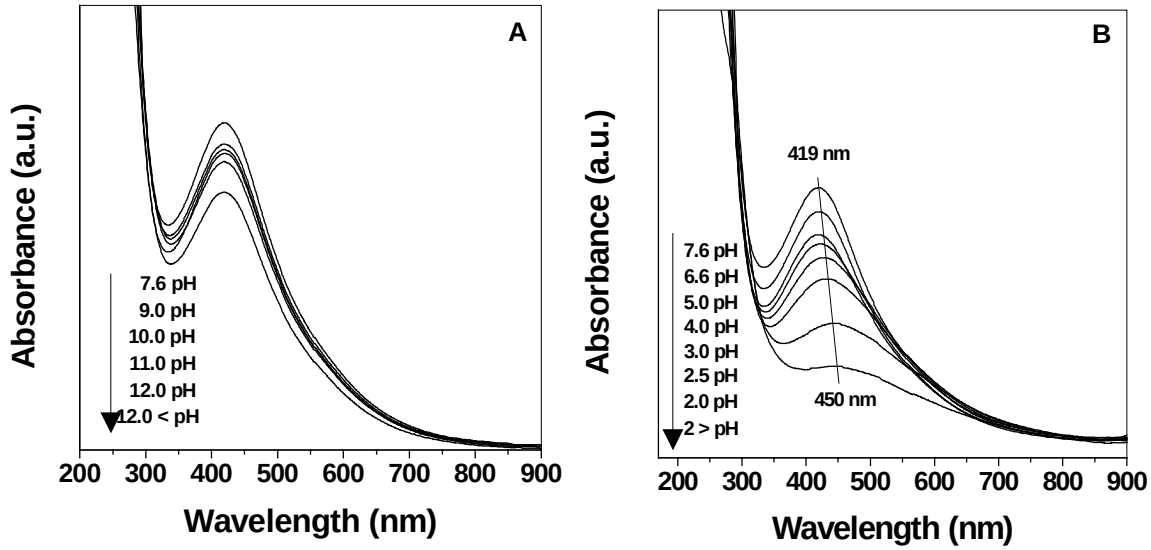

Figure 2.18. UV-Vis spectra of silver nanoparticle-fungus reaction mixture after 72 h of reaction at higher pH (A) and at lower pH (B).

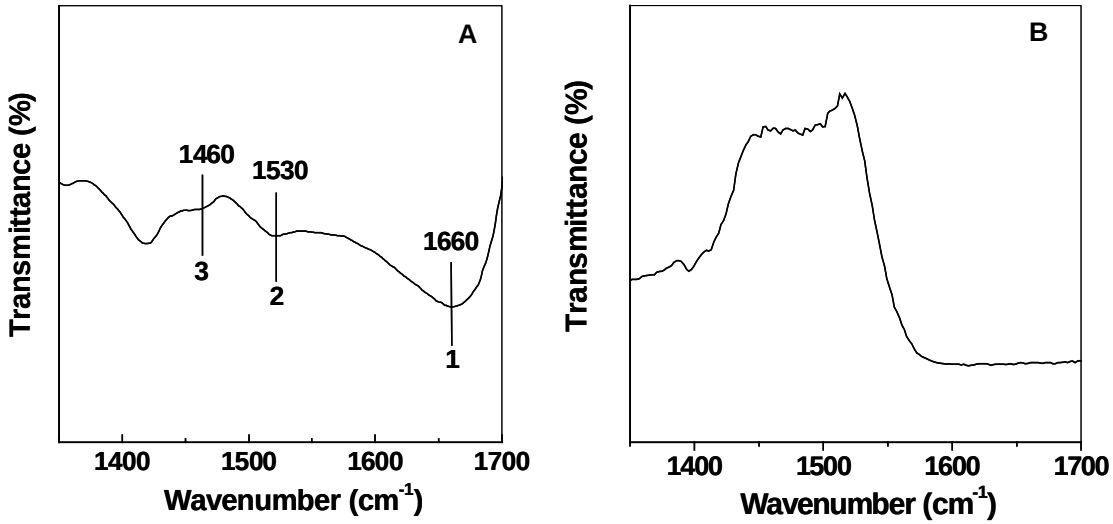

Figure 2.19. FTIR spectra recorded from a drop-coated film of nanoparticles–fungus reaction mixture after 48 h of reaction (A) at pH higher than 12 and (B) at pH less than 2.

2.3.6. Extracellular Synthesis of Bimetallic Gold Silver Alloy Nanoparticles

2.3.6.1. Visual Inspection

The inset of Figure 2.20 shows four test tubes (1–4) of the reaction mixture of $HAuCl_4$ and $AgNO_3$ solution after the treatment with 60 g *Fusarium oxysporum* wet biomass at different interval of time. The gradual change of color from purple to deep brown is the clear indicative of the formation of Au-Ag alloy nanoparticles. The color change from purple to deep brown is found to be dependent on the rate of reduction of Ag^+ ions by the fungus, *Fusarium oxysporum*.

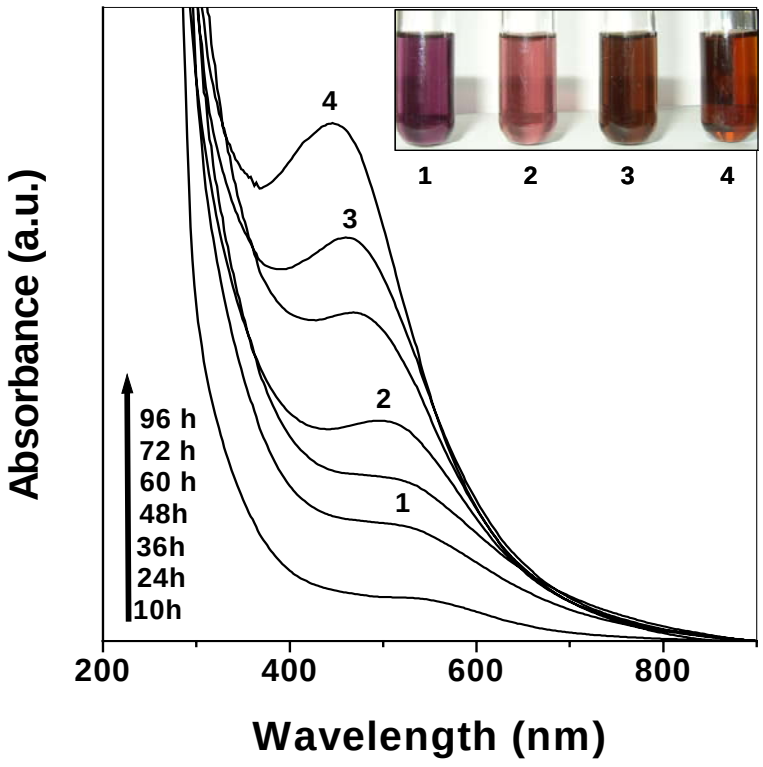

Figure 2.20. UV-Vis spectra of Au-Ag alloy nanoparticles, exhibiting increasing Ag mole fraction with time, after the reaction of a mixture of a solution containing 1 mM $HAuCl_4$ and 1 mM $AgNO_3$ with 60 g *Fusarium oxysporum* wet biomass for 96 h. The inset shows test tubes (1-4) containing these diluted colloidal solution.

2.3.6.2. UV-Vis Spectroscopy

The Figure 2.20 shows the UV-Vis absorption spectra of Au-Ag alloy nanoparticles solution recorded from the reaction mixture of a solution containing 1 mM $HAuCl_4$ and 1 mM $AgNO_3$ with 60 g *Fusarium oxysporum* biomass at different interval of time. The spectra show a gradual shift of surface plasmon bands, as a function of time for 96 h from 543 nm to 443 nm and are commensurate with the increasing Ag mole fraction. It can be observed that all the peaks are located at intermediate positions of pure nano Au and Ag plasmon bands (545 nm and 413 nm respectively, as described earlier in chapter 2). The presence of only one plasmon resonance, shifting gradually from nano gold to silver plasmon bands, clearly suggests the formation of gold silver alloy nanoparticles, rather than, segregated metal or core-shell type structure, otherwise, two bands for both nano gold and nano silver would have been observed.[25] The plasmon absorptions of the gold silver nano composites are linearly blue shifted from that of Au in proportion to the increase in the mol fraction of the Ag content and is shown in Figure 2.21, where, the UV-Vis absorption maximum is plotted against the mol fraction of Au.

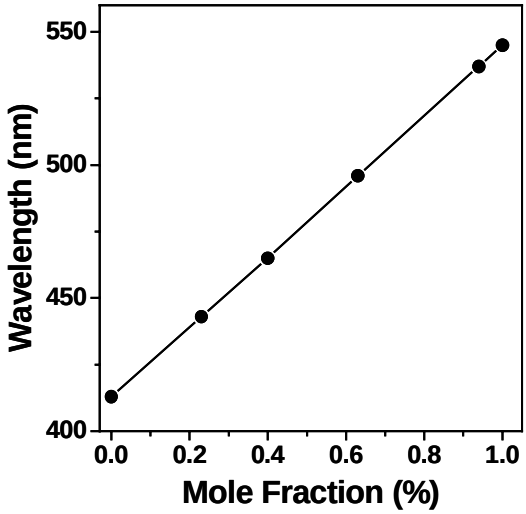

Figure 2.21. UV-Vis absorption position of the surface plasmon maximum is plotted against the mole fraction of gold in Au-Ag bimetallic nanoparticles.

2.3.6.3. X-ray Photoelectron Spectroscopy

A chemical analysis of drop-coated film on Si(111) of Au-Ag nano alloy solution exposed to fungal biomass for 96 h was carried out by XPS. All the recorded core level spectra were decomposed into individual chemical components using a nonlinear least-squares fitting procedure as shown in Figure 2.22. Au 4f spectrum resolved into two spin-orbit components 1 and 2 (Figure 2.22A). The Au $4f_{7/2}$ and $4f_{5/2}$ peaks occurred at a binding energy (BE) of 84.4 eV and 88.1 eV respectively and are assigned to the metallic gold. Figure 2.22B shows the Ag 3d spectrum resolved into a single spin-orbit pair. The Ag $3d_{5/2}$ peak occurred at a BE of 368.1 eV and corresponds to that of metallic silver. These results demonstrate that only one form of Au and Ag are present in solution and it is in the form of Au(0) and Ag(0). Thus, it is concluded from the XPS measurements that all the gold and silver ions used in the nanoparticle synthesis are reduced and are in the metallic form.

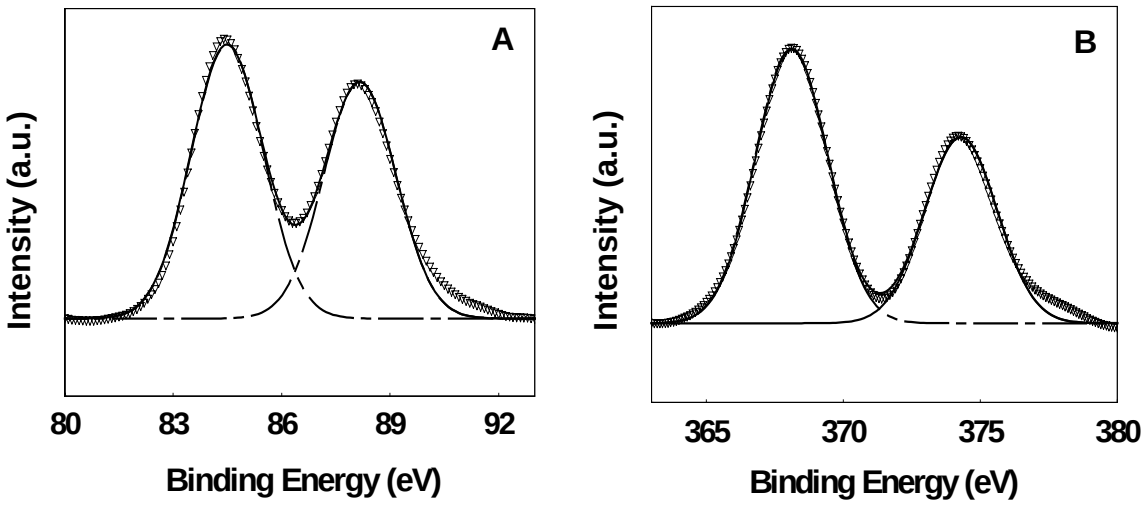

Figure 2.22. (A) Au 4f (B) Ag 3d core-level spectra recorded from a drop-coated Au-Ag nanoparticles solution on a Si(111) substrate. The two spin-orbit components are shown in the Figure of each element.

2.3.6.4. Transmission Electron Microscopy Measurements

Transmission electron microscopy was used to analyze the size and electron density of the alloy nanoparticles recorded from the drop-coated films of the bimetallic alloy nanoparticles synthesized using *Fusarium oxysporum* after treating an equimolar concentration of $HAuCl_4$ and $AgNO_3$ in 100 mL with the 60 g wet biomass for 96 h and are shown in Figure 2.23.

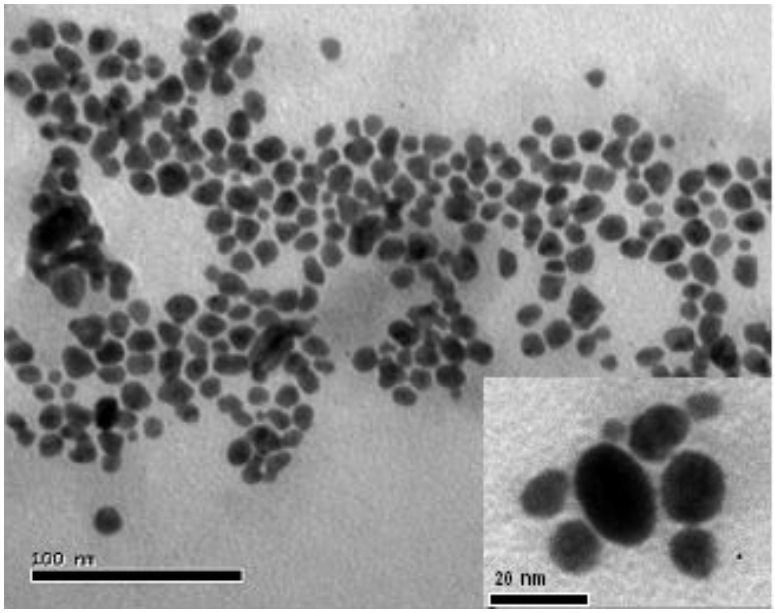

Figure 2.23. TEM images of Au-Ag nanoparticles formed by reaction of a mixture of 1 mM $HAuCl_4$ and 1 mM $AgNO_3$, with 60 g *Fusarium oxysporum* wet biomass for 96 h.

At lower magnification, well-separated nanoparticles with occasional aggregation in the size range 8–14 nm are clearly observed. TEM of bimetallic core-shell type nanoparticulate structures are known to show electron density banding with dark gold core and a lighter silver shell. However, the TEM analysis of our particles shows almost uniform contrast within each particle suggesting that the electron density is homogenous within the volume of the particle. This is not unexpected since gold and silver are completely miscible in all proportions due to their almost identical lattice constants. As a

result, the Au-Ag alloy unit-cell size changes only by less than 1 % over the whole range from pure Au to pure Ag.[26] The uniformity in contrast in the bimetallic particles observed herein clearly suggests the fact that the particles are in the alloy form and not of the core-shell structure. These results are in agreement with the UV-Vis data discussed earlier in section 2.7.2.

2.3.6.5. Effect of Biomass Concentration

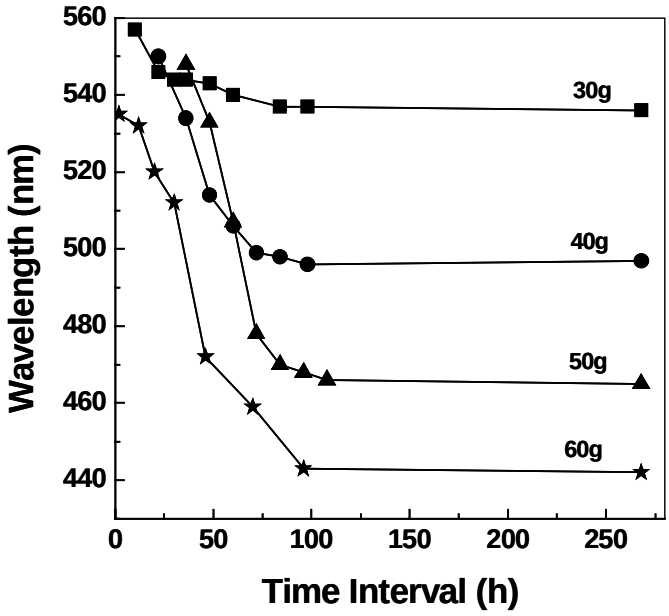

Figure 2.24. The graph showing the change in wavelength with respect to time of the mixture of a solution of 1 mM $HAuCl_4$ and 1 mM $AgNO_3$ after the treatment with different amount of *Fusarium oxysporum* wet biomass viz. 30 g, 40 g, 50 g and 60 g.

The Figure 2.24 shows the change in wavelength with respect to time of the reaction mixture of $HAuCl_4$ and $AgNO_3$ solution after the treatment with different amount of *Fusarium oxysporum* wet biomass viz. 30 g, 40 g, 50 g and 60 g respectively. It can be observed from Figure that when 30 g of wet biomass was used, the UV-Vis absorbance levels off at 96 h with λ_{max} of 543 nm. When the biomass amount was

increased to 40 g, 50 g, 60 g and 70 g, the absorbance leveled off at 96 h with λ_{max} of 496 nm, 470 nm, 443 nm, 440 nm respectively.

Thus, when amount of biomass was 30 g only gold nanoparticles are formed whereas with increase in biomass from 40 g to 60 g, Au-Ag alloy nanoparticles with higher mole fraction (w. r. t. silver) were formed. With further increase in the amount of biomass to 70 g, there was no further shift in the λ_{max} observed. In other words, when 30 g of wet biomass is exposed to a mixture of $HAuCl_4$ and $AgNO_3$, it is capable to reduce only $AuCl_4^-$ ions at that biomass concentration. However, when the biomass concentration is slightly increased to 40 g, the UV-Vis absorbance maxima blue shifts to 500 nm, indicating the beginning of reduction of Ag^+ ions along with $AuCl_4^-$ ions. This indicates that the critical biomass concentration is essential for reduction of Ag^+ in presence of Au^{3+} ions; below this critical biomass only gold ions will be reduced. On further increase in amount of biomass till 60 g, the UV-Vis absorbance maxima blue shifted to 443 nm, indicating the increase in the amount of silver in the synthesized alloy nanoparticles. However, on further increase in amount of biomass, no appreciable shift in the UV-Vis absorbance was observed. This suggests that the amount of biomass 60 g is the limiting amount of biomass; above this limiting value no further shift in the UV-Vis absorbance or no further increase in the amount of silver in the synthesized alloy nanoparticles will be observed.

2.3.6.6. Probable Mechanism of Formation of Au-Ag Alloy Nanoparticles

The fungus, *Fusarium oxysporum*, is known to secrete NADH dependent enzymes in reaction mixture as discussed earlier in section 2.4.[12, 27] To determine the relation between the biomass concentration and the ability of reduce both $AuCl_4^-$ and Ag^+ ions few controlled experiments were designed. Accordingly, 100 mL solution of

1mM $HAuCl_4$ and 1mM $AgNO_3$ was treated with different amounts, 100 μL, 200 μL, 300 μL and 400 μL, of NADH, (0.1% W/V) respectively (i) in the presence of 30g *Fusarium oxysporum* biomass (ii) and in absence of biomass. It was observed that the shift in the UV-Vis absorbance of these reaction mixtures after 24 h were similar when (i) the amount of biomass was increased from 30 to 60 g, or (ii) the amount of NADH was increased from 100 μL to 400 μL keeping the biomass amount constant at 30 g. However no shift in UV-Vis absorbance was observed when the experiment was performed in absence of biomass. It is clear from above experiments that as the amount of biomass are increased, more and more cofactor, NADH is being released by the fungus in solution and that enables the enzymes, secreted by the fungus, *Fusarium oxysporum*, in reaction mixture, to reduce the metal ions. The cofactor, NADH secreted by the 30 g biomass of fungus, *Fusarium oxysporum*, in reaction mixture for 96 h is sufficient only for more easily reducible Au^{3+} and thus UV-Vis absorbance is observed at 543 nm without any shift.[28] But as the amount of wet biomass is increased from 30 to 60 g, the fungus releases more NADH in reaction mixture, which helps the enzymes to reduce both Au^{3+} and Ag^{+} ions, thus a gradual shift in UV-Vis absorbance is observed. It should be mentioned here that the $HAuCl_4$ and $AgNO_3$ are not toxic to fungus, *Fusarium oxysporum*, as it found to grow on agar plate even after 96 h of reaction. Thus, the cofactor NADH plays an important role in controlling the composition of Au-Ag nanoparticles by the fungus, *Fusarium oxysporum.* In other words, by varying the amount of NADH, the different composition of Au-Ag alloy nanoparticles can be synthesized.

2.7. SUMMARY

In this chapter, it has been shown for the first time the use of eukaryotic system such as fungi in the extracellular synthesis of metal nanoparticles. The high stability of the nanoparticle solution is due to secretion of reducing enzyme and capping protein by the fungus, *Fusarium oxysporum*, in the reaction mixture and is responsible for both formation and capping of the metal nanoparticle. The preliminary study of protein extract obtained by suspending the fungus, *Fusarium oxysporum*, biomass for 72 h reveals the presence of NADH dependent reductases in the extract. The stability of capping protein is found to be pH dependent. At higher pH the nanoparticle solution remains stable while it aggregates at lower pH as the protein gets denatured. It has been observed that the *Fusarium oxysporum* lacks sufficient defence mechanism to circumvent the toxic effect of gold ions in compare to silver ions. In presence of $AuCl_4^-$ ions and at lower amount of biomass, the *Fusarium oxysporum* releases higher amount of reducing enzyme compare to capping protein in solution and results in the formation of aggregated nanoparticle while in presence of Ag^+ ions under similar condition, no aggregation of nanoparticle is observed. This efficient process of nanoparticle synthesis has been further extended for the synthesis of bimetallic Au-Ag alloy nanoparticle by using the equimolar mixture of gold and silver solution. It has been observed that the composition of Au-Ag nano alloy is cofactor NADH dependent. The Au-Ag alloy nanoparticle of varying composition can be synthesized by controlling the release of amount of cofactor by using the controlled amount of biomass, *Fusarium oxysporum*. The extracellular synthesis of nanoparticle makes it possible to harness and immobilize/deposit onto desired solid support for the use of different practical purposes.

2.8. REFERENCES

1. (a) J. Fritz, M. K. Baller, H. P. Lang, H. Rothuizen, P. Vettiger, E. Meyer, H. J. Guntherodt, C. Gerber, J. K. Gimzewski, *Science* **2000**, *288*, 316. (b) L. Stryer, *Biochemistry*, 4th edition, Freeman, New York, 1995. (c) J. Liu, J. Alvarez, A. E. Kaifer, *Adv. Mater.* **2000**, *12*, 1381. (d) M. Ludwig, W. Dettmann, H. E. Gaub, *J. Biophys.* **1997**, *72*, 445. (e) C. M. Paleos, D. Tsiourvas, *Adv. Mater.* **1997**, *9*, 695. (f) J. Spinke, M. Liley, H. J. Guder, L. Angermaier, W. Knoll, *Langmuir* **1993**, *9*, 1821.
2. (a) G. Southam, T. J. Beveridge, Geochimica et Cosmochimica Acta **1996**, *60*, 4369. (b) T. J. Beveridge, R. G. E. Murray, *J. Bacteriol.* **1980**, *141*, 876. (c) D. Fortin, T. J. Beveridge, *In Biomineralization. From Biology to Biotechnology and Medical Applications* (Ed. E. Baeuerien), Wiley-VCH, Weinheim, 2000, p. 7.
3. (a) T. Klaus, R. Joerger, E. Olsson, C. G. Granqvist, *Proc. Natl. Acad. Sci. USA* **1999**, *96*, 13611. (b) T. Klaus-Joerger, R. Joerger, E. Olsson, C. G. Granqvist, *Trends Biotechnol.* **2001**, *19*, 15. (c) R. Joerger, T. Klaus, C. G. Granqvist, *Adv. Mater*. **2000**, *12*, 407. (d) B. Nair, T. Pradeep, *Crys. Growth Des.* **2002**, *2*, 293.
4. (a) D. P. Cunningham, L. L. Lundie, *Appl. Environ. Microbiol.* **1993**, *59*, 7. (b) J. D. Holmes, P. R. Smith, R. Evans-Gowing, D. J. Richardson, D. A. Russell, J. R. Sodeau, *Arch. Microbiol.* **1995**, *163*, 0143. (c) P. R. Smith, J. D. Holmes, D. J. Richardson, D. A. Russell, J. R. Sodeau, *J. Chem. Soc., Faraday Trans.* **1998**, *94*, 1235.
5. M. Labrenz, G. K. Druschel, T. Thomsen-Ebert, B. Gilbert, S. A. Welch, K. M. Kemner, G. A. Logan, R. E. Summons, G. De Stasio, P. L. Bond, B. Lai, S. D. Kelly, J. F. Banfield, *Science* **2000**, *290*, 1744.
6. (a) D. R. Lovley, J. F. Stolz, G. L. Nord, E. J. P. Phillips, *Nature* **1987**, *330*, 252. (b) R. B. Frankel, R. P. Blakemore (Eds.) *Iron Biominerals*, Plenum Press, New York, 1991. (c) A. P. Philipse, D. Maas, *Langmuir* **2002**, *18*, 9977. (d) Y. Roh, R. J. Lauf, A. D. McMillan, C. Zhang, C. J. Rawn, J. Bai, T. J. Phelps, *Solid State Commun.* **2001**, *118*, 529.
7. (a) J. H. P. Watson, D. C. Ellwood, A. K. Sper, J. Charnock, *J. Magn. Magn. Mater.* **1999**, *203*, 69. (b) J. H. P. Watson, B. A. Cressey, A. P. Roberts, D. C. Ellwoood, J. M. Charnock, *J. Magn. Magn. Mater.* **2000**, *214*, 13.

8. M. Kowshik, W. Vogel, J. Urban, S. K. Kulkarni, K. M. Paknikar, *Adv. Mater.* **2002**, *14*, 815.
9. M. Kowshik, N. Deshmukh, W. Vogel, J. Urban, S. K. Kulkarni, K. M. Paknikar, *Biotech. Bioeng.* **2002**, *78*, 583.
10. M. G. Robinson, L. N. Brown, D. Beverley, *Biofouling*, **1997**, *11*, 59.
11. D. Mandal, A. Ahmad, M. I. Khan, R. Kumar, *J. Mol. Catal. A: Chem.* **2002**, *181*, 237.
12. (a) P. Mukherjee, S. Senapati, D. Mandal, A. Ahmad, M. I. Khan, R. Kumar, M. Sastry, *ChemBioChem* **2002,** *3,* 461. (b) A. Ahmad, P. Mukherjee, S. Senapati, D. Mandal, M. I. Khan, R. Kumar, M. Sastry, *Colloids Surf.* B **2003**, *28,* 313.
13. S. Senapati, A. Ahmad, M. I. Khan, M. Sastry, R. Kumar, *Small* **2005**, *1*, 517.
14. D. A. Shirley, *Phys. Rev. B.* **1972**, *5*, 4709.
15. (a) A. Henglein, *J. Phys. Chem.* **1993**, *97*, 5457. (b) M. Sastry, K. Bandyopadhyay, K. S. Mayya, *Colloid. Surf. A* **1997**, *127*, 221. (c) M. Sastry, V. Patil, S. R. Sainkar, *J. Phys. Chem. B* **1998,** *102*, 1404.
16. D. V. Leff, L. Brandt, J. R. Heath, *Langmuir* **1996**, *12*, 4723.
17. J. W. Jeffrey, *Methods in Crystallography*, Academic Press, New York, 1971.
18. C. S. Fadley, D. A. Shirley, *J. Res. Natl. Bur. Stand.* **1970**, *74A*, 543-545.
19. (a) C. D. Keating, K. K. Kovaleski, M. J. Natan, *J. Phys.Chem. B* **1998**, *102*, 9414. (b) A. Gole, C. Dash, V. Ramakrishnan, S. R. Sainkar, A. B. Mandale, M. Rao, M. Sastry, *Langmuir* **2001**, *17*, 1674. (c) A. Gole, C. Dash, S. R. Sainkar, A. B. Mandale, M. Rao, M. Sastry, *Anal. Chem.* **2000**, *72*, 1401.
20. A. Dong, P. Huang, W. S. Caughey, *Biochemistry* **1992**, *31*,182.
21. (a) M. R. Eftink, C. A. Ghiron, *Anal. Biochem.* **1981**, *114*, 199. (b) Cantor, Schimmel, (Eds.) *Biophysical Chemistry, Part II: Techniques for the Study of Biological Structure and Function*, H. Freeman and Co., San Francisco. 1980, Ch 7, p 377.
22. T. S. Magnuson, A. L. Hodges-Myerson, D. R. Lovley, *FEMS Microbiol. Lett.* **2000**, *185*, 205.
23. Y. Noguchi, T. Fujiwara, K. Y. Yoshimatsu, K. Fukumori, *J. Bacteriol.* **1999**, *181*, 2142.

24. (a) I. D. G. Macdonald, W. E. Smith, *Langmuir* **1996**, *12*, 706. (b) C. V. Kumar, G. L. McLendon, *Chem. Mater.* **1997**, *9*, 863.
25. S. Mandal, PR. Selvakannan, R. Pasricha, M. Sastry, *J. Am. Chem. Soc.* **2003**, *125*, 8440.
26. A. Bayler, A Schier, G. A. Bowmaker, H. Schmidbaur, *J. Am. Chem. Soc.* **1996**, *43*, 4519.
27. A Ahmad, P. Mukherjee, D. Mandal, S. Senapati, M. I. Khan, R. Kumar, M. Sastry, *J. Am. Chem. Soc.* **2002**, *124*, 12108.
28. Y. Xiao, V. Pavlov, S. Levine, T. Niazov, G. Markovitch, I. Willner, *Angew. Chem. Int. Ed. Engl.* **2004**, *43*, 4519.

3.1. INTRODUCTION

The synthesis of nanoparticles of controlled particle size and good monodispersity is essential to explore the unique physical and chemical properties of nanomaterials. Many potential applications of nanoparticles such as quantum dot, tunable laser diodes require extreme monodispersity of nanoparticles.[1] A number of chemical methods to control the size and distribution of the nanoparticles include micelle,[2] langmuir-Blodgett,[3] and organometallic techniques.[4] However, these techniques employ toxic and expensive chemicals and also the synthesized nanoparticles are relatively unstable and tend to agglomerate quickly. Thus, there is a growing need to develop clean, non-toxic and inexpensive synthesis protocols. Recently, the use of microbes has emerged as a novel method for the synthesis of nanoparticles.[5] Klaus and co-workers isolated a metal-resistant bacterium, *Pseudomonas stutzeri* AG259 from silver mine, and treated it with high concentrations of silver ions resulting in the intracellular formation of silver nanoparticles with polydispersed morphology.[6] Recently, Nair and Pradeep have demonstrated that exposure of large concentration of metal ions to bacteria *Lactobacillus* isolated from buttermilk found to synthesize the nanoparticles of variable morphology intracellularly.[7] Thus, the use of prokaryotes such as bacteria resulted in the intracellular synthesis of nanoparticles with polydispersed morphology. However, such biotransformation-based nanoparticle synthesis strategies would have greater application if the nanoparticles with controlled dispersity could be synthesized extracellularly as the harnessing of the nanoparticles from the cell is not easy.

It has been demonstrated in chapter 2 that the use of eukaryotic microorganism such as fungi, *Fusarium oxysporum* resulted in the synthesis of gold[8] and silver[9] but with polydispersity. Towards the objective to synthesize the nanoparticles with controlled

dispersity, a number of species of actinomycetes have been screened. It was observed that the alkalothermophilic (extremophilic) actinomycete, *Thermomonospora* sp., and alkalotolerant actinomycete, *Rhodococcus* sp., are quite promising as an exciting candidate for the synthesis of metal nanoparticles. We observed that the exposure of metal ions to *Thermomonospora* sp. resulted in the extracellular synthesis of nanoparticles with fairly monodispersity while the use of *Rhodococcus* sp. resulted in the formation of high concentration of nanoparticles with good monodispersity within the actinomycete cells.[10] Although the intracellular synthesis of metal and semiconductor nanoparticles has until now been reported only from bacteria and fungi, the use of actinomycetes in the intracellular synthesis of nanoparticles is yet to be investigated.[5, 8, 9]

3.2. EXPERIMENTAL

3.2.1. Extracellular Biosynthesis of Metal Nanoparticles using Actinomycete, *Thermomonospora* sp.

An alkalothermophilic (extremophilic) actinomycete, *Thermomonospora* sp., having optimum growth at pH 9 and 50 °C was isolated from self heating compost from the Barabanki district of Uttar Pradesh, India. The extremophiles are microorganisms which can grow under extreme conditions e.g. extremes of temperature, from –14 °C (psychrophiles) to 45 °C (thermophiles) to 110 °C (hyperthermophiles)]; extremes of pH [from 1 (acidophiles) to 9 (alkalophiles)]; very high barostatic pressure (barophiles); non-aqueous environment containing 100 % organic solvents; excess heavy metal concentration; etc. These microorganisms have developed numerous special adaptations to survive in such extreme habitats, which include new mechanisms of energy

transduction, regulating intracellular environment and metabolism, maintaining the structure and functioning of membrane and enzymes, etc.

The actinomycete, *Thermomonospora* sp., was maintained on MGYP (malt extract, glucose, yeast extract and peptone) agar slants and was maintained by subculturing at monthly intervals. The actinomycete was grown at pH 9 and 50 °C for four days and the slants were preserved at 15 °C. From an actively growing stock culture, subcultures were made on fresh slants and after four days of incubation at pH 9 and 50 °C and were used as the starting material for nanoparticles synthesis.

For the synthesis of nanoparticles, the actinomycete, *Thermomonospora* sp., was grown in 250 mL Erlenmeyer flasks containing 50 mL MGYP medium which is composed of malt extract (0.3 %), glucose (1.0 %), yeast extract (0.3 %) and peptone (0.5 %). Sterile 10 % sodium carbonate was used to adjust the pH of the medium to 9. The culture was grown with continuous shaking on a rotary shaker (200 rpm) at 50 °C for 96 h. The mycelia (cells) were then separated from the culture broth by centrifugation (5000 rpm) at 20 °C for 20 minutes and were washed thrice with sterile distilled water under sterile conditions. Some of the harvested mycelial mass (10 g) was then used for the synthesis of metal nanoparticles.

3.2.2. Intracellular Biosynthesis of Gold Nanoparticles using Actinomycete, *Rhodoccocus* sp.

An alkalotolerant actinomycete, *Rhodococcus* sp., having optimum growth at pH 7 at 27 °C was isolated from fig trees (*Ficus carica* family Moraceae) from the Pune district of Maharashtra, India. The alkalotolerant organisms are those, which can grow over a broad pH range (pH 5–10), the optimum being more towards the alkaline pH. The alkalotoretant actinomycete was maintained on potato-dextrose-agar (PDA) slants. Stock

cultures were maintained by subculturing at monthly intervals. After growing at pH 7 and 27 °C for four days the slants were preserved at 15 °C. From an actively growing stock culture, subcultures were made on fresh slants and, after 4 days incubation at pH 7 and 27 °C, were used as the starting material for fermentation experiments.

For the synthesis of metal nanoparticles, the actinomycete mycelia were grown in 500 mL Erlenmeyer flasks containing 100 mL MGYP medium which is composed of malt extract (0.3 %), glucose (1.0 %), yeast extract (0.3 %) and peptone (0.5 %). The culture was grown with continuous shaking on a rotary shaker (200 rpm) at 27 °C for 96 h. The mycelia (cells) were separated from the culture broth by centrifugation (5000 rpm) at 10 °C for 20 min and washed thrice with sterile distilled water under sterile conditions. Some of the harvested mycelial mass (10 g) was then used for the synthesis of metal nanoparticles.

3.2.3. Biosynthesis of Gold Nanoparticles

For the extracellular synthesis of gold nanoparticles, 10 g wet biomass of *Thermomonospora* sp. was exposed to 50 mL aqueous solution of 1 mM chloroauric acid ($HAuCl_4$) in 250 mL of Erlenmeyer flask at pH 9. The pH of the solution was adjusted using 10 % Na_2CO_3 solution. The whole mixture was put into a shaker at 50 °C (200 rpm) for 5 days and maintained in the dark.

For the intracellular synthesis of gold nanoparticles, 10 g wet biomass of *Rhodococcus* sp. was incubated with 1 mM aqueous solution of $HAuCl_4$ in 500 mL of Erlenmeyer flask at pH 7 and the whole mixture was put onto a shaker at 25–28 °C (200 rpm) for 48 h.

3.2.4. Biosynthesis of Silver Nanoparticles

In a typical synthesis of silver nanoparticle extracellularly, 50 mL aqueous solution of 1 mM silver nitrate ($AgNO_3$) was treated with 10 g wet biomass of *Thermomonospora* sp. in 250 mL of Erlenmeyer flask at pH 9. The pH was adjusted using 10 % Na_2CO_3 solution. The whole mixture was put into a shaker at 50 °C (200 rpm) and maintained in the dark.

3.2.5. Instruments for Characterization

The bioreduction of the Au^{3+} / Ag^{+} ions in solution was monitored by periodic sampling of aliquots (2 mL) of the aqueous component and by measuring the UV-Vis spectra of the solution. For the intracellular synthesis of gold nanoparticles, after the reaction periods, the biomass was washed thrice with copious amounts of sterile distilled water and films of the actinomycete cells (both before and after exposure to $AuCl_4^-$ ions for 24 h) for UV–Vis spectroscopy and X-ray diffraction (XRD) studies were prepared by solution-casting the washed fungal cells onto a Si(111) wafers and thoroughly drying the film in flowing N_2. UV–Vis spectroscopy measurements of the films were made on a Shimadzu dual-beam spectrophotometer (model UV-1601PC) operating in the reflection mode at a resolution of 1 nm. It is pertinent to mention here that, since the films of the Au-*Rhodococcus* cells were rough, the results are not quantitative and have been merely used to detect the presence of gold nanoparticles in the biomaterial. UV-Vis spectra of the aqueous $HAuCl_4$ solution after reaction with the actinomycete cells for 24 h were recorded in the transmission mode on the same instrument.

X-ray diffraction (XRD) measurements of the bioreduced chloroauric acid / silver nitrate solution drop-coated on glass substrate as well as the Au nano actinomycete

biofilm on Si(111) substrate were carried out on a Philips PW 1830 instrument operating at 40 kV voltage and a current of 30 mA with Cu K_α radiation.

For Fourier transform infrared (FTIR) spectroscopy measurement, the gold / silver nanoparticle solution was drop-coated on Si(111) wafer and was carried out on a Perkin-Elmer instrument in the diffuse reflectance mode at a resolution of 4 cm^{-1}.

The transmission electron microscopy (TEM) analysis of extracellularly synthesized gold / silver nanoparticles were prepared by drop-coating biosynthesized gold / silver nanoparticles solution on carbon-coated copper TEM grids (40 µm × 40 µm mesh size). TEM measurements were performed on a JEOL model 1200EX instrument operated at an accelerating voltage at 120 kV. For the intracellularly synthesized gold nanoparticles, transmission electron microscopy (TEM) studies of thin sections of the Au nano-actinomycete cells were carried out on the same instrument to examine the exact location of the reduction of gold nanoparticles by the enzymes. Thin sections of the *Rhodococcus* cells, after reaction with $AuCl_4^-$ ions were prepared for TEM analysis as follows:

Approximately 1 mm^3 aliquots of the Au nano-*Rhodococcus* biomass were taken and fixed in 2.5 % gluteraldehyde in distilled water for 2 h at room temperature. After fixation, the cells were sedimented (1500 rpm, 10 min) and washed three times with distilled water. Without post fixation, the pellet was subjected to dehydration with 30, 50, 70 and 90 % ethanol for 15 min at each concentration followed by two changes in absolute ethanol. Since ethanol is poorly miscible with epoxy resins, propylene oxide was used as a linking agent. The dehydrated pellet was kept in propylene oxide for 15 min following which the infiltration of the resin was carried out by placing the pellet in a 1:1 mixture of propylene oxide and Epon 812 overnight at room temperature. Embedding

was carried out by using a mixture of the resin (Epon 812) and hardeners (DDSA: dodecynyl succinic anhydride and MNA: methyl nadic anhydride) in the ratio 1:1.5. To this, two drops of tridimethylaminomethyl phenol (DMP30) was added to accelerate the polymerization process. Polymerization was carried out using this mixture at 60 °C for 3 days. Ultrathin sections were cut using an ultramicrotome (Leica Ultracut UCT) and were taken on copper TEM grids (40 mm × 40 mm mesh size). The sections were slightly stained with uranyl acetate and lead citrate prior to TEM analysis.

To identify the number of proteins secreted by the actinomycete, *Thermomonospora* sp. and their molecular weights in the extracellular synthesis of gold and silver nanoparticles, the actinomycete biomass [10.0 g of wet mycelia (cells)] was resuspended in 100 mL of sterile distilled water at pH 9 and the whole mixture was put into a shaker at 50 °C for a period of 4 days. The mycelia were then removed by centrifugation, and the aqueous supernatant thus obtained was concentrated by ultrafiltration using an YM3 (molecular weight cutoff 3K) membrane and then dialyzed thoroughly against distilled water using a 3K cutoff dialysis bag. This concentrated aqueous extract containing protein was analyzed by PAGE (polyacrylamide gel electrophoresis) and carried out at pH 8.3 according to the procedure published by Laemmli.[11]

3.3. CHARACTERIZATION

3.3.1. Extracellular Biosynthesis of Gold and Silver Nanoparticles using Actinomycete, *Thermomonospora* sp.

3.3.1.1. Visual Inspection and UV-Vis Spectroscopy

The picture of test tubes of chloroauric acid and silver nitrate solution after exposure to actinomycete, *Thermomonospora* sp. are shown in the inset of Figure 3.1A and 3.1B respectively. The appearance of the ruby red and brown color clearly indicates the formation of gold and silver nanoparticles respectively in the reaction mixture. The characteristics ruby red and brown color of colloidal gold and silver solution respectively is due to the excitation of surface plasmon vibrations in the nanoparticle and provides a convenient spectroscopic signature of their formation.[12]

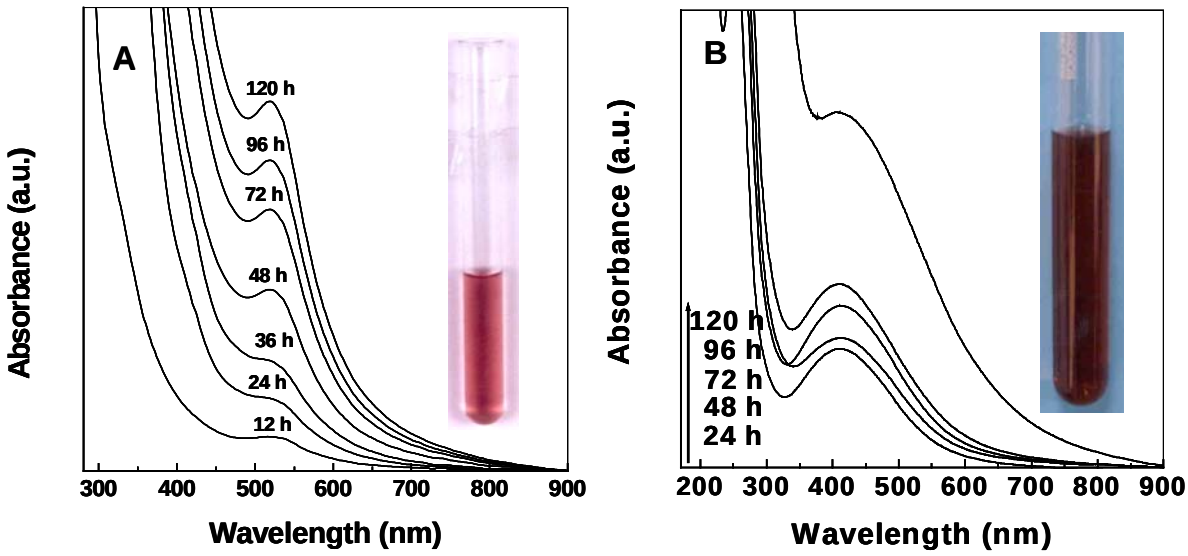

Figure 3.1. UV-Vis spectra recorded as a function of time of reaction of 1 mM aqueous solution of (A) $HAuCl_4$ and (B) $AgNO_3$ with *Thermomonospora* sp. biomass. The inset of respective Figures show a test tube of the gold (A) and silver (B) nanoparticle solution formed at the end of the reaction.

The UV-Vis spectra recorded from the aqueous chloroauric acid- and silver nitrate-actinomycete reaction medium as a function of time of reaction are shown in Figure 3.1 (A and B). It can be observed that the gold surface plasmon band occurs at *ca.* 520 nm while that of silver occurs at 410 nm respectively and steadily increases in intensity as a function of time of reaction. The surface plasmon band in the gold and silver nanoparticles solution remains close to 520 and 410 nm respectively throughout the reaction period, suggesting that the particles are dispersed in the aqueous solution with no evidence for aggregation. After completion of the reaction, the gold and silver nanoparticles solution was separated from the actinomycete biomass and tested for stability. It was observed that the nanoparticle solution of gold and silver was extremely stable for more than six months with no signs of aggregation even at the end of this period. The particles are thus stabilized in solution by the capping agent that is likely to be proteins secreted by the biomass.

3.3.1.2. X-ray Diffraction

Figure 3.2 (A and B) show the X-ray diffraction pattern recorded from gold and silver nanoparticles film deposited on a Si(111) substrate respectively. Prominent Bragg reflections corresponding to fcc gold and silver nanoparticles have been identified in the Figure.[13] An estimate of the mean size of the gold and silver nanoparticles formed in the cells were made by using the Debye–Scherrer equation by determining the width of the (111) Bragg reflection.[14] The size of the gold and silver nanoparticles was calculated to be about 9 and 18 nm respectively.

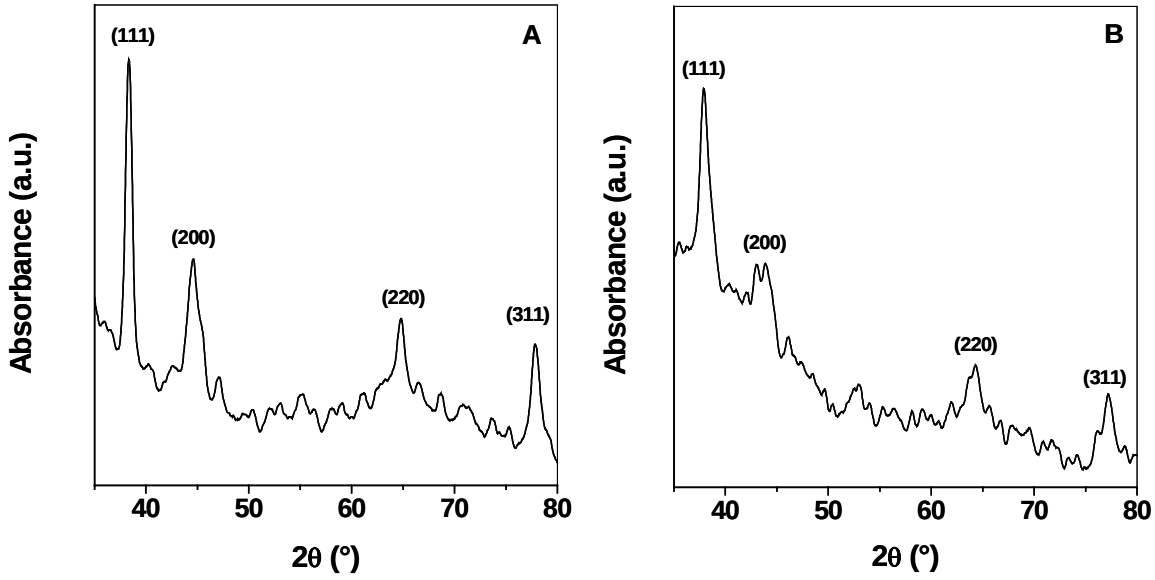

Figure 3.2. X-ray diffraction patterns recorded from (A) gold and (B) silver nanoparticles films deposited on a Si(111) wafer.

3.3.1.3. Transmission Electron Microscopy

Figure 3.3 (A and B) show TEM pictures recorded from drop-coated films of the gold nanoparticles. The low magnification TEM image clearly shows dense assembly of uniformly sized gold nanoparticles (Fig. 3.3A). The whole surface of the grid was evenly covered with gold nanoparticles as shown in this image. At higher magnification, the morphology and size of the particles can be clearly visualized (Fig. 3.3B). The particles are essentially spherical and appear to be reasonably monodispersed. The particle size histogram derived from the particles shown in this image and other similar images is shown in Fig. 3.3C. It can be seen that the mean particle size is *ca*. 8.5 nm with some particles of 9–10 nm size and a very small percentage having diameters 7 and 12 nm. Figure 3.3D shows the selected area electron diffraction (SAED) pattern obtained from the gold nanoparticles shown in Fig. 3.3B. The Scherrer ring pattern characteristic of

face centered cubic (fcc) gold is clearly observed showing that the structures seen in the TEM images are nanocrystalline in nature.

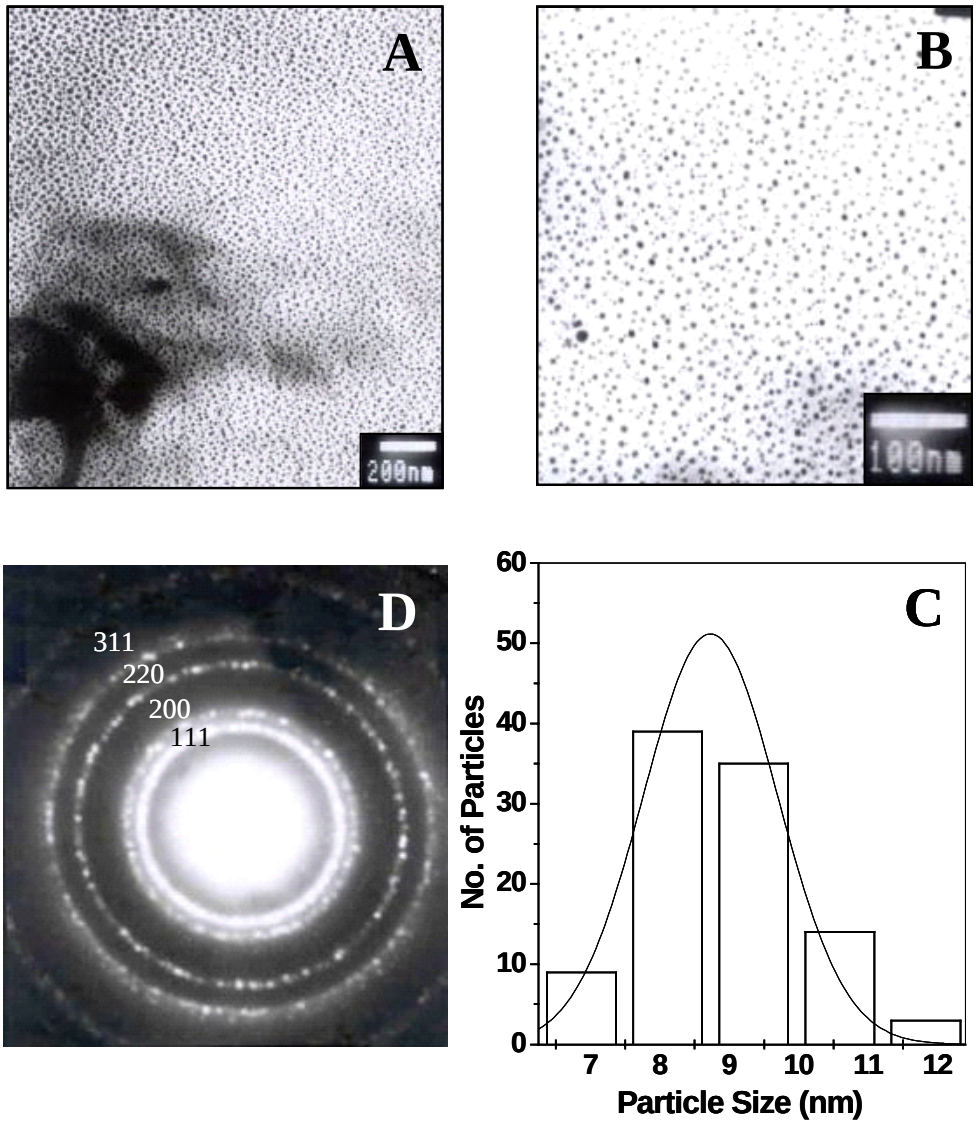

Figure 3.3. (A and B) TEM micrographs recorded from drop-cast films of the gold nanoparticle solution formed by the reaction of chloroauric acid solution with *Thermomonospora* sp. biomass for 120 h at different magnifications. (C) Particle size distribution histogram determined from the TEM micrograph shown in Fig B. (D) Selected area diffraction pattern recorded from the gold nanoparticles shown in Fig. B.

A representative TEM picture recorded from the silver nanoparticles film deposited on a carbon-coated copper TEM grid is shown in Figure 3.4. It can be seen

from TEM micrograph that the distribution of silver nanoparticles are polydispersed. The morphology of the particles is highly variable. Careful inspection of the image shows that the silver nanoparticles with different variable morphology as well as smaller, polydispersed spherical particles. Optical microscopy analysis of many such TEM images gave an average size of dimensions of 8–30 nm.

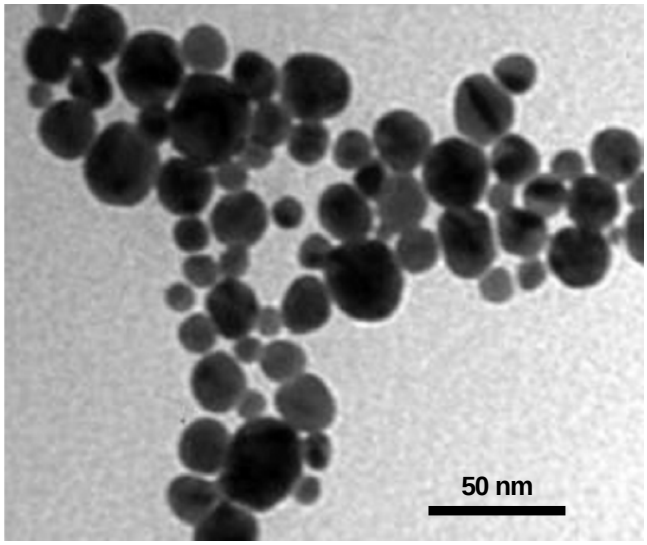

Figure 3.4. TEM micrograph recorded from drop-cast film of silver nanoparticle solution formed by the reaction of silver nitrate solution with *Thermomonospora* sp. biomass.

3.3.1.4. Probable Mechanism of Formation of Metal Nanoparticles Using Thermomonospora sp.

The presence of amide linkages between amino acid residues in polypeptides provides a well known signature in the infrared region of the electromagnetic spectrum. The positions of –N-H and –CO stretching vibrations in the FTIR spectra of proteins are a sensitive indicator to conformational changes in the secondary structure of proteins.[15] The Fourier Transform Infrared (FTIR) spectra recorded from the chloroauric acid (a) and silver nitrate (b) solution after reaction with *Thermomonospora* sp. for 120 h and are shown in Figure 3.5. The spectra show the presence of three bands at 1650, 1540 and

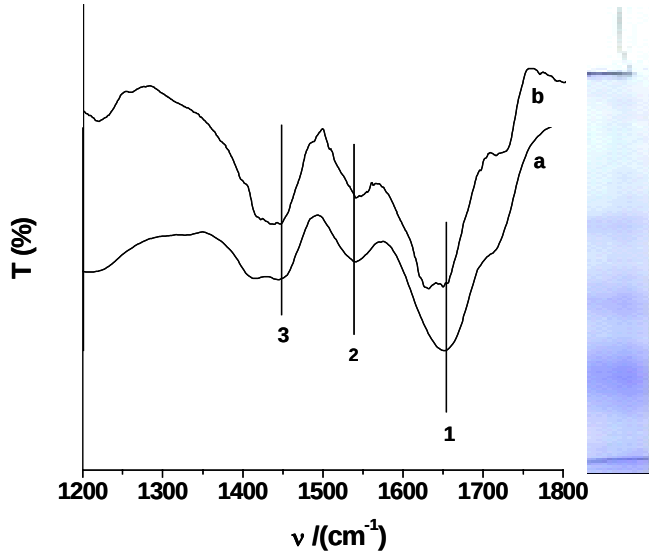

Figure 3.5. FTIR spectrum recorded from drop-cast films of (a) $HAuCl_4$ and (b) $AgNO_3$ solution after reaction with *Thermomonospora* sp. for 120 h. The amide I and II bands are identified in the Figure. The inset shows the native gel electrophoresis of aqueous protein extract obtained from *Thermomonospora* sp. mycelia (cells); 7.5 % (w/v) polyacrylamide slab gel, at pH 8.3.

1450 cm^{-1} for both gold and silver nanoparticle solution. The 1650 and 1540 cm^{-1} bands may be assigned to the amide I and II bands (labeled as 1 and 2 in Fig. 3.5) and are due to –CO stretch and –N-H stretch vibrations in the amide linkages of proteins respectively.[16] It is well known that proteins can bind to gold and silver nanoparticles either through free amine groups or cysteine residues in the proteins,[17] therefore, stabilization of the nanoparticles by proteins is a possibility.

To understand the exact mechanism of reduction of metal ions by actinomycete, the release of protein into reaction mixture by *Thermomonospora* sp. in terms of the number of different proteins secreted and their molecular weights have been analyzed. Preliminary gel electrophoresis measurement (inset in Fig. 3.5) indicates that the actinomycete secretes atleast four different proteins of molecular masses between 80 kDa

and 10 kDa. One or more of these proteins may be enzymes that reduce chloroaurate ions and silver ions and cap the gold and silver nanoparticles formed by the reduction process.

The actinomycete is found to synthesize the metal nanoparticle with different particle size distribution, e.g. the gold nanoparticle synthesized by *Thermomonospora* sp. is fairly monodispersed while silver nanoparticles are polydispersed. These phenomena may be a pointer towards the specific interaction between gold nanoparticles and one of the capping proteins and non specific interaction of silver nanoparticles with different capping proteins giving fairly monodispersed gold nanoparticles and silver with polydispersity. This can be indicative of subtle difference in activity of gold and silver nanoparticles. In other words, the nature and strength of interaction of different proteins with different crystallographic faces of metal nanocrystals may vary and this may lead to complex morphologies and size control. Recently, Heuer et al. reported that the complex morphology of calcium carbonate crystals in red abalone shells is modulated by insoluble proteins present in the organism,[18] and a similar mechanism may be operative in this study.

3.3.2. Intracellular Biosynthesis of Gold Nanoparticles using Actinomycete, *Rhodococcus* sp.

3.3.2.1. Visual Inspection

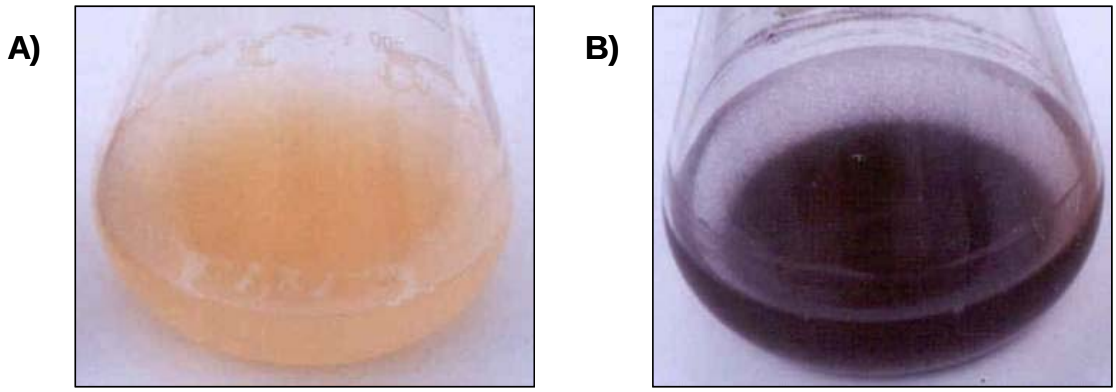

Figure 3.6. (A) *Rhodococcus* sp. biomass after removal from the culture medium. (B) *Rhodococcus* sp. actinomycete cells after exposure to 1 mM aqueous solution $HAuCl_4$ for 24 h.

Figure 3.6 shows a conical flask of the actinomycete cells after removal from the culture medium and before immersion in $HAuCl_4$ solution (A). The saffron color of the actinomycete cells can clearly be seen in the Figure 3.6A. A picture of the conical flask containing the actinomycete cells after exposure to 1 mM aqueous solution of $HAuCl_4$ for 24 h is shown in Figure 3.6B. A vivid purple color of the actinomycete cells can clearly be observed, which indicates the formation of Au nanoparticles by the cells. It is also clear that the aqueous $HAuCl_4$ medium is colorless, thereby strongly indicating that the extracellular reduction of the $AuCl_4^-$ ions has not occurred.

3.3.2.2. UV-Vis Spectroscopy

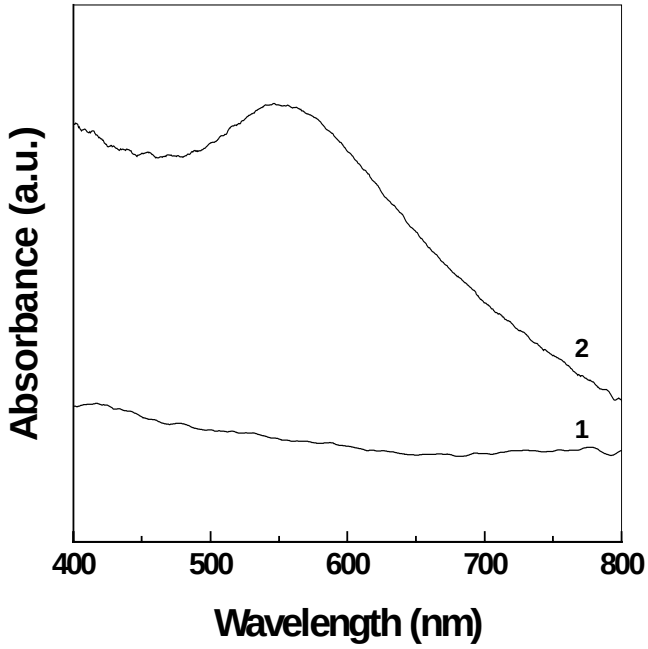

Figure 3.7. UV–Vis spectra recorded from biofilms of the *Rhodococcus* sp. biomass before (curve 1) and after exposure to 1 mM aqueous $HAuCl_4$ solution for 24 h (curve 2).

Figure 3.7 shows the UV–Vis spectra recorded from a film of the actinomycete cells before (curve 1) and after immersion in 1 mM $HAuCl_4$ solution for 24 h (curve 2). The gold nanoparticles absorb radiation in the visible region of the electromagnetic spectrum due to the excitation of surface plasmon vibrations giving gold nanoparticles striking colors in various media. The UV–Vis spectra (Figure 3.7) show no evidence of absorption in the spectral window 400–800 nm for the as-harvested actinomycete cells (curve 1), whereas the actinomycete cells exposed to $AuCl_4^-$ ions show distinct absorption at around 540 nm (curve 2). The presence of the broad resonance indicates an aggregated structure of the gold particles in the film. As mentioned earlier, scattering from the rough biomass surface would also contribute to the broadening of the

resonance. This absorption is close to that observed for thin films of gold nanoparticles grown by different techniques.[19]

3.3.2.3. X-ray Diffraction

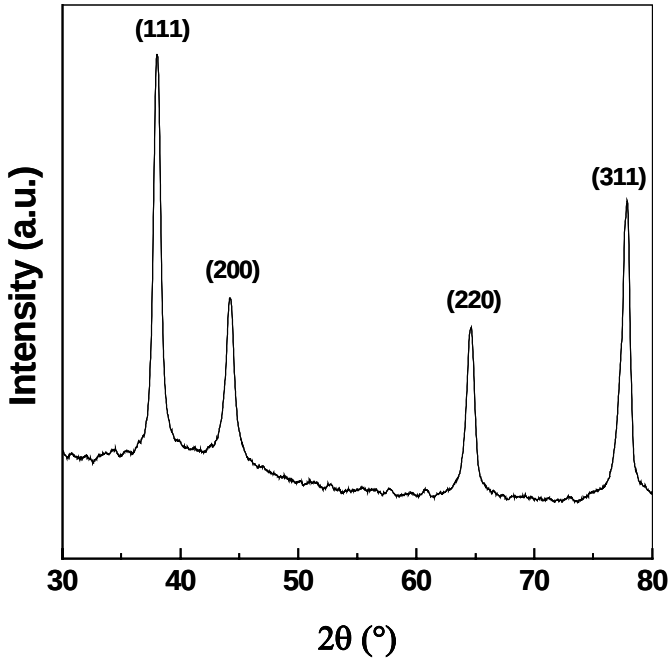

Figure 3.8. XRD pattern recorded from an Au nano-*Rhodococcus* biofilm deposited on a Si(111) wafer. The principal Bragg reflections are identified.

Further evidence for the intracellular formation of gold nanoparticles is provided by XRD analysis of the Au nano-actinomycete biofilm deposited on a Si(111) substrate (Figure 3.8). The prominent peaks corresponding to (111), (200), (220) and (311) Bragg reflections are characteristic of fcc gold and agrees with those reported for gold nanocrystals. An estimate of the mean size of the gold nanoparticles formed in the cells was made by using the Debye–Scherrer equation by determining the width of the (111) Bragg reflection. The average size of the gold nanoparticles thus calculated was found to be about 12 nm.

3.3.2.4. Transmission Electron Microscopy

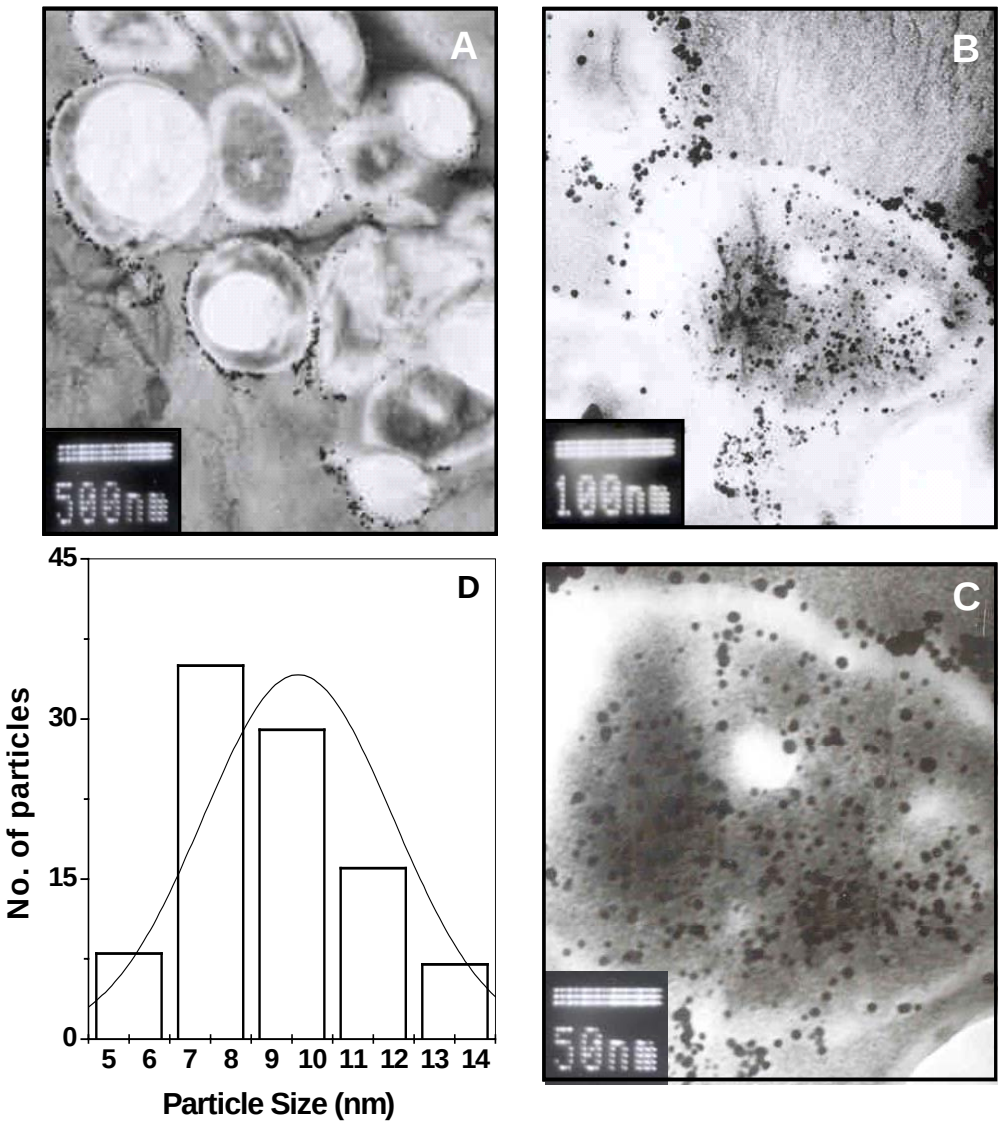

Figure 3.9. (A-C) Representative TEM micrographs recorded at different magnifications from thin sections of stained *Rhodococcus* cells after reaction with $AuCl_4^-$ ions for 24 h. (D) A particle size distribution histogram determined from the TEM image shown in Figure 3.9C.

Figure 3.9 (A-C) shows representative TEM pictures of the thin sections of the Au nano-actinomycete cells synthesized by using actinomycete after reacting with chloroauric acid for 24 h. At lower magnification, the image shows small particles of

gold organized on the walls of the actinomycete cells (Figure 3.9A). At slightly higher magnification, one TEM image shows the junction between two cells wherein the individual cells are more clearly resolved (Figure 3.9B). The gold nanoparticles can clearly be seen on the cell wall as well as on the cytoplasmic membrane. Furthermore, the concentration of gold nanoparticles is much higher on the cytoplasmic membrane than on the cell wall. At a still higher magnification, a better idea of the morphology and the size of the particles may be obtained (Figure 3.9C). The highly concentrated particles are essentially spherical with occasional evidence of aggregation. The size distribution of particles is represented in a histogram after considering > 100 gold nanoparticles shown in the many TEM images and is shown in Figure 3.9D. It can be seen that the average particle size is ~ 9 nm with some particles of 10–12 nm size and a very small percentage having diameters 5, 14 and 16 nm.

3.4. SUMMARY

In this chapter, extra- and intracellular biosynthesis of metal nanoparticles with controlled monodispersity using actinomycetes, *Thermomonospora* sp. and *Rhodococcus* sp. have been demonstrated. It has been observed that on exposure of $AuCl_4^-$ ions to alkalothermophilic (extremophilic) actinomycete, *Thermomonospora* sp. results in the synthesis of gold nanoparticles in solution (extracellularly). However, the use of alkalotolerant actinomycete, *Rhodococcus* sp. results in the formation of gold nanoparticles within the *Rhodococcus* cells. It has been demonstrated earlier in chapter 2, that the fungi, *Fusarium oxysporum*, when exposed to aqueous solution of chloroauric acid, resulted in the extracellular formation of gold nanoparticles with variable morphology. The reduction was faster with *Fusarium oxysporum* than *Thermomonospora* sp. (48 h vs 120 h). However, the gold nanoparticles synthesized using the fungi were polydisperse and ranged in size from 8–40 nm. If biosynthesis of metal nanoparticles using microorganisms is to be a viable alternative to chemical methods currently, then greater control over particle size and polydispersity would need to be established. This was one of the goals in screening different species of fungi and now, actinomycetes. Thus, a significant improvement in the monodispersity has been achieved using actinomycetes. The size and dispersity control may be the consequence of larger amounts of proteins/enzymes secreted by actinomycetes in comparison with fungi. It is also to be noted that the synthesis conditions are completely different. In the case of actinomycetes, *Thermomonospora* sp., the reaction is carried out under alkaline conditions and at slightly elevated temperatures. Under these extreme conditions, fungi such as *Fusarium oxysporum* would not survive. The use of extreme biological conditions in the synthesis could also be contributory factors in the size and

monodispersity control observed using actinomycetes. It has also been observed that the same actinomycete, *Thermomonospora* sp. cannot synthesize different metal nanoparticles with similar monodispersity. This may be due to the difference in mode of interactions between different metal nanoparticles and the capping proteins.

3.5. REFERENCES

1. G. Cao, *Nanostructures & Nanomaterials:Synthesis, Properties & Applications*, Imperial College Press, London, 2004.
2. (a) A. Taleb, C. Petit, M. P. Pileni, *Chem. Mater.* **1997**, *9*, 950. (b) L. Motte, F. Billoudet, E. Lacaze, J. Douin, M. P. Pileni, *J. Phys.Chem. B* **1997**, *101*, 138.
3. J. H. Fendler, F. C. Meldrum, *Ad*v. *Mater.* **1995**, *7*, 607.
4. C. B. Murray, D. J. Norris, M. G. Bawendi, *J. Am. Chem. Soc.* **1993**, *115*, 8706.
5. (a) Mann, S. (ed.) *Biomimetic Materials Chemistry*, VCH Publishers, 1996. (b) D. R. Lovley, J. F. Stolz, G. L Nord, E. J. P. Phillips, *Nature* **1987**, *330*, 252. (c) S. Oliver, A. Kupermann, N. Coombs, A. Lough, G. A. Ozin, *Nature* **1995**, *378*, 47. (d) D. Pum, U. B. Sleytr, *Trends Biotechnol.* **1999**, *17*, 8. (e) J. R. Stephen, S. J. Maenaughton, *Curr. Opin. Biotechnol.* **1999**, *10*, 230. (f) R. K. Mehra, D. R. Winge, *J. Cell. Biochem.* **1991**, *45*, 30. (g) T. J. Beveridge, R. G. E. Murray, *J. Bacteriol.* **1980**, *141*, 876.
6. (a) T. Klaus, R. Joerger, E. Olsson, C. G. Granqvist, *Proc. Natl. Acad. Sci. USA* **1999**, *96*, 13611. (b) T. Klaus-Joerger, R. Joerger, E. lsson, C. G. Granqvist, *Trends Biotechnol.* **2001**, *19*, 15. (c) R. Joerger, T. Klaus, C. G. Granqvist, *Adv. Mater.* **2000**, *12*, 407.
7. B. Nair, T. Pradeep, *Crys. Growth Des*. **2002**, *2*, 293.
8. P. Mukherjee, S. Senapati, D. Mandal, A. Ahmad, M. I. Khan, R. Kumar, M. Sastry, *ChemBioChem* **2002**, *3*, 461.
9. A. Ahmad, P. Mukherjee, S. Senapati, D. Mandal, M. I. Khan, R. Kumar, M. Sastry, *Colloids Surf.* B **2003**, *28*, 313.
10. (a) A. Ahmad, S. Senapati, M. I. Khan, R. Kumar, R. Ramani, V. Srinivas, M. Sastry, *Nanotechnology* **2003**, *14*, 824. (b) A. Ahmad, S. Senapati, M. I. Khan, R. Kumar, M. Sastry, *Langmuir* **2003**, *19*, 3550.
11. U. K. Laemmli, *Nature* **1970**, *227*, 680.
12. (a) P. Mulvaney, *Langmuir* **1996**, *12*, 788. (b) S. Underwood, P. Mulvaney, *Langmuir* **1994**, *10*, 3427. (c) M. D. Musick, C. D. Keating, L. A. Lyon, S. L. Botsko, D. J. Pena, W. D. Holliway, T. M. MeEvoy, J. N. Richardson, M. J. Natan, *Chem. Mater.* **2000**, *12*, 2869.
13. D. V. Leff, L. Brandt, J. R. Heath, *Langmuir* **1996**, 12, 4723.

14. J. W. Jeffrey, *Methods in Crystallography*, Academic Press, New York, 1971.

15. F. Caruso, D. N. Furlong, K. Ariga, I. Ichinose, T. Kunitake, *Langmuir* **1998**, *14*, 4559.

16. (a) I. D. G. Macdonald, W. E. Smith, *Langmuir* **1996**, *12*, 706. (b) C. D. Keating, K. K. Kovaleski, M. J. Natan, *J. Phys. Chem. B* **1998**, *102*, 9414. (c) C. V. Kumar, G. L. McLendon, *Chem. Mater.* **1997**, *9*, 863. (d) A. Gole, C. Dash, S. R. Sainkar, A. B. Mandale, M. Rao, M. Sastry, *Anal. Chem.* **2000**, *72*, 1401.

17. A. Gole, C. Dash, V. Ramakrishnan, S. R. Sainkar, A. B. Mandale, M. Rao, M. Sastry, *Langmuir* **2001**, *17*, 1674.

18. X. Su, A. M. Belcher, C. M. Zaremba, D. E. Morse, G. D. Stucky, A. H. Heuer, *Chem. Mater.* **2002**, *14*, 3106.

19. (a) J. J. Storhoff, C. A. Mirkin, *Chem. Rev.* **1999**, *99*, 1849. (b) V. Patil, R. B. Malvankar, M. Sastry, *Langmuir* **1999**, *15*, 8197.

4.1. INTRODUCTION

Among the various nanoparticles, colloidal semiconductor nanoparticles have attracted significant attention of researchers due to their quantum confinement effects and size dependent photoemission characteristics.[1-3] The semiconductor nanoparticles have been applied to many different technological areas including light-emitting diodes, electroluminescent devices, photovoltaic devices, lasers, and single-electron transistors.[4] The ability to tune the optical properties of semiconductor nanoparticles during UV-light irradiation by simply changing the nanoparticle size is particularly attractive in diverse areas of application such as cell labeling,[5] cell tracking,[6] *in vivo* imaging,[7] diagnostics and DNA detection.[8]

Semiconductor nanoparticles having variable sizes and different shapes have been synthesized by various solution-phase synthetic processes.[9-12] CdSe nanoparticles have been the intensively studied; while relatively little work has been done on semiconductor sulfide nanoparticles. Steigerwald et al. demonstrated the synthesis of sulfide nanoparticles from the reaction of alkaline solution of metal salt with H_2S in the presence of a suitable stabilizing agent.[10] Recently, several groups reported the synthesis of sulfide nanoparticles from the thermolysis of single-source precursors.[11] Most of the colloidal solutions of nanoparticles prepared by these methods are less stable against agglomeration, environmental unfriendly, cumbersome and non-uniform in size distribution. Therefore, the researchers in the field of nanoparticles synthesis have been seeking inspiration from biological systems where biominerals are routinely synthesized.[13-17] Of late, bacteria and yeast have been used successfully in the synthesis of CdS and PbS nanoparticles.[18-20] Holmes and coworkers have demonstrated that on exposure of cd^{2+} ions to the bacterium, *Klebsiella aerogenes* results in the intracellular

formation of CdS nanoparticles in the size range 20–200 nm.[18] Dameron and coworkers reported that the yeasts such as *Schizosaccharomyces pombe* and *Candida glabrata* produced intracellular CdS nanoparticles when challenged with aqueous solution of cadmium salt.[19] Recently, Kowshik and coworkers have identified the yeast, *Turolopsis* sp. and found to synthesis intracellular PbS nanoparticles when exposed to aqueous lead salt solution.[20]

As mentioned in previous chapters 2 and 3, that the use of eukaryotic and prokaryotic microorganisms like fungi and actinomycetes respectively, in the synthesis of nanoparticles is a relatively new and exciting area of research with considerable potential for development. It was demonstrated that the reaction of metal ions with the fungus, *Verticillium* sp. resulted in the intracellular synthesis of metal nanoparticles such as gold[21] and silver.[22] For the extracellular synthesis of gold,[23] silver[24] and bimetallic gold silver alloy[25] nanoparticles, the fungus, *Fusarium oxysporum*, was identified (as described in chapter 2). These results encouraged us to try to use the fungus, *Fusarium oxysporum*, to synthesize quite important semiconductor metal nanoparticles extracellularly by a purely enzymatic process.[26] It is observed that *Fusarium oxysporum* secretes sulfate reductase enzymes when exposed to aqueous MSO_4 (where M = Cd, Pb, Mn and Zn) solution and results in the formation of extremely stable metal sulfide nanoparticles in solution.

4.2. EXPERIMENTAL

It may be recalled from chapter 2 that the fungus, *Fusarium oxysporum*, was obtained from National Collection of Industrial Microorganisms (NCIM), NCL, Pune and maintained on potato-dextrose agar slants at 25 °C. Stock cultures were maintained

by subculturing at monthly intervals. From an actively growing stock culture, subcultures were made on fresh slants at pH 7.0 and 25 °C and were used after 5-6 days as the starting material for fermentation experiments.

The fungus was grown in 500 mL Erlenmeyer flasks each containing MGYP media (100 mL), composed of malt extract (0.3 %), glucose (1.0 %), yeast extract (0.3 %), and peptone (0.5 %) at 25–28 °C under shaking at 200 rpm for 96 h. After 96 h of fermentation, mycelial mass were separated from the culture broth by centrifugation (5000 rpm) at 10 °C for 20 min and the settled mycelia were washed thrice with sterile distilled water. Some of the harvested mycelial mass (20 g) was then used for the synthesis of metal sulfide quantum dots.

4.2.1. Biosynthesis of Metal Sulfide Nanoparticles

For the syntheses of cadmium, lead, zinc, manganese and nickel sulfide nanoparticles, 20 g wet biomass of *Fusarium oxysporum* was incubated with an aqueous solution of 1 mM metal sulfate ($CdSO_4$, $PbSO_4$, $ZnSO_4$, $MnSO_4$ and $NiSO_4$) and the reaction mixture was then put onto a shaker at 28 °C (200 rpm) and kept for 15 days.

4.2.2. Instruments for Characterization

The optical properties of metal sulfide nanoparticles have been characterized by using UV-Vis and fluorescence spectroscopy. The measurements were performed on a Shimadzu dual-beam spectrophotometer (model UV-1601 PC) operated at a resolution of 1 nm and Perkin-Elmer LS 50B luminescence spectrophotometer, respectively.

The metal sulfide nanoparticles were characterized by using transmission electron microscopy (TEM), X-ray diffraction (XRD) measurements and the effect of the structure of enzymes/proteins due to interaction with metal sulfide nanoparticles was

studied by Fourier transform infrared spectroscopic (FTIR) measurements of the reaction mixtures. The films of nanoparticles were made on Si(111) substrates by drop-coating the metal nanoparticle solution to study FTIR and XRD. FTIR studies were performed on a Shimadzu FTIR-8201 PC instrument in the diffuse reflectance mode at a resolution of 4 cm^{-1}. XRD patterns were obtained in the transmission mode on a Philips PW 1830 instrument operating at 40 kV and a current of 30 mA with Cu K_α radiation (λ = 1.5404 Å). Transmission electron microscopy (TEM) images were scanned on a JEOL 1200EX instrument operated at an accelerated voltage of 120 kV.

To determine the number of proteins released by *Fusarium oxysporum* in the extracellular synthesis of metal sulfide nanoparticles, 20 g of biomass was immersed in 100 ml of distilled water for 12 days. The aqueous extract thus obtained after filtration was concentrated by ultrafiltration using an YM3 (molecular weight cut off 3K) membrane and then dialyzed against distilled water using a 3K cutoff dialysis bag. The concentrated aqueous extract containing protein was analyzed by polyacrylamide gel electrophoresis (PAGE) carried out at pH 4.3.

4.3. CHARACTERIZATION

4.3.1. Cadmium Sulfide Nanoparticles

The inset of Figure 4.1A shows test tubes of the $CdSO_4$ reaction solution at the beginning (left) and after 12 days of reaction (right) with the *Fusarium oxysporum* biomass. The bright yellow color of the solution after reaction indicates the presence of CdS nanoparticles in solution. The Figure 4.1A shows the UV-Vis spectra recorded from the *Fusarium oxysporum*–$CdSO_4$ solution reaction medium at different time intervals (in days). The spectra exhibit a well-defined absorption band at around 380 nm, which is

considerably blue shifted relative to the bulk band gap for CdS crystals (515 nm).[27] Thus, with the reduction in particle size, the band gap of the semiconductor becomes larger due to quantum size effect and there is concomitant blue shift in the absorption spectra.[27] The absorption maximum is progressively increases in intensity as the reaction progresses. It has been observed that the colloidal solution of CdS nanoparticles was extremely stable with no evidence of aggregation even after six months of storage. An absorption band at *ca*. 270 nm can be observed in the Figure 4.1A, which is due to electronic excitations in tryptophan and tyrosine residues of proteins[28] and suggests the release of proteins into the solution by *Fusarium oxysporum*. The long-term stability of the CdS nanoparticle solution is due to the presence of the proteins in the nanoparticle solution that bind to the surface of the nanoparticles and hence prevents aggregation.

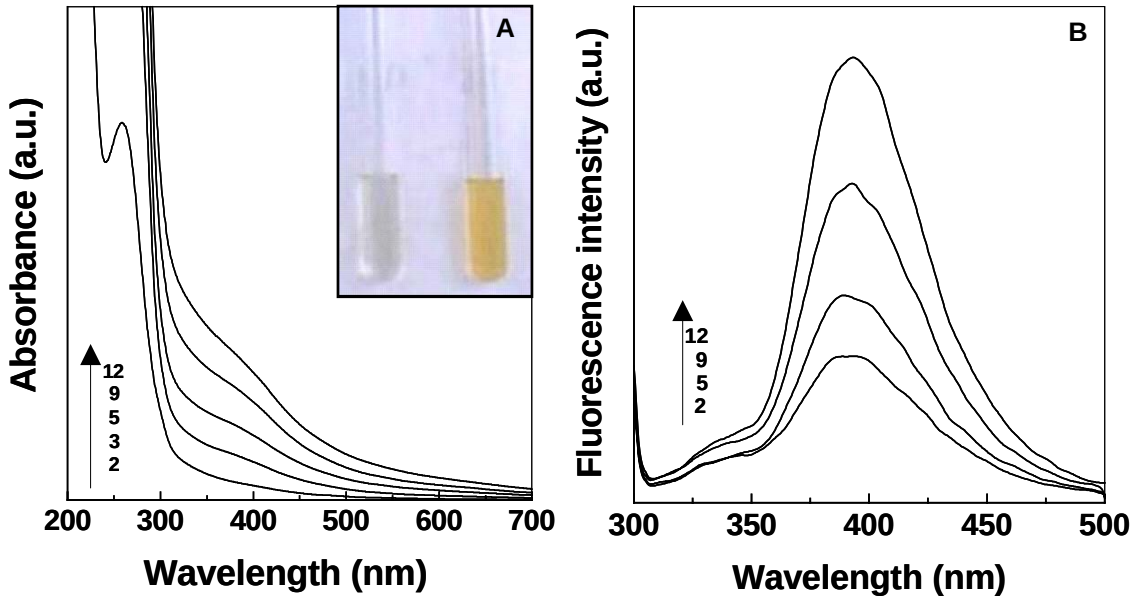

Figure 4.1. (A) UV-Vis spectra recorded from the aqueous 1 mM $CdSO_4$ solution as a function of time (in days) of addition of the fungal biomass. The inset shows test tubes containing $CdSO_4$ solution before (left) and after reaction with the fungal biomass for 12 days (right). (B) Fluorescence emission spectra recorded from the same solution used for UV-Vis measurements.

The luminescence characteristics shown by semiconductor particles have potential implications in the field of optoelectronic (light emitting) devices[29] and biosensors.[30] This property is dependent on the nature of the semiconductors, physical dimensions as well as the chemical environments of the particles.[27,29] This was studied by fluorescence measurement of the CdS nanoparticle after exciting the reaction mixture at 320 nm and is shown in Figure 4.1B. The emission band at 410 nm is considerably red shifted compared to its absorption onset and is attributed to the band gap or near band gap emission resulting from the recombination of the electron-hole pairs in the CdS nanoparticles.[31] The small stokes` shift of the band indicates that the nanocrystals possess a continuous surface with most surface atom exhibiting the coordination and oxidation states of their bulk counterparts.[32] The intensity of the peak gradually increases as the reaction progresses, but the emission spectra have the same general features. The absence of any red shifted emission band with respect to time in the fluorescence spectra indicates the synthesis of uniformly distributed cadmium sulfide nanoparticles.

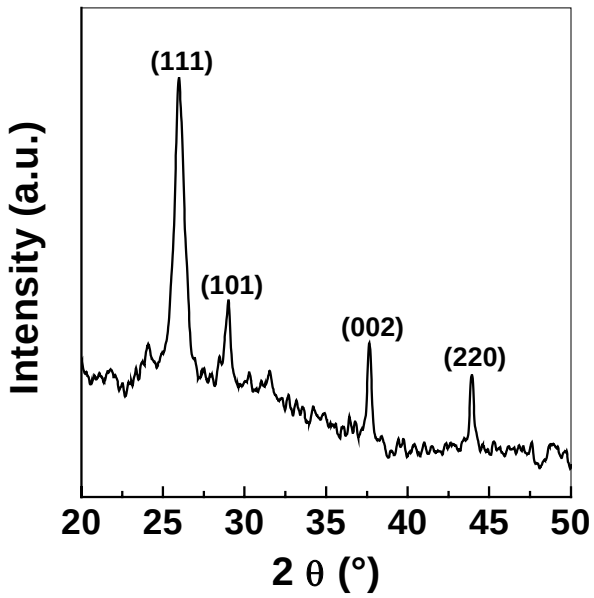

Figure 4.2. XRD pattern recorded from the CdS nanoparticle film deposited on a Si(111) wafer.

Another evidence for the formation of CdS nanoparticles in solution by *Fusarium oxysporum* is provided by X-ray diffraction (XRD) pattern recorded from a CdS nanoparticle film prepared by drop-coating the *Fusarium oxysporum*–$CdSO_4$ reaction mixture on Si(111) substrate and is shown in Figure 4.2. The Prominent Bragg reflections due to (111), (101), (002) and (220) reveals the hexagonal structure of CdS crystal.[33] The crystal size of CdS nanoparticles calculated, from the line broadening of (111) reflection using the Debye–Scherrer formula, was found to be ~10 nm.[34]

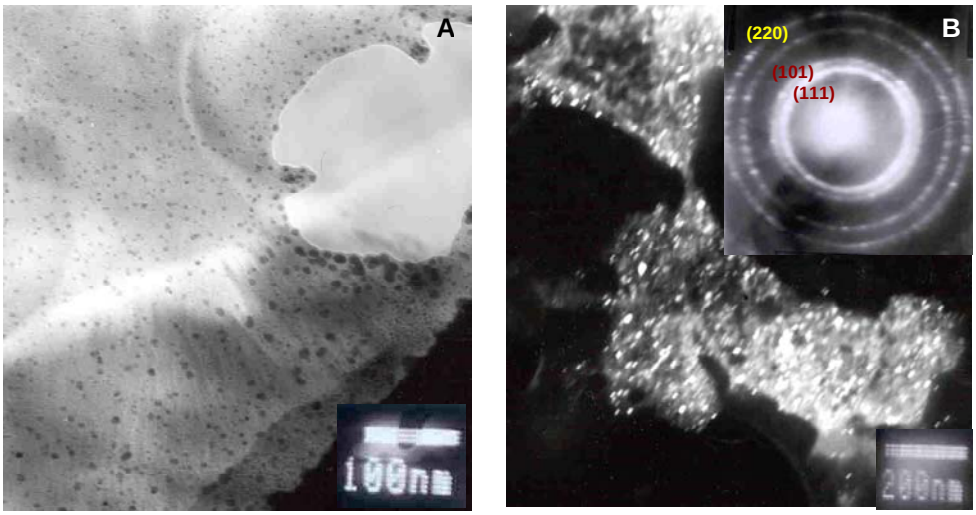

Figure 4.3. Bright field (A) and dark field (B) TEM pictures of CdS nanoparticles formed by reaction of $CdSO_4$ with the fungal biomass for 12 days. The inset of Figure (B) shows the selected area diffraction pattern recorded from one of the CdS nanoparticles shown in (A). The diffraction rings have been indexed with reference to hexagonal CdS.

A bright and dark field transmission electron microscopy (TEM) images obtained from a drop-coated film of the CdS nanoparticles solution and are shown in Figure 4.3. The assemblies of well-dispersed spherical particles are observed in the bright field image while individual shining particles in the dark field image (Fig. 4.3B). Under observation of these images in an optical microscope, the size of CdS nanoparticles

found to be in the range 5–15 nm. The hexagonal CdS particles are crystalline, as can be observed from the selected area diffraction pattern recorded from one of the nanoparticles in the TEM micrograph (inset of Fig. 4.3B).

Similarly, other metal sulfides (PbS, ZnS, MnS and NiS), prepared in the same way as CdS nanoparticles were synthesized, have been characterized and described below.

4.3.2. Lead Sulfide Nanoparticles

Like other semiconductors, lead sulfide is also quite interesting material. The bulk PbS exhibits a very small band gap of 0.41 eV at room temperature, with an absorption onset at 3020 nm and is very sensitive against the finite size effect of PbS crystals.[35] By changing the size and shape from bulk material to nanoparticles, it is possible to tune the band gap energy from ~0.41 eV to 5.2 eV [36] and could be used to build the optical sensors with adjustable properties. Lead sulfide can also be used in other applications such as in photography,[37] near-IR communication[38] and a solar absorber.[39] This interesting material has been synthesized using fungus, *Fusarium oxysporum*, with particle of nanosize range. The Figure 4.4A displays the UV-Vis spectrum of *Fusarium oxysporum*–$PbSO_4$ reaction mixture. The spectrum reveals a weak absorption edge at ~ 360 nm, corresponding to an energy band gap of ~3.43 eV. Thus, the absorption edge of PbS shows a large blue shift (~2660 nm) when the crystallite size is reduced to the nanometer size range. The origin of large blue-shift can be attributed to quantum confinement of charge carrier in the nanoparticles.

The surface quality of the PbS nanoparticles has been examined by fluorescence measurement. The Figure 4.4A shows the fluorescence spectrum of PbS nanoparticle recorded from *Fusarium oxysporum*–$PbSO_4$ reaction mixture. A relatively broad

emission band is observed at 425 nm and is ascribed to deep trap emission, which arises from the recombination of trapped electrons and holes with broad energy distributions.[32] The broadness of emission band indicates that the surface of PbS nanocrystals are irregular.[32]

Furthermore, the X-ray diffraction (XRD) pattern of PbS nanoparticles showed in Figure 4.4B reveals the characteristic of cubic rock salt structure of PbS nanoparticles. The crystal size of the nanoparticles calculated using Debye–Scherrer formula was about 14 nm.[34]

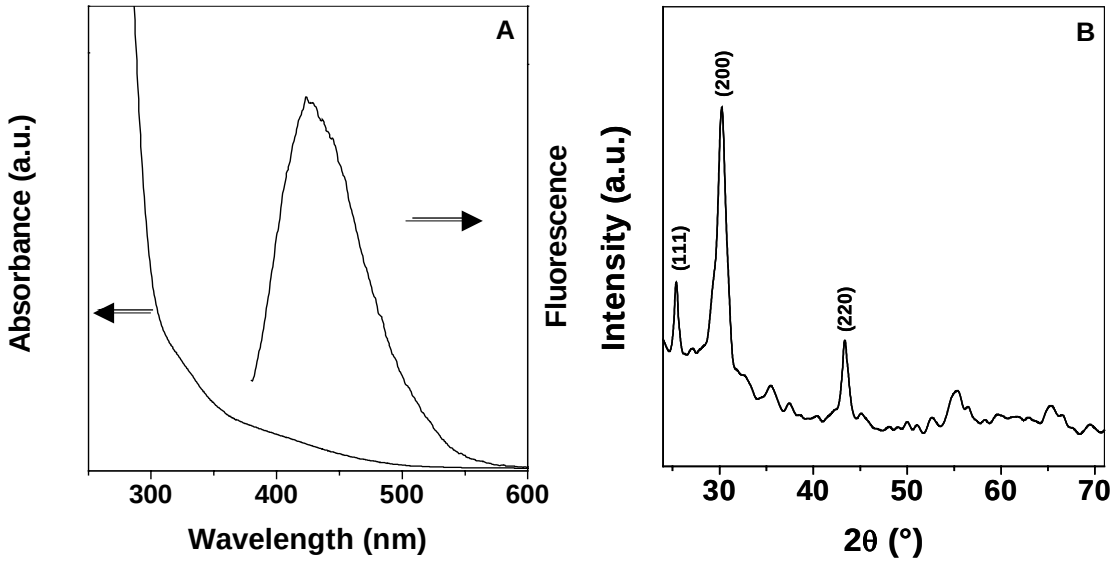

Figure 4.4. (A) UV-Vis spectrum (left) and fluorescence emission spectrum (right) recorded from the aqueous 1 mM $PbSO_4$ solution of addition of the fungal biomass. (B) XRD pattern recorded from the PbS nanoparticle film deposited on a Si(111) wafer.

The transmission electron microscopy (TEM) images of PbS nanoparticles are shown in Figure 4.5. The lower magnification TEM image shows a thallus like structure of PbS nanoparticles [Fig. 4.5 (A and B)]. On careful inspection of the micrographs at higher magnification reveal that these thalli like structures consist of star shaped fractal units [Fig. 4.5 (C and D)]. It can be suggested that the individual PbS nanoparticles

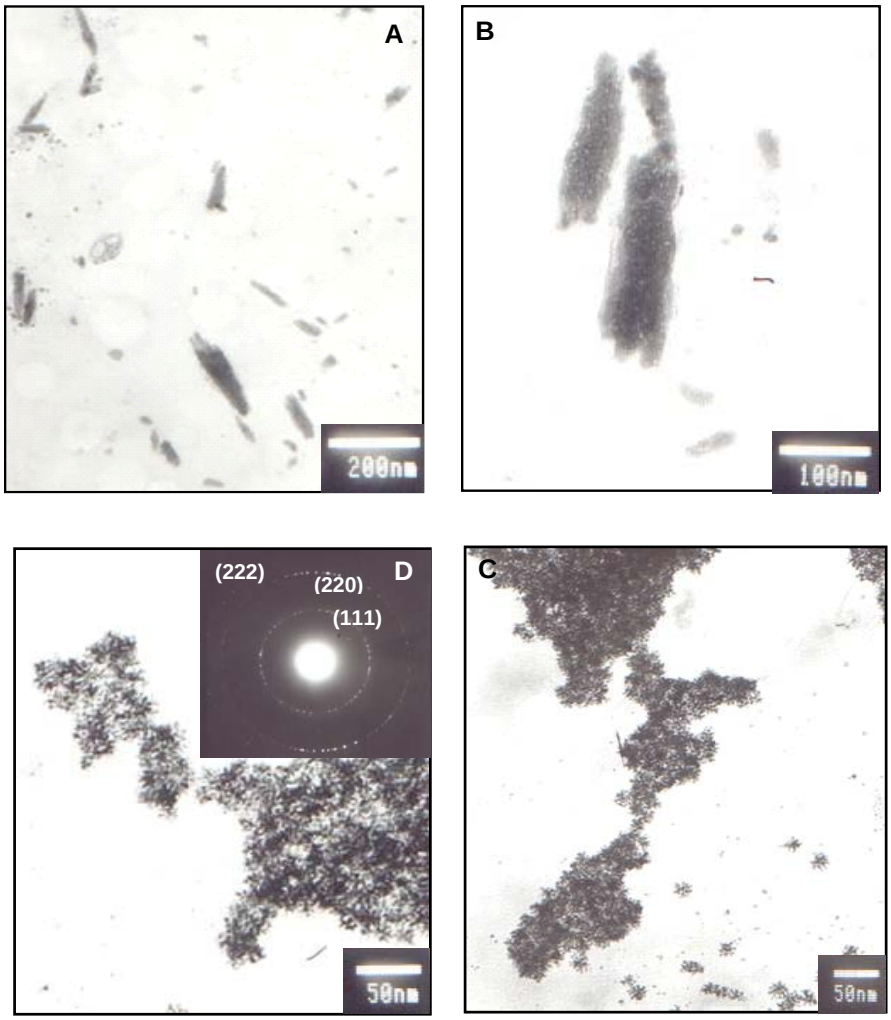

Figure 4.5. (A-D) TEM images of PbS nanoparticles at different magnifications recorded from *Fusarium oxysporum*–$PbSO_4$ reaction mixture. The inset of Figure (D) shows the selected area diffraction pattern of PbS nanoparticle. The diffraction rings have been indexed with reference to cubic PbS.

(primary unit) arranged themselves in star like fractals (secondary unit), which in turn form the thallus like body (tertiary structure) while maintaining the crystalinity of PbS nanoparticles as evident from the selected area electron diffraction pattern (inset of Fig. 4.5D). It is to emphasize that the transition of PbS nanoparticles from primary to secondary units and finally to tertiary structure do not lead to any aggregation. The

analysis of the number of areas of the TEM grid showed the similar results. The stars like structures are of dimension of 15–20 nm.

4.3.3. ZnS Sulfide Nanoparticles

Zinc sulfide semiconductor has been used in a wide range of applications, such as, in nonlinear optical devices,[40] as an LED when doped,[41] and as a pigment.[42] The UV-Vis spectrum of ZnS nanoparticles is shown in Figure 4.6A, exhibiting a very weak absorption edge at 335 nm and is blue shifted (~10 nm) compared to the bulk ZnS, which shows the the absorption onset at 345 nm.[27] This shift can be attributed to the decrease in size of synthesized ZnS particles to nano range. The Figure 4.6A shows the fluorescence spectrum of the same solution. It exhibits a broad trap state emission centered at around 425 nm. A marked blue shift of the emission band position relative to that of the bulk ZnS (450–500 nm) also clearly indicates the formation of ZnS nanoparticles of quantum size regime.

The X-ray diffraction (XRD) pattern of ZnS nanoparticle solution recorded from a thin film of *Fusarium oxysporum*–$ZnSO_4$ reaction mixture deposited onto Si(111) substrate is shown in Figure 4.6B. The XRD pattern indicates the characteristic of zinc blende structure and is good agreement with the literature.[43] The size of the blende particles calculated from the half-width of the diffraction peaks using Debye–Scherrer formula was ~13 nm.[34] The TEM micrographs recorded from the ZnS nanoparticle film deposited on a carbon coated TEM grid is shown in Figure 4.6C. It indicates the larger fractal and diffused thallus like structures of ZnS nanoparticles whereas in case of PbS nanoparticles formed under similar conditions (as described earlier) were more defined. The high crystalinity of the ZnS particle can be seen from the selected area electron diffraction pattern (Fig. 4.6D).

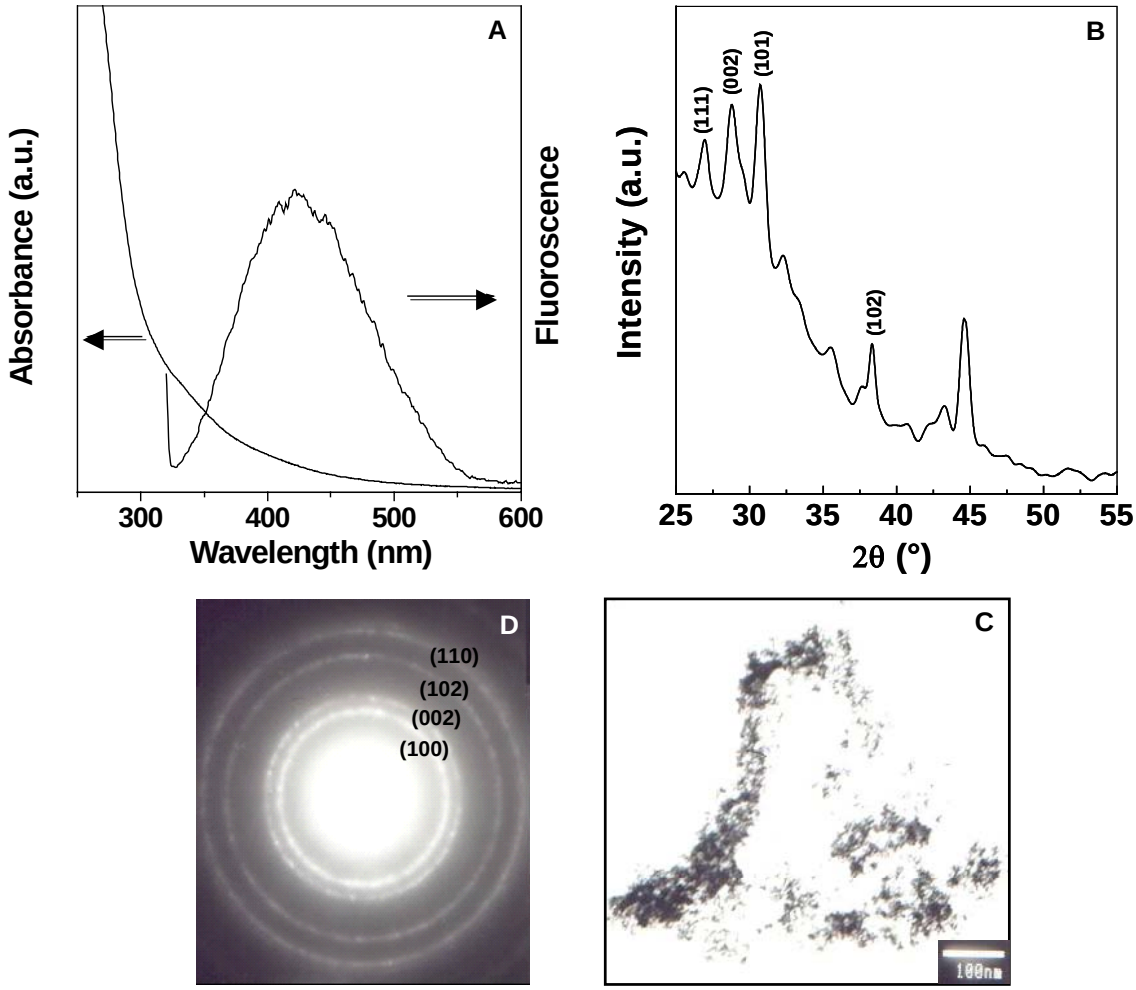

Figure 4.6. (A) UV-Vis spectrum (left) and fluorescence emission spectrum (right) recorded from *Fusarium oxysporum*–$ZnSO_4$ reaction mixture. (B) XRD pattern recorded from the ZnS nanoparticle film deposited on a Si(111) wafer. (C) TEM images of ZnS nanoparticles recorded from *Fusarium oxysporum*–$ZnSO_4$ reaction mixture. (D) Selected area diffraction pattern of ZnS nanoparticle. The diffraction rings have been indexed with reference to zinc blende ZnS.

4.3.4. Manganese sulfide Nanoparticles

The synthesis of MnS is important due to its most extensive study as diluted magnetic semiconductors, which show unique optomagnetic properties and could find application in solar cell as a window/buffer material.[44] The transmission electron

micrograph images recorded from the manganese sulfide nanoparticle film deposited on a carbon coated TEM grid is shown in Figure 4.7A. The picture shows individual, well separated MnS particles with polydispersed morphology. Optical microscopy analysis of such images yielded nanoparticles of 10–15 nm. The MnS particles are crystalline as can be observed in the selected area electron diffraction pattern (inset of Fig. 4.7B).

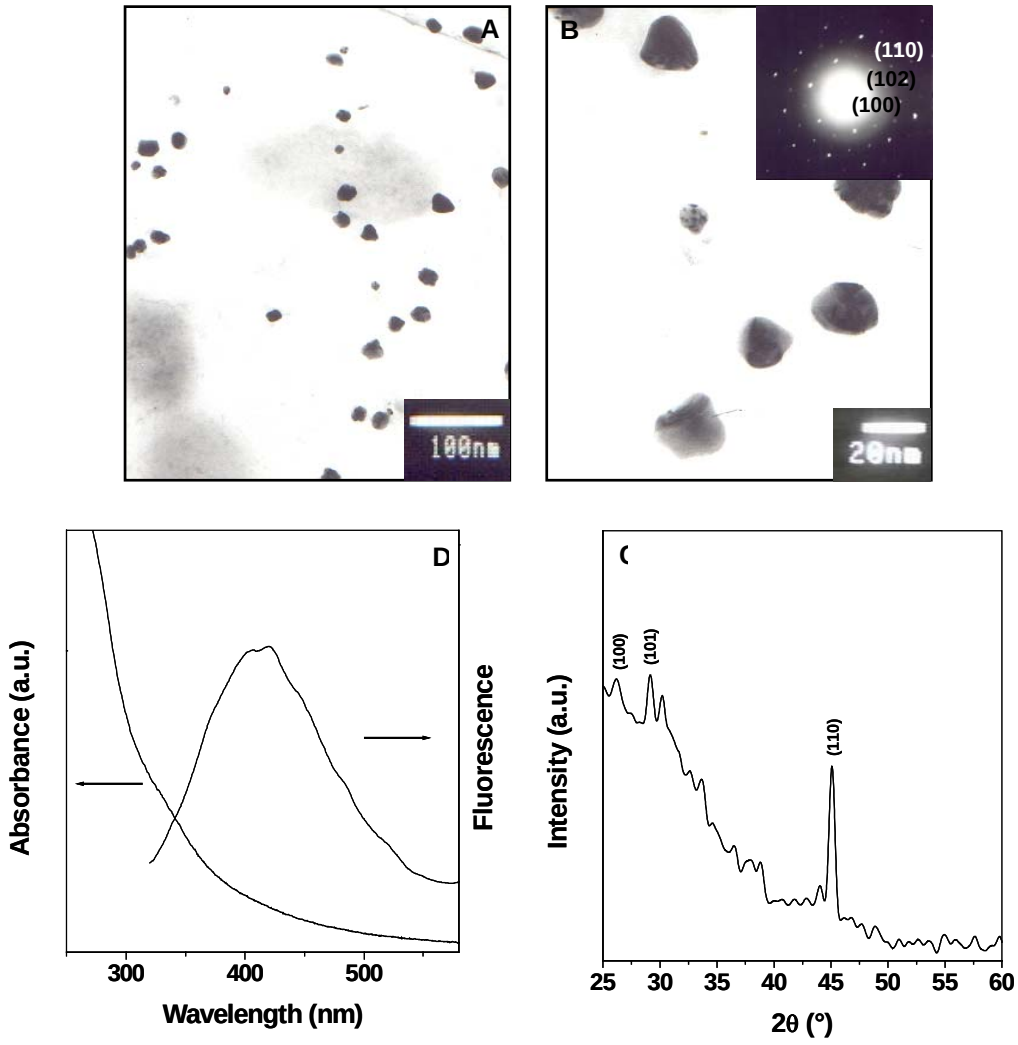

Figure 4.7. (A and B) TEM images of MnS nanoparticles at different magnifications recorded from *Fusarium oxysporum*–$MnSO_4$ reaction mixture. The inset of Figure (B) shows the selected area electron diffraction pattern of MnS particle. The diffraction rings have been indexed with reference to hexagonal MnS. (C) XRD pattern recorded from the MnS nanoparticle film deposited on a Si(111) wafer. (D) UV-Vis spectrum (left) and fluorescence emission spectrum (right) of MnS nanoparticle solution.

The Figure 4.7C shows the XRD of the MnS nanoparticles. The observed peaks in the XRD spectrum are the characteristic of hexagonal wurtzite structure of MnS crystals. The average particle size is 10 nm, as estimated from the Debye–Scherrer formula, which is nearly consistent with the size of the MnS nanoparticles as determined by TEM measurements.[34]

A weak absorption edge is observed in the UV-Vis spectrum of *Fusarium oxysporum*–$MnSO_4$ reaction mixture (Fig. 4.7D). The appearance of absorption edge at 350 nm is clear indication of the formation of MnS nanoparticles. A broad emission band is observed in the fluorescence spectrum of the same solution (Fig 4.7D) and is attributed to deep trap emission. The broad feature of the deep trap emission indicates that the presence of number of trap states.[32]

4.3.5. Nickel Sulfide Nanoparticles

Figure 4.8A shows the UV-Vis spectra of NiS nanoparticles recorded from the reaction mixture of $NiSO_4$ and *Fusarium oxysporum* biomass. The appearance of absorption edge at 360 nm indicates the formation of NiS nanoparticles of band gap energy 3.43 eV. The fluorescence spectrum (Fig. 4.8A) of the NiS shows a broad emission band centered at around 440 nm and is due to broad trap state emission.[32] The broad feature of the trap state emission band suggests the existence of large number of trap states. The large stokes' shift shown by PbS, ZnS, MnS and NiS nanoparticles indicates the occurrence of surface irregularity in the semiconductor particles that can arise due to missing atoms, uncommon oxidation states or adsorbed impurities on the surface of the particle. The presence of these defects in the synthesized metal sulfide nanoparticles can be attributed to the fact that when nanoparticles size is reduced in such a way that the particle is essentially on surface, the curvature of the surface becomes so

high that virtually all of the surface atoms have a slightly different coordination and/or effective oxidation state.[32]

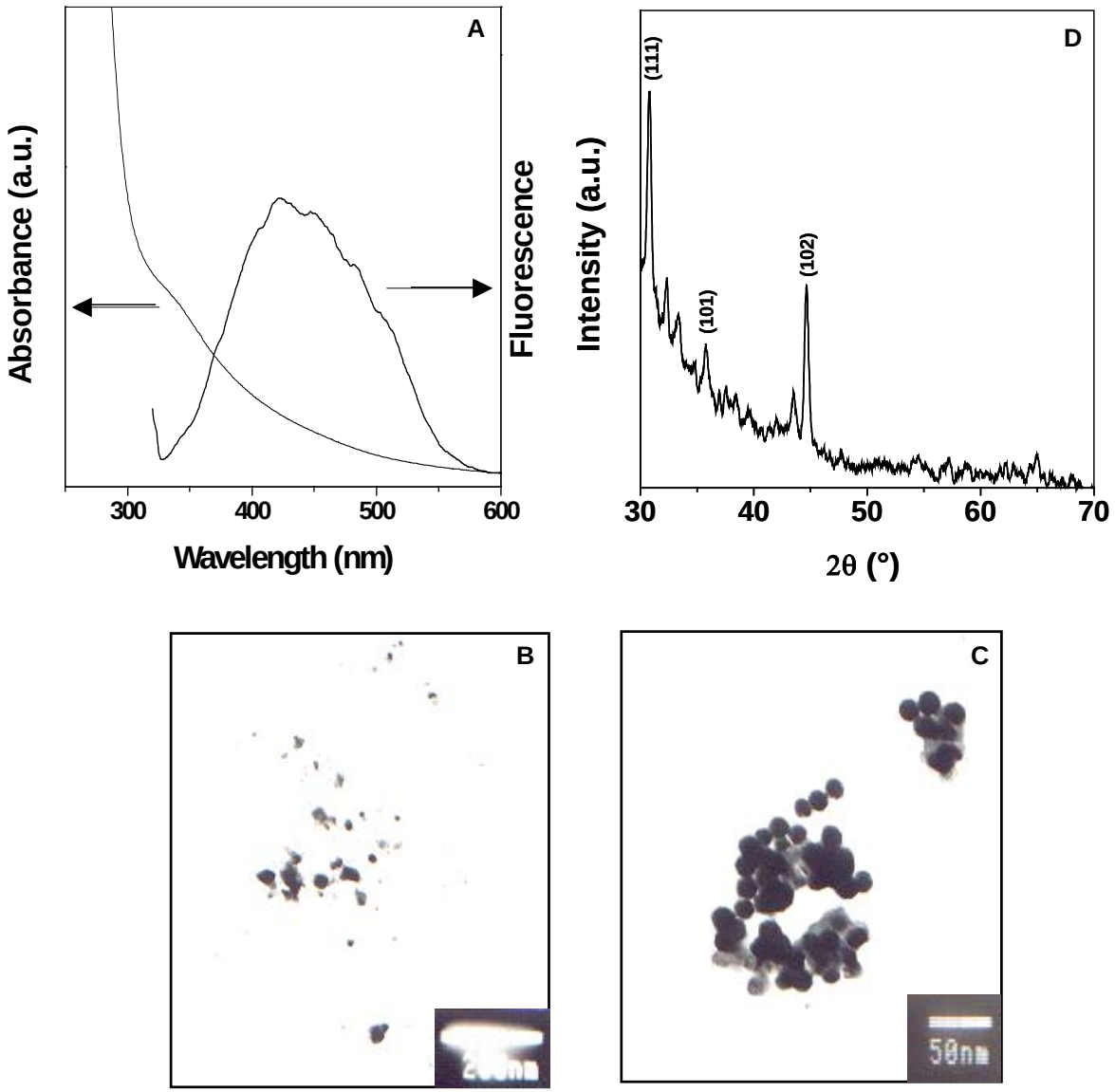

Figure 4.8. (A) UV-Vis spectrum (left) and fluorescence emission spectrum of NiS nanoparticle solution. (B and C) TEM micrographs of NiS nanoparticles recorded from *Fusarium oxysporum*–$NiSO_4$ reaction mixture at different magnifications. (D) XRD pattern recorded from the NiS nanoparticle film deposited on a Si(111) wafer.

The transmission electron microscopy analysis of NiS nanoparticle solution at lower magnification shows the well-separated polydispersed particles (Fig. 4.8B). At

higher magnification, it shows spherical and some aggregated nanoparticles (Fig. 4.8C). On careful examination of this image indicates that the nickel sulfide nanoparticles are enclosed by the proteins secreted by fungus in the reaction mixture. This suggests the high stability of nanoparticles is due to stabilization by surface bound proteins present in the solution. The average particle size calculated under optical microscope was found to be about 7–15 nm. The intense peaks observed in the XRD pattern of the NiS nanoparticles (Fig. 4.8D) revealed the characteristic of hexagonal structure of nickel sulfide crystals. The average size is 11.2 nm as calculated using Debye–Scherrer equation, which is in good agreement with the size of the NiS nanoparticles determined by the TEM observations.[34]

4.4. PROBABLE MECHANISM OF FORMATION OF METAL SULFIDE NANOPARTICLES

The Fourier Transform Infrared (FTIR) spectrum recorded from the cadmium sulfide solution (Fig. 4.9A) exhibits bands at 1650 (1) and 1540 (2) cm^{-1} and are due to carbonyl stretch and –N-H stretch vibrations in the amide linkages of proteins respectively.[45] The nanoparticles are known to interact with protein either through free amine groups or cysteine residues and therefore the high stability of metal sulfide nanoparticles solutions may be due to the capping of nanoparticles by surface-bound proteins present in reaction mixture. An absorption band at *ca.* 270 nm is observed (Fig. 4.1A) in the UV-Vis spectra of metal sulfide nanoparticle solution, which is due to electronic excitations in tryptophan and tyrosine residues of proteins[28] and suggesting a possible sulfate reducing enzyme secreted by *Fusarium oxysporum* in solution for the synthesis of metal sulfide nanoparticles. To establish the secreted enzymes are indeed

sulfate reductase, few set of reactions were designed wherein the *Fusarium oxysporum* biomass was reacted with (i) a 1 mM aqueous solution of MNO_3 and (ii) an aqueous solution containing a mixture of the salts MCl_2 and Na_2SO_4 (1:1 M^{2+}:SO_4^{2-} concentration in solution = 1 mM), where M= Cd, Pb, Zn, Mn and Ni. Metal sulfide nanoparticles were observed to form in the latter case after just 4 days of reaction, while in the former case; there was no evidence of nanoparticle formation even after 21 days of reaction. To rule out the possibility of entrapment of the M^{2+} ions in the fungal mass followed by reaction with sulfide ions and then release of the nanoparticles into solution, another control experiment was performed wherein the fungal biomass was immersed in sterile water for 12 days, the reaction mixture was filtered, and the filtrate was reacted with 1 mM MSO_4 solution.

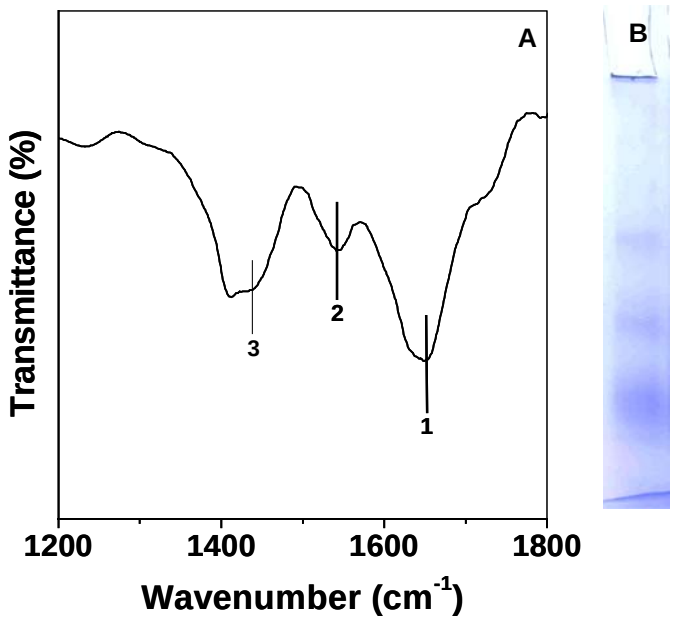

Figure 4.9. (A) FTIR spectrum recorded from drop-cast films of the cadmium sulfide nanoparticle solution. The carbonyl stretch (1) and –N-H stretch (2) are identified in the Figure. (B) The native gel electrophoresis of aqueous protein extract obtained from *Fusarium oxysporum* mycelia; 10 % (w/v) polyacrylamide slab gel, pH 4.3.

It was observed that metal sulfide nanoparticles formed readily within 6 days of reaction. From the above experiments, it is clear that *Fusarium oxysporum* releases reductase enzymes into solution that are responsible for the formation of metal sulfide nanoparticles from M^{2+} and SO_4^{2-} ions. The aqueous solution exposed to the fungal biomass for 12 days was analyzed for its protein content. The inset of Figure 4.9B shows the polyacrylamide gel electrophoresis (PAGE) results of the aqueous extract carried out at pH 4.3. The electrophoresis measurement indicates the presence of at least four different proteins of molecular masses between 66 kDa and 10 kDa. Addition of an aliquot of the aqueous protein extract after dialysis to remove small molecular weight compounds (using a dialysis bag of 3 K molecular weight cutoff) to an aqueous solution of metal sulfate did not result in the formation of sulfide nanoparticles. However, addition of ATP and NADH to the protein dialysate restores the nanoparticle formation ability of the protein solution either by direct reaction with metal sulfate solution or by an aqueous solution consisting of a mixture of MCl_2 and Na_2SO_4. This clearly indicates that the reduction of SO_4^{2-} to S^{2-} ions by NADH dependent reductases in the extract and the subsequent formation of metal sulfide nanoparticles.

4.5. SUMMARY

In this chapter, the extracellular biosynthesis of technologically important semiconductor metal sulfide nanoparticles using fungus, *Fusarium oxysporum*, has been demonstrated. The extracellular synthesis of metal sulfide is due to the release of NADH dependent sulfate reductase enzyme in solution by the fungus, *Fusarium oxysporum*, which results in the reduction of SO_4^{2-} ions to S^{2-} and subsequent formation of metal sulfide nanoparticles. While such processes are known in sulfate reducing bacteria (which are strictly anaerobic),[46] this is the first demonstration on the secretion of sulfate reducing enzymes by a fungus. The high stability of the metal sulfide nanoparticle solution is due to stabilization by surface bound proteins present in the reaction mixture. It has also been observed that the presence of protein moiety on the surface of the metal sulfide does not affect their optoelectronic property. The fluorescence measurements recorded from CdS solution reveal the small stokes' shift indicating that the surfaces of sulfide are regular with most surface atoms satisfying the coordination or oxidation states of their bulk counterpart. However, the measurements recorded from other sulfides, PbS, ZnS, MnS and NiS exhibit broad emission band, indicating the surfaces of sulfides are irregular, which may arise due to the uncommon oxidation or missing of atom or adsorbed impurities on the surface of the particle.[32]

4.6. REFERENCES

1. (a) K. J. Klabunde, *Nanoscale Materials in Chemistry*; Wiley-Interscience, New York, 2001. (b) J. H. Fendler, *Nanoparticles and Nanostructured Films*, Wiley-VCH, Weinheim: Germany, 1998. (c) H. Weller, *Angew. Chem. Int. Ed. Engl.* **1993**, *32*, 41.
2. (a) S. Sun, C. B. Murray, D. Weller, L. Folks, A. Moser, *Science* **2000**, *287*, 1989. (b) T. Hyeon, *Chem. Commun*. **2003**, 927. (c) P. Michler, A. Imamoglu, M. D. Mason, P. J. Carson, G. F. Strouse, S. K. Buratto, *Nature* **2000**, *406*, 968. (d) M. G. Bawendi, M. L. Steigerwald, L. E. Brus, *Annu. Rev. Phys. Chem.* **1990**, *41*, 477.
3. (a) A. P. Alivisatos, *Science* **1996**, *271*, 933. (b) C. B. Murray, C. R. Kagan, M. G. Bawendi, *Annu. Rev. Mater. Sci.* **2000**, *30*, 545.
4. (a) J. Hu, L. S. Li, W. Yang, L. Manna, L. W. Wang, A. P. Alivisatos, *Science* **2001**, *292*, 2060. (b) V. C. Sundar, H. J. Eisler, M. G. Bawendi, *Adv. Mater*. **2002**, *14*, 739. (c) W. C. W Chan, S. Nie, *Science* **1998**, *281*, 2016.
5. X. Wu, H. Liu, J. Liu, K. N. Haley, J. A. Treadway, J. P. Larson, N. Ge, F. Peale, M. P. Bruchez, *Nature Biotechnol.* **2003**. *21*, 41.
6. W. J. Parak, R. Boudreau, M. L. Gros, D. Gerion, D. Zanchet, C. M. Micheel, S. C. Williams, A. P. Alivisatos, C. Larabell, *Adv. Mater.* **2002**, *14*, 882.
7. B. Dubertret, P. Skourides, D. J. Norris, V. Noireaux, A. H. Brivanlou, A. Libchaber, *Science* **2002**, *298*, 1759.
8. (a) J. R. Taylor, M. M. Fang, S. Nie, *Anal. Chem.* **2000**, *72*, 1979. (b) H. Xu, M. Y. Sha, E. Y. Wong, J. Uphoff, Y. Xu, J. A. Treadway, A. Truong, E. O'Brien, S. Asquith, M. Stubbins, N. K. Spurr, E. H. Lai, W. Mahoney, *Nucleic Acids Res.* **2003**, *31*, e 43.
9. (a) C. B. Murray, D. J. Norris, M. G. Bawendi, *J. Am. Chem. Soc.* **1993**, *115*, 8706. (b) Z. A. Peng, X. Peng, *J. Am. Chem. Soc.* **2002**, *124*, 3343. (c) D. V. Talapin, A. L. Rogach, E. V. Shevchenko, A. Kornowski, M. Haase, H. Weller, *J. Am. Chem. Soc.* **2002**, *124*, 5782. (d) M. W. DeGroot, N. J. Taylor, J. F. Corrigan, *J. Am. Chem. Soc.* **2003**, *125*, 864. (e) X. Peng, *Adv. Mater*. **2003**, *15*, 459. (f) L. Qu, Z. A. Peng, G. Peng, *Nano Lett.* **2001**, *1*, 333.

10. M. L. Steigerwald, A. P. Alivisatos, J. M. Gibson, T. D. Harris, R. Kortan, A. J. Muller, A. M. Thayer, T. M. Duncan, D. C. Douglass, L. E. Brus, *J. Am. Chem. Soc.* **1988**, *110*, 3046.
11. (a) S. M. Lee, Y. W. Jun, S. N. Cho, J. Cheon, *J. Am. Chem. Soc.* **2002**, *124*, 11244. (b) Y. W. Jun, Y. Y. Jung, J. Cheon, *J. Am. Chem. Soc.* **2002**, *124*, 615. (c) N. Pradhan, S. Efrima, *J. Am. Chem. Soc.* **2003**, *125*, 2050.
12. (a) X. Peng, *Chem. Eur. J.* **2002**, *8*, 335. (b) M. W. Yu, X. G. Peng, *Angew. Chem. Int. Ed. Engl.* **2002**, *41*, 2368. (c) Z. A. Peng, X. G. Peng, *J. Am. Chem. Soc.* **2001**, *123*, 183.
13. (a) L. Addadi, S. Weiner, *Angew. Chem., Int. Ed. Engl.* **1992**, *31*, 153. (b) S. Mann, G. A. Ozin, *Nature* **1996**, *382*, 313. (c) S. Oliver, A. Kupermann, N. Coombs, A. Lough, G. A. Ozin, *Nature*, **1995**, *378*, 47. (d) D. R. Lovley, J. F. Stolz, G. L. Nord, E. J. P. Phillips, *Nature*, **1987**, *330*, 252.
14. (a) U. B. Sleytr, P. Messner, D. Pum, M. Sara, *Angew. Chem. Int. Ed. Engl.* **1999**, *38*, 1034. (b) G. Southam, T. J. Beveridge, *Geochim. Cosmochim. Acta* **1996**, *60*, 4369.
15. (a) T. J. Beveridge, R. J. Doyle, (Eds.) *Metal Ions and Bacteria*, Wiley, New York, 1989. (b) T. J. Beveridge, R. G. E. Murray, *J. Bacteriol.* **1980**, *141***,** 876. (b) D. Fortin, T. J. Beveridge, *Biomineralization. From Biology to Biotechnology and Medical Applications*, E. Baeuerien (eds.), Weinheim: Wiley–VCH, 2000, p 7.
16. (a) T. Klaus, R. Joerger, E. Olsson, C. G. Granqvist, *Proc. Natl Acad. Sci. USA* **1999**, *96*, 13611. (b) T. Klaus-Joerger, R. Joerger, E. Olsson, C. G. Granqvist, *Trends Biotechnol.* **2001**, *19***,** 15. (c) R. Joerger, T. Klaus, C. G. Granqvist, *Adv. Mater.* **2000**, *12*, 407.
17. B. Nair, T. Pradeep, *Cryst. Growth Des.* **2002**, *2*, 293.
18. (a) J. D. Holmes, P. R. Smith, R. Evans-Gowing, D. J. Richardson, D. A. Russell, J. R. Sodeau, *Arch. Microbiol.* **1995**, *163*, 143. (b) P. R. Smith, J. D. Holmes, D. J. Richardson, D. A. Russell, J. R. Sodeau, *J. Chem. Soc.*, *Faraday Trans.* **1998**, *94*, 1235.
19. C. T. Dameron, R. N. Reese, R. K. Mehra, A. R. Kortan, P. J. Carroll, M. L. Steigerwald, L. E. Brus, D. R. Winge, *Nature* **1989**, *338*, 596.

20. (a) M. Kowshik, W. Vogel, J. Urban, S. K. Kulkarni, K. M. Paknikar, *Adv. Mater.* **2002**, *14*, 815. (b) M. Kowshik, N. Deshmukh, W. Vogel, J. Urban, S. K. Kulkarni, K. M. Paknikar, *Biotechnol. Bioengineer.* **2002**, *78*, 583.
21. P. Mukherjee, A. Ahmad, D. Mandal, S. Senapati, S. R. Sainkar, M. I. Khan, R. Ramani, R. Parischa, P. V. Ajaykumar, M. Alam, M. Sastry, R. Kumar, *Angew. Chem. Int. Ed. Engl.* **2001**, *40*, 3585.
22. P. Mukherjee, A. Ahmad, D. Mandal, S. Senapati, S. R. Sainkar, M. I. Khan, R. Parischa, P. V. Ajaykumar, M. Alam, R. Kumar, M. Sastry, *Nano Lett.* **2001**, *1*, 515.
23. P. Mukherjee, S. Senapati, D. Mandal, A. Ahmad, M. I. Khan, R. Kumar, M. Sastry, *ChemBioChem* **2002**, *3*, 461.
24. A. Ahmad, P. Mukherjee, S. Senapati, D. Mandal, M. I. Khan, R. Kumar, M. Sastry, *Coll. Surf. B: Biointerfaces* **2003**, *28*, 313.
25. S. Senapati, A. Ahmad, M. I. Khan, M. Sastry, R. Kumar, *Small* **2005**, *1*, 517.
26. A. Ahmad, P. Mukherjee, D. Mandal, S. Senapati, M. I. Khan, R. Kumar, M. Sastry, *J. Am. Chem. Soc.* **2002**, *124*, 12108.
27. (a) A. Henglein, *Chem. Rev.* **1989**, *89*, 1861. (b) L. Spanhel, M. Haase, H. Weller, A. Henglein, *J. Am. Chem. Soc.* **1987**, *109*, 5649.
28. Cantor, Schimmel, (Eds.) *Biophysical Chemistry, Part II: Techniques for the Study of Biological Structure and Function*, H. Freeman and Co., San Francisco. 1980, Ch 7, p 377.
29. (a) M. L. Steigerwald, L. E. Brus, *Acc. Chem. Res.* **1990**, *23*, 183. (b) M. Nirmal, L. Brus, *Acc. Chem. Res.* **1999**, *32*, 407. (c) S. Empedocles, M. G. Bawendi, *Acc. Chem. Res.* **1999**, *32*, 389.
30. (a) A. P. Alivisatos, *J. Phys. Chem.* **1996**, *100*, 13226. (b) X. Peng, J. Wickham, A. P. Alivisatos, *J. Am. Chem. Soc.* **1998**, *120*, 5343. (c) M. Jr. Bruchez, M. Moronne, P. Gin, S. Weiss, A. P. Alivisatos, *Science* **1998**, *281*, 2013. (d) W. C. W. Chan, S. Nie, *Science* **1998**, *281*, 2016.
31. (a) S. Gallardo, M. Gutierrez, A. Henglein, E. Janata, *Ber. Bunsen-Ges. Phys. Chem.* **1989**, *93*, 1080. (b) J. L. Machol, F. W. Wise, R. Patel, D. B. Tanner, *Phys A* **1994**, *207*, 427. (c) L. Brus, *J. Phys. Chem.* **1986**, *90*, 2555.

32. (a) C. F. Landes, S. Link, M. B. Mohamed, B. Nikoobakth, M. A. El-Sayed, *Pure Appl. Chem.* **2002**, *74*, 1675. (b) E. Lifshitz, I. Dag, I. D. Litvitn, G. Hodes. *J. Phys. Chem. B* **1998**, *102*, 9245. (c) A. P. Alivisatos. *J. Phys. Chem B* **1996**, *100*, 13226.
33. (a) V. L. Colvin, A. N. Goldstein, A. P. Alivisatos, *J. Am. Chem. Soc.* **1992**, *114*, 5221. (b) M. Kundu, A. A. Khosravi, S. K. Kulkarni, *J. Mater. Sci.* **1997**, *32*, 245.
34. J. W. Jeffrey, *Methods in Crystallography*, Academic Press, New York, 1971.
35. (a) L. Brus, *J. Phys. Chem.* **1986**, *90*, 2555. (b) L. E. Brus, *J. Chem. Phys.* **1984**, *80*, 4403.
36. (a) Y. Wang, A. Suna, W. Mahler, R. Kasowski, *J. Chem. Phys.* **1987**, *87*, 7315. (b) R. Thielsch, T. Bohme, R. Reiche, D. Schlafer, H. D. Bauer, H. Bottcher, *Nanostruct. Mater.* **1998**, *10*, 131. (c) Y. Wang, *Acc. Chem. Res.* **1991**, *24*, 133.
37. P. K. Nair, O. Gomezdaza, M. T. S. Nair, *Adv. Mater. Opt. Electron*. **1992**, *1*, 139.
38. P. Gadenne, Y. Yagil, G. Deutscher, *J. Appl. Phys*. **1989**, *66*, 3019.
39. T. K. Chaudhuri, S. Chatterjee, *Proc*. *Int. Conf. Thermoelectro*. **1992**, *11*, 40.
40. J. Xu, W. Ji, *J. Mater. Sci. Lett.* **1999**, *18*, 115.
41. E. J. Donahue, A. Roxburgh, M. Yurchenko, *J. Mater. Res. Bull.* **1998**, *33*, 323.
42. D. H. Parker, *Principles of Surface Coating Technology*, Interscience Publishers, New York, 1965, p. 79.
43. D. H. Gray, S. Hu, D. L. Gin, *Adv. Mater.* **1997**, *9*, 731.
44. (a) J. K. Furdyna, *J. Appl. Phys.* **1988**, *64*, R29. (b) O. Goede, W. Heimbrodt, *Phys. Status Solidi B* **1988**, *146*, 11.
45. (a) C. D. Keating, K. K. Kovaleski, M. J. Natan, *J. Phys.Chem. B* **1998**, *102*, 9414. (b) A. Gole, C. Dash, V. Ramakrishnan, S. R. Sainkar, A. B. Mandale, M. Rao, M. Sastry, *Langmuir* **2001**, *17*, 1674.
46. (a) M. Labrenz, G. K. Druschel, T. Thomsen-Ebert, B. Gilbert, S. A. Welch, K. M. Kemner, G. A. Logan, R. E. Summons, G. De Stasio, P. L. Bond, B. Lai, S. D. Kelly, J. F. Banfield, *Science* **2000**, *290*, 1744. (b) J. D. Holmes, P. R. Smith, R. Evans-Gowing, D. J. Richardson, D. A. Russell, J. R. Sondeau, *Arch. Microbiol.* **1995**, *163*, 143.

5.1. INTRODUCTION

Oxidation of cyclohexane to adipic acid in air using heterogeneous catalysts is an important reaction of industrial importance.[1] The oxidation of cyclohexane, via, cyclohexanol and cyclohexanone, leads to adipic acid, which is an important precursor for the production of nylon–6 and nylon–66 polymers, fibers, plastics, and lubricant additive as well as important intermediate for pharmaceuticals and insecticides industries.[2]

Commercially, adipic acid is manufactured in a two-step process by the oxidation of cyclohexanol and cyclohexanone (KA oil), obtained either by the oxidation of cyclohexane or hydrogenation of phenol. First step involves the cyclohexane oxidation to a mixture of cyclohexanol-cyclohexanone (KA oil) using a soluble cobalt catalyst at around 150 °C and 1–2 MPa pressure. In the second step, this mixture, KA oil is further oxidized to adipic acid using 40–60 % HNO_3 in presence of copper and vanadium catalysts.[3] Table 5.1 summarizes salient feature of various processes reported on cyclohexane to KA oil using the range of reaction conditions.

However, the use of nitric acid as oxidant causes environmental constraints since it generates NO_x effluent, which contributes to global warming and ozone layer depletion.[4] Thus, there is an increasing need to replace the present commercial hazardous processes with a more effective catalytic process. The greater environmental concerns among scientists in recent years demand the use of benign oxidant such as molecular oxygen or hydrogen peroxide. Sato et al. reported the oxidation of cyclohexene to adipic acid with 30 % H_2O_2 in presence of Na_2WO_4 and $[CH_3(n\text{-}C_8H_{17})_3N]HSO_4$ as a phase transfer catalyst.[5] Recently, Pillai et al. reported that a calcined vanadium phosphorus oxide (VPO) catalyst with a P/V ratio of 1:1 using H_2O_2 gave 91 % conversion with a

Table 5.1. Reaction conditions for aerial oxidation of cyclohexane

Process and Company	Temp., °C	Press., MPa	Catalyst or Additives	Reactor Type	Cyclo -hexane Conv., Mol %	KA yield, Mol %	Ref.
Metal-Catalyzed							
Du Pont	170	1.1	Co	Column	6	76	6
Stamicarbon	155	0.9	Co	Tank	4	77	7
High Peroxide							
BASF							
Oxidation	145	1.1	None	Tank	3	83	8
Deperoxidation	125		Co/NaoH				
Du Pont							
Oxidation	160	1.0	Co	Column	4	82	9
Deperoxidation	120		Co, Cr				
Rhone Poulenc							10
Oxidation	175	1.8	None	Tank	4	84	
Deperoxidation	115		Cr, V, Mo				
Stamicarbon							11
Oxidation	160	1.3	None	Tank	3	86	
Deperoxidation	100		Co/NaOH				
Boric acid							
Halcon	165	1.0	H_3BO_4	Tank	3	87	12
ICI	165	1.0	H_3BO_4	Tank	5	85	13 14
IFB	165	1.2	H_3BO_4		12	85	15
Solutia (formerly Monsanto)	165	1.0	H_3BO_4	Tank	4	87	

product distribution of oxidation with *tert*-butylhydroperoxide or iodosylbenzene over 36 % cyclohexanol and 64 % cyclohexanone.[16] The extensive study of cyclohexane using metal phthalocyanine complexes incapsulated in zeolite–Y has well been documented in literature.[17] Tanaka reported a single step, liquid phase oxidation of cyclohexane to adipic acid using cobalt acetate catalyst with the addition of a promoter like acetaldehyde, H_2O_2 etc. at 90 °C under oxygen atmosphere. Very recently, Thomas et al. oxidized cyclohexane and n-hexane with air over metal containing aluminum phosphate molecular sieves.[18]

Among the transition metals, gold is chemically inert because of its smooth surface and unusual properties shown by individual gold atom. Thus, it is considered to be the least catalytically active.[19] The unusual properties of gold atom are attributable to the so-called relativistic effect that stabilizes the $6s^2$ electron pairs and thus much of the chemistry (including the catalytic properties) of the novel group elements is determined by the high energy and reactivity of the 5d electrons.[19b] This explains the low catalytic activity of gold catalyst in comparison to platinum group metal for many reactions. Recently, Hammer and Norskov had explained theoretically why the smooth surface of gold is noble in the dissociative adsorption of molecular hydrogen.[19a] However, a substantial amount of work done by Haruta et al.[20] has established that nanosized gold particles when deposited on certain oxides, such as Fe_2O_3, NiO, MnO_2.γ-alumina[21] and titania,[22] exhibits surprisingly high catalytic activity in oxidation of carbon monoxide at or below ambient temperatures. The excellent catalytic activity of supported gold nanoparticles for partial and complete oxidation of hydrocarbons, oxidation of carbon monoxide, nitric oxide and unsaturated hydrocarbons has been reported.[20c] Thiol-stabilized gold nanoparticles have also been exploited in asymmetric hydroxylation

reactions,[23] carboxylic ester cleavage[24] and particle-bound ring opening metathesis polymerization.[25]

The remarkably high catalytic activity of gold arises from the formation of very small particles. It is known that the bulk metal and larger metallic particles cannot chemisorb most of the reactant molecules and the chemisorption occurs only when a satisfactory number of low-coordination number surface atoms are present, preferably on smaller particles lacking complete metallic character. Recent literature on supported gold catalysts suggests that the main factors for attaining high catalytic activity are (i) smaller particle size and (ii) support.[20d]

Recognizing the immense importance of nanocomposites in many application including catalysis, the extracellularly synthesized gold nanoparticles using fungus, *Fusarium oxysporum*,[26] (as described in chapter 2), has been supported on amorphous (fumed) silica and also intracellularly synthesized gold nanoparticles by fungus, *Verticillium* sp.,[27] have been explored for oxidation reaction.

In this chapter, the catalytic potential of the supported Au-SiO_2 nanocomposite will be exploited in an aerial oxidation of cyclohexane to adipic acid in a solvent free system in batch type reactor. The effect of reaction temperature, air pressure and amount of catalyst is extensively studied. A comparative study on the effect of nano gold particle size on the conversion of cyclohexane has also been studied. A possible pathway of formation of adipic acid by oxidation of cyclohexane using supported gold nanocomposites as catalyst for has also been discussed.

5.2. EXPERIMENTAL

5.2.1. Synthesis of Gold Nanoparticles Supported on Fumed Silica

Gold nanoparticles supported on amorphous (fumed) SiO_2 (Au-SiO_2-FO) using *Fusarium oxysporum* were synthesized as follows: 20 g of fungus, *Fusarium oxysporum*, was taken in a conical flask containing 100 mL of distilled water. An appropriate quantity of $HAuCl_4$ was added to conical flask to yield an overall concentration of 1 mM gold in aqueous solution. To this mixture 500 mg of amorphous (fumed) silica was added and the whole mixture was thereafter put into a shaker at 28 °C (200 rpm) for 48 h. On reduction of $AuCl_4^-$ ions by *Fusarium oxysporum* for 48 h (as discussed in chapter 2), the gold nanoparticle solution was subjected to filtration to separate solid from the liquid solution. The solid Au-SiO_2-FO along with biomass was washed several times with sterile water and heated at 150 °C overnight to remove water from solid including the fungal biomass.

5.2.2. Synthesis of Gold Nanoparticle Supported on Fungal Biomass

The gold nanoparticle supported on fungal biomass, *Verticillium* sp. (Au-Vert) was synthesized as follows: The acidophillic fungus, *Verticillium* sp., was isolated from the Taxus plant and maintained on potato-dextrose agar slants at 25 °C. The fungus was grown in 500 mL Erlenmeyer flasks each containing MGYP media (100 mL), composed of malt extract (0.3 %), glucose (1.0 %), yeast extract (0.3 %), and peptone (0.5 %) at 25–28 °C under shaking (200 rpm) for 96 h. After 96 h of fermentation, mycelia were separated from the culture broth by centrifugation (5000 rpm) at 10 °C for 20 minutes and the settled mycelia were washed thrice with sterile distilled water. Some of the harvested mycelial mass (10 g) was re-suspended in sterile distilled water (100 mL) in 500 mL Erlenmeyer flasks at pH 5.5–6.0 and to this suspension an aqueous solution of

chloroauric acid (1 mM $HAuCl_4$, 100 mL) was added. The whole mixture was put into a shaker at 28 °C (200 rpm) and left for 72 h. The nano Au-Vert thus synthesized for 72 h is filtered and thoroughly washed several times with distilled water, dried at 110 °C overnight under vacuum.

5.2.3. *In Situ* Preparation of Nanogold-Fumed Silica Composite Materials

The nano-Au-SiO_2 (Au-SiO_2-Chem) composite material of 8 nm size of nano gold was prepared using chemical method by *in situ* reduction of $AuCl_4^-$ ions as reported by Mukherjee et al.[28] It was achieved by treating 500 mg of amorphous (fumed) silica with 100 mL of 0.1 mM $HAuCl_4$ solution for 96 h at ambient conditions followed by filtration, washing thoroughly with copious amount of water and acetone and finally dried under vacuum. This material was used to study the cyclohexane oxidation for comparative purpose.

5.2.4. Instruments for Characterization

The presence of gold nanoparticles on Au-SiO_2-Chem, Au-SiO_2-FO and Au-Vert composite materials were confirmed by recording XRD on the same Rigaku MiniFlex instrument between 30–80° at a scan rate of 2 °/min. From the broadening of the Au(111) reflection, the average size of the gold nanoparticles was evaluated using the Debye–Scherrer equation: $D = k\lambda / \beta\cos\theta$, where, D = thickness of the nanoparticle, k is a constant, λ = wavelength of X-rays (1.5404 Å), β = width at half maxima of (111) reflection at Bragg's angle 2θ.

The UV-Vis spectra of the gold nanoparticles on Au-SiO_2-Chem, Au-SiO_2-FO and Au-Vert composite materials were recorded on a Shimadzu UV-2102 PC spectrophotometer operating at the reflectance mode at a resolution of 1 nm using barium

sulfate as a standard for the background correction. Since the films of the bionanocomposite were rough, the results are not quantitative and have been used to merely detect the presence of gold nanoparticles in the biomaterial.

To estimate the mass loading of gold nanoparticles on Au-SiO_2-Chem, Au-SiO_2-FO and Au-Vert nanocomposites, the atomic absorption spectrophotometer was used. Fifty milligrams of each of the catalyst bound with gold nanoparticles were dissolved in 10 mL of aqua regia (concentrated HCl/concentrated HNO_3, 3:1), and volume was adjusted up to 100 mL using deionized water. The solutions were analyzed by Chemito 201 atomic absorption spectrophotometer and were compared with a standard gold solution to estimate the weight percent of loading of gold nanoparticles in the supports.

The reaction mixtures and esterified acid products were analyzed by an Agilent 6890 series gas chromatography (GC) containing chiral capillary column (10 % permethylated β-cyclodextrin, 30 m × 0.32 mm × 0.25 μm film thickness) and flame ionization detector. The acid products were also confirmed by GC-Mass spectroscopy (GCMS) on a Shimadzu GCMS-QP 2000A instrument. The gaseous products were analyzed by 5765 NUCON GC containing 1/8" SS Packed Poropak-Q column of 3 m long and TCD detector.

5.2.5. Catalytic Reaction of Cyclohexane to Adipic acid

Catalytic reaction of aerial oxidation of cyclohexane was performed in a high pressure autoclave using 30 mL (278.2 mmol) of cyclohexane in presence of 25 mg of Au-SiO_2-FO or Au-*Verticillium* sp. or Au-SiO_2-Chem in a solvent free condition at different temperatures (110 to140 °C) and pressures (2.1 to 4.3 MPa). After the complete consumption of oxygen (observed by pressure drop), the reaction was stopped and the reactor was cooled to 25 °C. A crystalline solid product was observed, which was not

observed in a controlled experiment in absence of catalyst. The solid product was esterified to test the presence of acids, and analyzed by GC with FID detector. The acid products were also confirmed by GC-MS. The detailed mass balance was calculated by analyzing the liquid products by GC with FID detector. The gaseous products were analyzed using GC with TCD detector.

5.3. CHARACTERIZATION

5.3.1. Powder X-Ray Diffraction

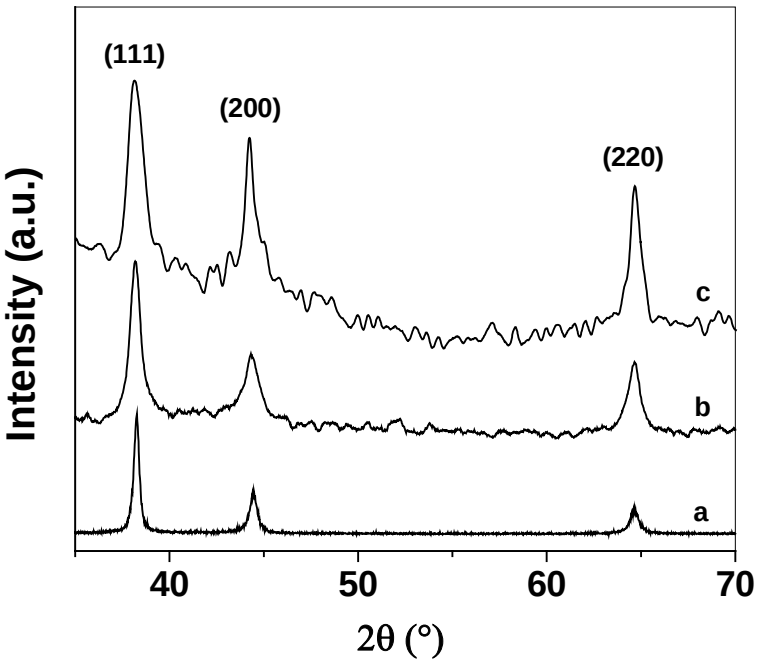

Figure 5.1. XRD patterns recorded from (a) Au-Vert, (b) Au-SiO_2-FO (c) Au-SiO_2-Chem samples.

The presence of gold nanoparticles on (a) Au-Vert (b) Au-SiO_2-FO and (c) Au-SiO_2-Chem nanocomposites were confirmed by XRD measurements between 35–80° at a scan rate of 2 °/min. and are shown in Figure 5.1. The occurrence of intense peaks in all the spectra at (111), (200) and (220) Bragg's reflections are the characteristic of face

centred cubic structures of gold crystals.[29] An estimate of the mean size of the gold nanoparticles on these nanocomposites were calculated using the Debye–Scherrer equation by determining the width of the (111) Bragg reflection.[30] The average size of the gold nanoparticles in Au-SiO_2-Chem, Au-SiO_2-FO and Au-Vert nanocomposites was found to be about 8, 13 and 20 nm respectively.

5.3.2. UV-Vis Spectroscopy

Figure 5.2 depicts the DR UV–Vis spectra of Au-SiO_2-Chem, Au-SiO_2-FO and Au-Vert. The broad resonance at around 550 nm in all spectra indicates the presence of the gold in these nanocomposites. As mentioned earlier, scattering from the rough surface would also contribute to the broadening of the resonance. This absorption is close to that observed for thin films of gold nanoparticles grown by different techniques.[31]

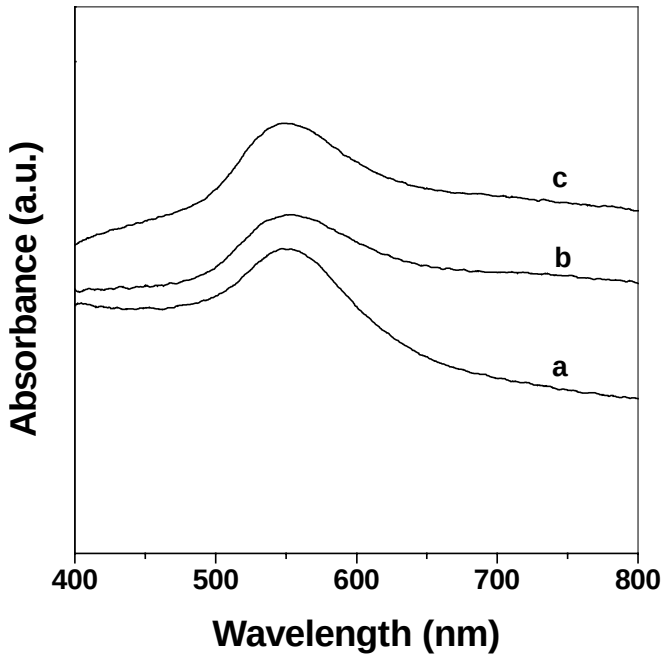

Figure 5.2. UV-Vis spectra recorded from (a) Au-SiO_2-Chem (b) Au-SiO_2-FO and (c) Au-Vert nanocomposites.

The estimation of the mass loading of gold nanoparticles on Au-SiO_2-Chem, Au-SiO_2-FO and Au-Vert. nanocomposites was performed by the atomic absorption spectrophotometer analysis. The weight percentage loading of gold nanoparticles in Au-SiO_2-Chem, Au-SiO_2-FO and Au-Vert. nanocomposites was found to be 0.4463, 1.4880 and 1.6208 respectively.

5.4. CATALYTIC ACTIVITY OF Au-SiO_2-FO ON AERIAL OXIDATION OF CYCLOHEXANE

5.4.1. Effect of Temperature

The influence of reaction temperature on aerial oxidation of cyclohexane to adipic acid at 4.3 MPa in a solvent free condition using Au-SiO_2-FO is shown in Figure 5.3. It has been observed that a smaller amount of cyclohexane is oxidized to cyclohexanol and cyclohexanone at 110 °C. However, the conversion of cyclohexane increases with the increase in reaction temperature till 120 °C and reaches plateau as the oxygen concentration becomes the limiting factor for higher conversion. Selectivity of cyclohexanone and acid products is more at 120 °C and gradually decreases as the temperature is further increased. Selectivity of cyclohexanol is less at this temperature and increases on further increase in reaction temperature. The increase in selectivity of cyclohexanone at lower temperature may be attributed to the preferential conversion of cyclohexanol to cyclohexanone as the former is more reactive than cyclohexane. The decrease in selectivity of acid products beyond 120 °C is due to the oxidation and decomposition of adipic acid to lower acids viz., glutaric, succinic acids. The lower acids may also further react with available oxygen in the reaction medium to give finally gaseous oxidative products such as CO_2, H_2 and water, which are evident from the analysis of gaseous products by GC with TCD detector.

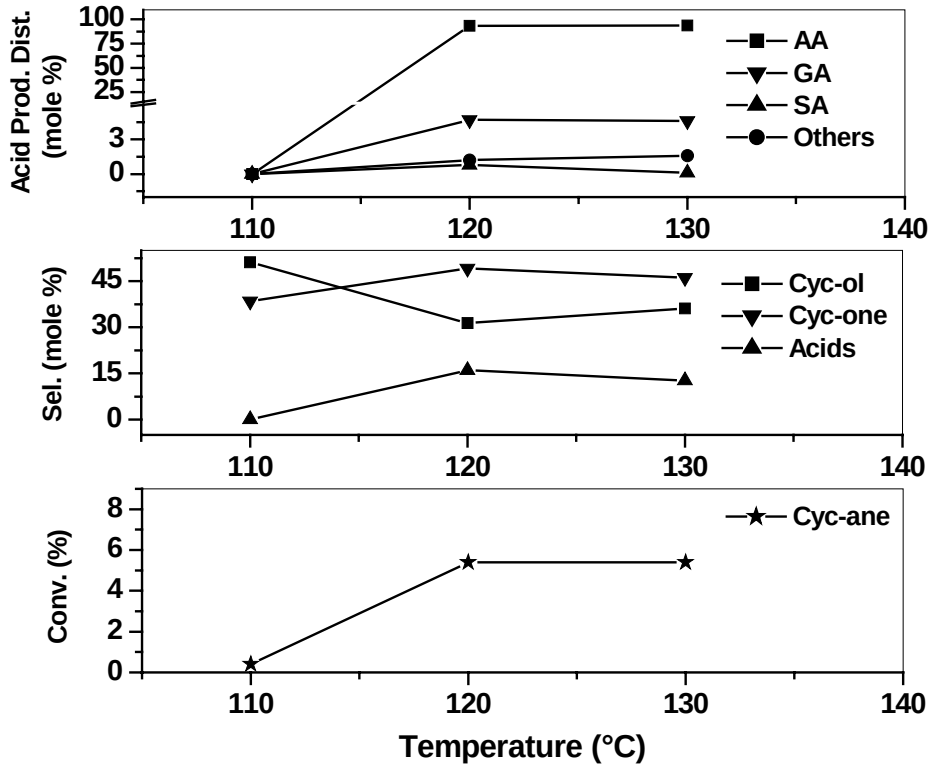

Figure 5.3. Influence of temperature on conversion, selectivity and acid product distribution in aerial oxidation of cyclohexane catalyzed by Au-SiO_2-FO. Reaction condition: Duration = 8 h, Air Pressure = 4.3 MPa, Stirring speed = 400 rpm.

To ascertain the effect of cyclohexane conversion and products selectivities after complete consumption of oxygen in air, the autoclave was refilled twice (Figure 5.4). It has been observed that the rate of cyclohexane conversion increases linearly and selectivity of acids continue to increase further. However, on further refilling (4^{th} time), the rate of cyclohexane conversion slows down and selectivity of adipic acids decreases (Table 5.2). The decrease in the rate of cyclohexane conversion can be attributed to various reasons like deactivation of the catalyst either due to leaching of gold nanoparticles or adsorption of products on the surface of Au-SiO_2-FO and preferred oxidation of products (acids) vis-à-vis reactant. The leaching of gold nanoparticles from catalyst after each refilling with air was monitored by AAS analysis and the data is

shown table 5.3. The decrease in selectivity of acid products is attributed to the oxidation of more reactive products and oxidative decomposition of adipic acid to lower acids viz., glutaric, succinic acids as the gold catalyst gets deactivated after refilling four times with air as evident from the table 5.2. Thus, the oxygen present in the reaction mixture is used up in the oxidation of more reactive products and oxidative decomposition of adipic acid.

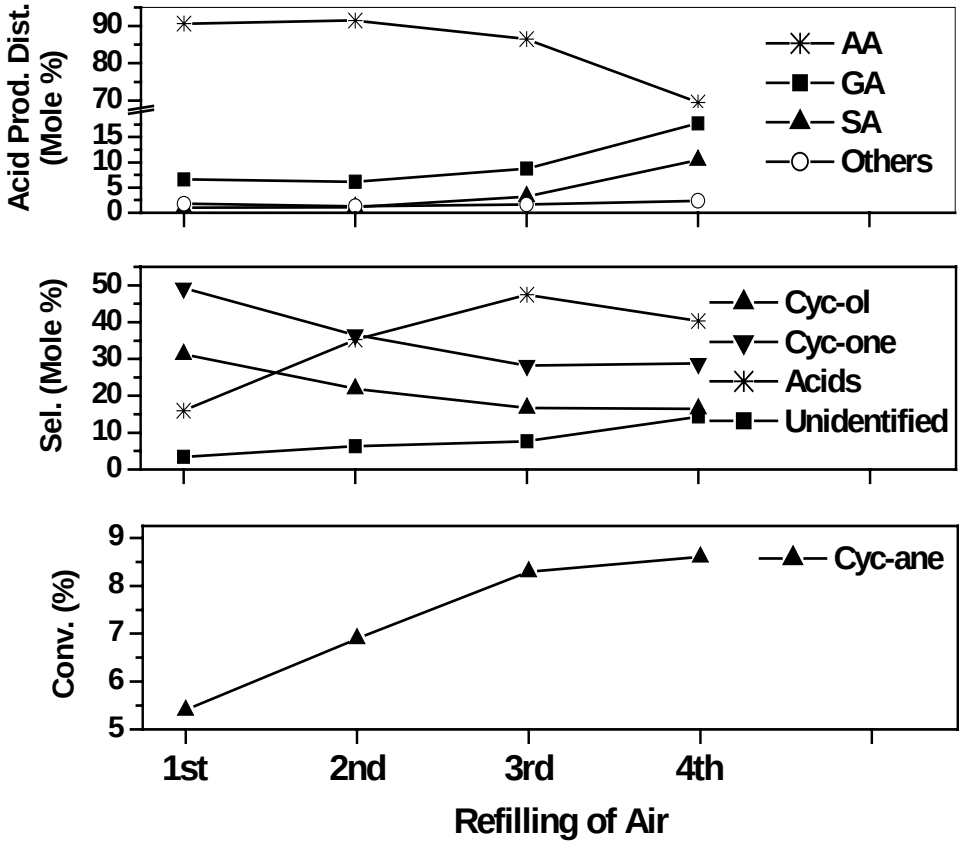

Figure 5.4. Influence of oxygen concentration on conversion, selectivity and acid product distribution in aerial oxidation of cyclohexane catalyzed by Au-SiO_2-FO in a solvent free condition. Reaction condition: Duration = 8 h (1st), 3 h 30 min (2nd), 2 h (3rd) and 2 h (4th), Temperature = 120 °C, Air Pressure = 4.3 MPa (each time), Stirring speed = 400 rpm.

Table 5.2. Influence of oxygen concentration on conversion, selectivity and acid product distribution in aerial oxidation of cyclohexane catalyzed by Au-SiO_2-FO at 120 °C.

No. of Refilling with Air	Air Press. (MPa)	C_6H_{12} Conv. (%)	Time (h)	Product Selectivity (%)				Acid Product Distribution (%)			
				-nol	-none	acids	UDP	AA	GA	SA	other acids
1.	4.3	5.4	8	31.3	49.2	16.0	3.5	90.6	6.6	1.0	1.8
2.	4.3	6.9	11.5	21.9	36.5	35.3	6.3	91.5	6.1	1.1	1.3
3.	4.3	8.3	13.5	16.7	28.2	47.4	7.7	86.5	8.7	3.2	1.6
4.	4.3	8.6	15.5	16.5	28.8	40.3	14.4	69.5	17.7	10.4	2.4

(a) Reaction condition: Cyclohexane = 30 mL, Catalyst = 25 mg, Temperature = 120 °C, Stirring Speed = 400 rpm. (b) Overall Yield: Product Abbreviations: -nol = Cyclohexanol; -none = Cyclohexanone; UDP = Unidentified Products; AA = Adipic Acid; GA = Gluteric Acid; SA = Succinic Acid.

Table 5.3. AAS analysis of catalyst, Au-SiO_2-FO after each refilling of reaction mixture with air.

Catalyst (Au-SiO_2-FO)	Au Wt (%)	% Leaching	Conv. (%)	% Increase in Conv.
First Charge	1.42	–	5.4	–
Second Recharge	1.40	1.4	6.9	1.5
Third Recharge	1.35	5	8.3	2.9
Fourth Recharge	1.30	8.5	8.6	3.2

5.4.2. Effect of Pressure

The Figure 5.5 depicts the effect of pressure on aerial oxidation of cyclohexane to adipic acid at 120 °C in a solvent free condition using Au-SiO_2-FO as catalyst. It can be clearly seen that the cyclohexane conversion as well as selectivity of acid products is increased with increasing pressure. This observation is anticipated, as more oxygen was available at higher pressure. Selectivity of cyclohexanol decreases, while cyclohexanone increases with increasing pressure, which again indicates that the cyclohexanol is first getting converted to cyclohexanone. The cyclohexanone is further oxidized to 1,2-dione to produce adipic acid by ring opening of cyclohexane as reported earlier.

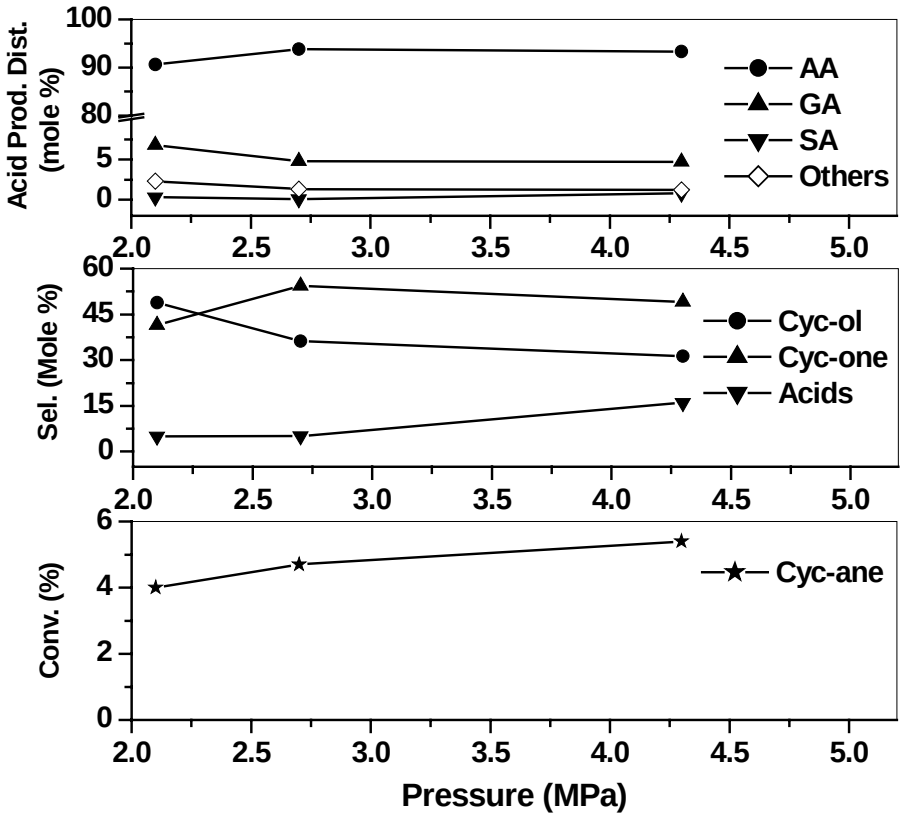

Figure 5.5. Influence of air pressure on conversion, selectivity and acid product distribution in the oxidation of cyclohexane catalyzed by Au-SiO_2-FO in a solvent free condition. Reaction condition: Duration = 6.5 h (2.07 MPa), 7 h (2.7 MPa) and 8 h (4.3 MPa), Temperature = 120 °C, Stirring speed = 400 rpm.

5.4.3. Effect of Amount of Catalyst

The effect of the amount of catalyst on the aerial oxidation of cyclohexane to adipic acid at 120 °C and 4.3 MPa without using any solvent is shown in Figure 5.6. The conversion of cyclohexane increases with increasing amount of catalyst. It has been observed that the selectivity of cyclohexanol increases while that of cyclohexanone decreases with increasing amount catalyst. The decrease in selectivity of cyclohexanone can be due to the preferential oxidation to acid products. Selectivity of acid products is found to decrease slightly with the increasing amount of catalyst.

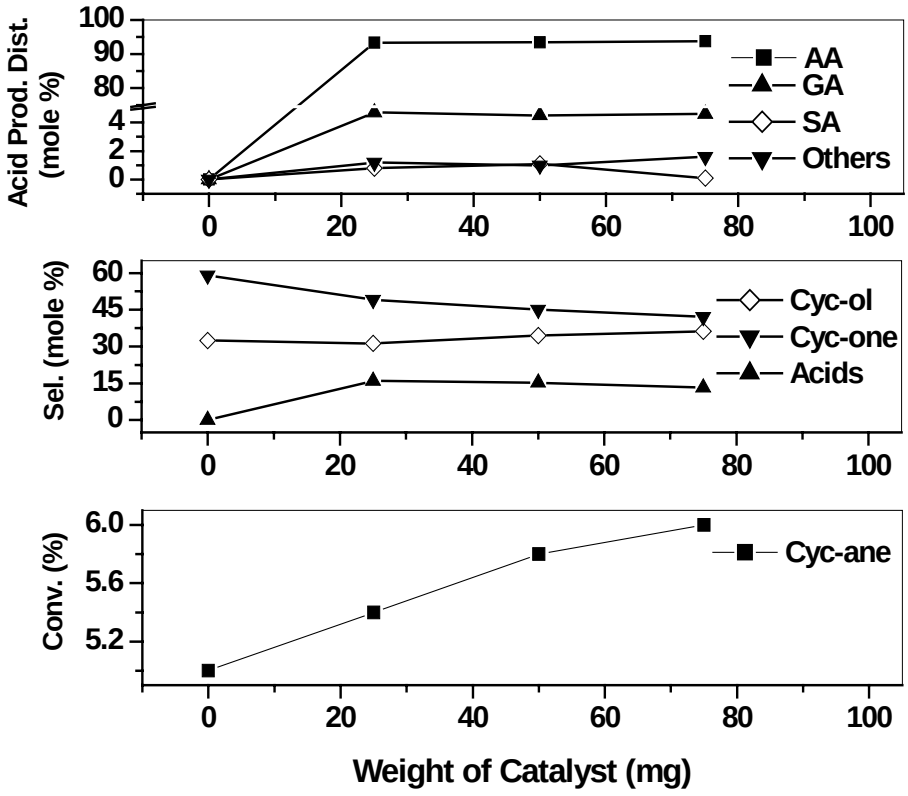

Figure 5.6. Influence of concentration of Au-SiO_2-FO catalyst on conversion, selectivity and acid product distribution in aerial oxidation of cyclohexane. Reaction conditions: Duration = 8 h, Temperature = 120° C, Air Pressure = 4.3 MPa, Stirring speed = 400 rpm.

5.4.4. Comparative Study using Au-SiO_2-Chem, Au-SiO_2-FO and Au-Vert with Different Particle Size of Nano Gold

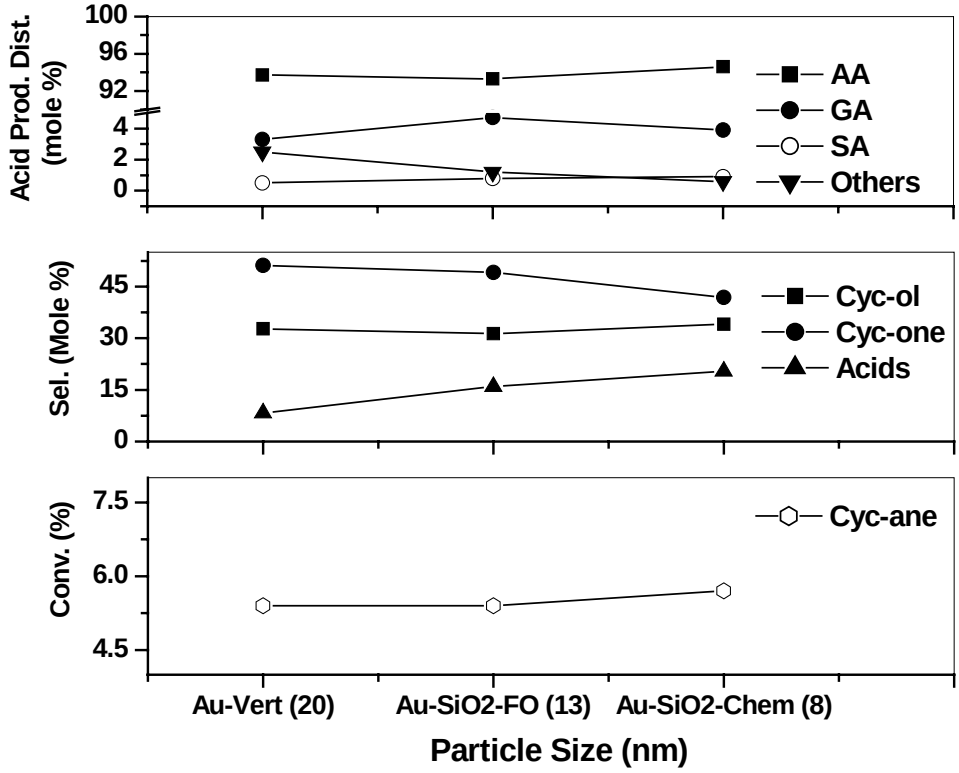

Figure 5.7. Influence of nano Au particle size on conversion, selectivity and acid product distribution in aerial oxidation of cyclohexane. Reaction conditions: Duration = 5 h (Au-SiO_2-Chem), 8 h (Au-SiO_2-FO) and 12 h (Au-Vert), Temperature = 120 °C Air Pressure = 4.3 MPa, Stirring speed = 400 rpm.

The influence of the particle size of nano gold on the catalytic activity and selectivity of Au-SiO_2-Chem, Au-SiO_2-FO and Au-Vert having gold particles of diameter 8 nm, 13 nm and 20 nm, respectively, and is presented in Figure 5.7. It has been observed that among Au-SiO_2-Chem, Au-SiO_2-FO and Au-Vert catalysts, Au-SiO_2-Chem show nearly same cyclohexane conversion. However, among the products, selectivity of acids and cyclohexanol increases while of cyclohexanone decreases with the decrease in particle size of nano Au containing catalysts. This may be due to the

increased oxidation of cyclohexanone to a more reactive species, 1,2 dione, which subsequently oxidized to adipic acid. The extent of oxidation of cyclohexanone is found to increase with the decrease in size of gold nanoparticles, obviously due to availability of more surface area for the reactant molecules to get adsorbed onto the nano gold surface. This also explains the lower concentration of cyclohexanone in the reaction mixture for Au-SiO_2-Chem compare to other catalysts, Au-SiO_2-FO and Au-Vert.

5.5. PROBABLE REACTION PATHWAY OF CYCLOHEXANE OXIDATION TO ADIPIC ACID

The aerial oxidation of cyclohexane in the absence of catalyst at 120 °C and 2.1-4.3 MPa, results in the formation of only cyclohexanol and cyclohexanone. The reaction may be schematically represented as follows:

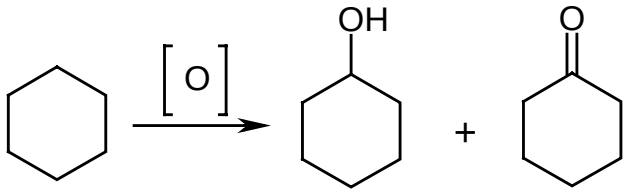

However, the use of gold nanoparticles as catalyst under similar condition along with cyclohexanol and cyclohexanone forms acid products, such as adipic acid (AA), gluteric acid (GA) and succinic acid (SA). The oxidation of cyclohexane to adipic acid involves 1,2-cyclohexanedione as an intermediate, which results due to oxidation of cyclohexanone.[2,32] This keto-form yields the desire adipic acid while the enol-form leads to other lower acids. The lower acids (such as GA, SA, etc.) can also form by oxidative degradation of adipic acid. Thus, the oxidation of cyclohexanone to 1,2-cyclohexanedione intermediate, is the key step for adipic acid formation. It can be inferred from above observation that the oxidation of cyclohexanone to 1,2-

cyclohexanedione may involve relatively high activation energy pathway and may not be achievable in absence of catalyst. However, the use of supported gold nanoparticles may lower this activation energy, which results in the formation of adipic acid and other lower acids. This may be schematically represented as follows:

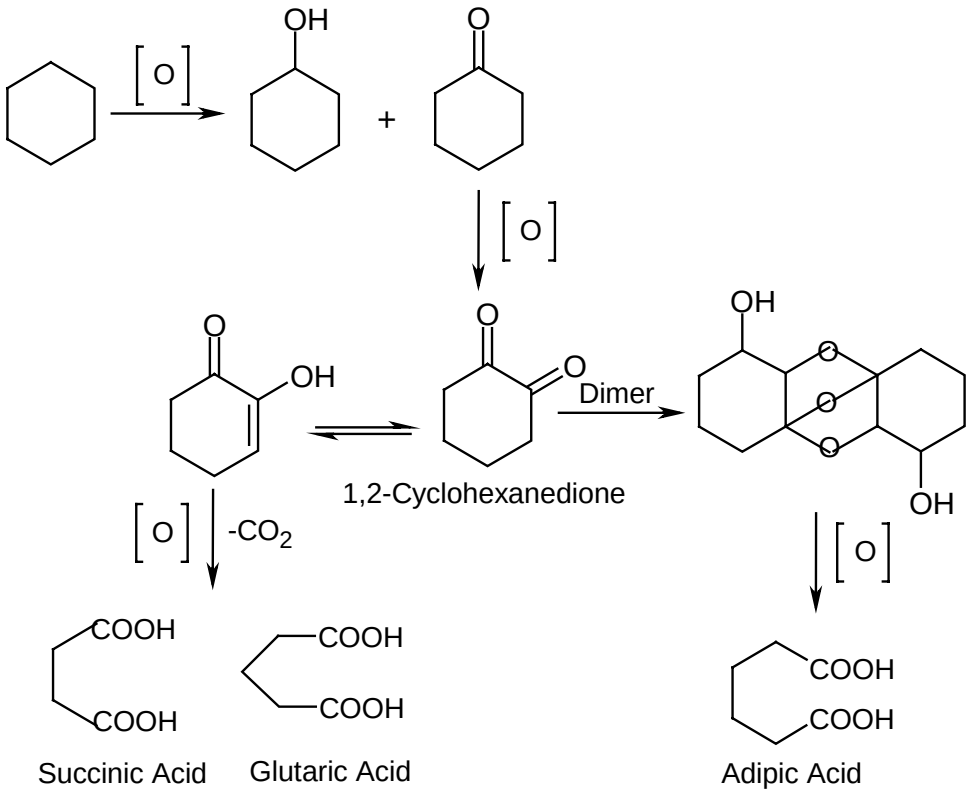

5.6. SUMMARY

In this chapter, a novel, solvent free, aerial oxidation of cyclohexane to adipic acid using gold nanoparticles supported on amorphous (fumed) silica, as catalyst, in an environmentally benign oxidation process has been efficiently demonstrated. The cyclohexane conversion and acid selectivity was found to be dependent on temperature, pressure and amount of catalyst used. The conversion of cyclohexane oxidation is ~ 5-6 % but with respect to the concentration of oxygen in reaction mixture, the consumption of oxygen is almost 100 %. The particle size of nano gold plays an important effect on the product distribution in the aerial oxidation of cyclohexane. It has been observed that the selectivity of cyclohexanol and acid increases while cyclohexanone decreases with the decrease in particle size.

5.7. REFERENCES

1. (a) J. M. Thomas, *Nature* **1985**, *314*, 669. (b) T. Ito, J. H. Lunsford, *Nature* **1985**, *314*, 721.
2. D. D. Davis, D. R. Kemp in *Kirk-Othmer Encyclopedia of Chemical Technology*, J. I. Kroschwitz, M. Howe-Grant, (Eds.) 4th ed., Wiley, New York, 1991, vol. 1 pp 466-493.
3. A. Castellan, J. C. J. Bart, S. Cavallaro, *Catal. Today* **1991**, *9*, 237.
4. K. Tanaka, *Hydrocarbon Process* **1974,** 114.
5. K. Sato, M. Aoki, R. Noyori, *Science* **1998**, *281*, 1646.
6. U. S. Pat, 3,530,185 (Sept. 22, 1970), K. Pugi (to E. I. du pont de Nemours & Co., Inc.).
7. *Hydrocarbon Process*, **1969**, *48*, 163.
8. (a) U. S. Pat. 4,163,027 (July 31, 1979), P. Magnussen, G. Herrman, E. Frommer, (to Badische Anilin-und Soda-Fabrik A. G.). (b) Ger. Offen. 3,328,771 (Feb. 28, 1985), Stoessel and co-workers, (to Badische Anilin-und Soda-Fabrik A. G.). (c) U. S. Pat. 4,704,476 (Nov. 3, 1987), J. Hartig, G. Herrman, E. Lucas, (to Badische Anilin-und Soda-Fabrik A. G.).
9. (a) U. S. Pat. 3,957,876 (May 18, 1976), M. Rapoport, J. O. White, (to E. I. du pont de Nemours & Co., Inc.). (b) U. S. Pat. 3,987,100 (Oct. 19, 1976), W. J. Barnette, D. L. Schmitt, J. O. White, (to E. I. du pont de Nemours & Co., Inc.). (c) U. S. Pat. 4,465,861 (Aug. 14, 1984), J. Hermolin, (to E. I. du pont de Nemours & Co., Inc.).
10. (a) U. S. Pat. 3,925,316 (Dec. 9, 1975), J. C. Brunie, N. Creene, F. Maurel, (to Rhone-Poulenc S. A.). (b) Adapted from L. L. van Dierendonck, J. A. de Leeuw den Bouter, *PT/Procestechnick* **1984**, *39(3)*, 44-48. (c) U. S. Pat. 3,923,895 (Dec. 2, 1975), M. Costantini, N. Creene, M. Jouffret, J. Nouvel (to Rhone-Poulenc S. A.). (d) U. S. Pat. 3,927,105 (Dec. 16, 1975), J. C. Brunie, N. Creene, (to Rhone-Poulenc S. A.).
11. (a) U. S. Pat. 4,326,085 (Apr. 20, 1982), M. De Cooker, (to Stamicarbon N. V.) (b) Eur. Pat. 092,867 (Nov. 2, 1983), J. G. Housmans and co-workers, (to Stamicarbon N. V.). (c) U. S. Pat. 4,238,415 (Dec. 9, 1980), W. O. Bryan, (to Stamicarbon N. V.).

12. (a) U. S. Pat. 3,932,513 (Jan. 13, 1976), J. L. Russell, (to Halcon International, Inc.). (b) U. S. Pat. 3,796,761 (Aug. 18, 1971), Marcell and co-workers, (to Halcon International, Inc.).

13. Brit. Pat. 1,590,958 (June 10, 1981), J. F. Risebury, (to Imperial Chemical Industries, Ltd.).

14. (a) J. Alagy and co-workers, *Hydrocarbon Process* **1968**, *47*, 131. (b) H. Van Landeghem, *Ind. Eng. Chem. Process. Des.* **1974**, *13*, 317.

15. U. S. Pat. 3, 895,067 (Jan. 12, 1973), G. H. Mock and co-workers, (to Monsanto Co.).

16. U. R. Pillai, E. Sahle-Demessie, *Chem. Commun.* **2002**, 2142.

17. (a) R. F. Parton, I. F. J. Vankelecom, M. J. A. Casselman, C. P. Bezoukhane. J. B. Uytterhoeven, P. A. Jacobs, *Nature* **1994**, *370*, 541. (b) R. F. Parton, G. J. Peere, P. E. Neys, P. A. Jacobs, R. A. Claessens, G. V. Baron, *J. Mol. Catal.* A **1996**, *113*, 445. (c) K. J. Balkus, M. Eissa, R. Lavado, *J. Am. Chem. Soc.* **1995**, *117*, 10753. (d) N. Herron, G. D. Stucky, C. A. Tolman, *J. Chem. Soc. Chem. Commun.* **1986**, 1521. (e) R. Raja, P. Ratnasamy, *Catal. Lett.* **1997**, *48*, 1.

18. (a) M. Dugal, G. Sankar, R. Raja and J. M. Thomas, *Angew. Chem. Int. Ed. Engl.* **2000**, *39*, 2310. (b) R. Raja, G. Sankar, J. M. Thomas, *Angew. Chem. Int. Ed. Engl.* **2000**, *39*, 2313.

19. (a) B. Hammer, J. Norskov, *Nature* **1995**, *376*, 238. (b) P. Pyykko, *Chem. Rev.* **1988**, *88*, 563. (c) G. C. Bond, *Catal. Today* **2002**, *72*, 5.

20. (a) M. Haruta, N. Yamada, T. Kobayashi, S. Iijima, *J. Catal.* **1989**, *115*, 301. (b) M. Haruta, S. Tsubota, T. Kobayashi, H. Kageyama, M. J. Genet, B. Delmon, *J. Catal.* **1993**, *144*, 175. (c) M. Haruta, *Catal. Today* **1997**, *36*, 153. (d) M. Haruta, M. Date, *Appl. Catal. A: General* **2001**, *222*, 427. (e) M. Okumura, M. Haruta, *Chem. Lett.* **2000**, 396.

21. R. J. H. Grisel, B. E. Nieuwenhuys, *J. Catal.* **2001**, *199*, 48.

22. (a) M. Valden, X. Lai, D. W. Goodman, *Science* **1998**, *281*, 1647. (b) V. Bondzie, S. C. Parker, C. T. Campbell, *Catal. Lett.* **1999**, *63*, 143.

23. H. Li, Y. Y. Luk, M. Mrksich, *Langmuir* **1999**, *15*, 4957.

24. L. Pasquato, F. Rancan, P. Scrimin, F. Mincin, C. Frigeri, *Chem. Commun.* **2000**, 2253.

25. M. Bartz, J. Kuther, R. Seshadri, W. Tremel, *Angew. Chem. Int. Ed. Engl.* **1998**, *37*, 2466.

26. P. Mukherjee, S. Senapati, D. Mandal, A. Ahmad, M. I. Khan, R. Kumar, M. Sastry, *ChemBioChem* **2002**, *3*, 461.

27. P. Mukherjee, A. Ahmad, D. Mandal, S. Senapati, S. R. Sainkar, M. I. Khan, R. Ramani, R. Parischa, P. V. Ajaykumar, M. Alam, M. Sastry, R. Kumar, *Angew. Chem. Int. Ed. Engl.* **2001**, *40*, 3585.

28. P. Mukherjee, C. R. Patra, A. Ghosh, R. Kumar, M. Sastry, *Chem. Mater.* **2002**, *14*, 1678.

29. D. V. Leff, L. Brandt, J. R. Heath, *Langmuir* **1996**, *12*, 4723.

30. J. W. Jeffrey, *Methods in Crystallography* Academic Press, New York, 1971.

31. (a) V. Patil, R. B. Malvankar, M. Sastry, *Langmuir* **1999**, *15*, 8197. (b) J. J. Storhoff, C. A. Mirkin, *Chem. Rev.* **1999**, *99*, 1849.

32. (a) J. R. Chen, H. H. Yang, C. H. Wu, *Org. Process. Res. Dev.* **2004**, *8***,** 252. (b) Y. Wen, O. E. Potter, T. Sridhar, *Chem. Eng. Sci.* **1997**, *52*, 4593. (c) A. E. Shilov, G. B. Shulpin, *Activation and Catalytic Reactions of Saturated Hydrocarbons in the Presence of Metal Complexes*, Kluwer Academic Publishers, 2001.

6.1. SUMMARY

The thesis gives an account of

(i) The extracellular syntheses of gold, silver, metal sulfide (CdS, PbS, ZnS, MnS and NiS) nanoparticles and gold silver alloy nanoparticles using eukaryotic microorganisms like fungi.

(ii) The intra- and extracellular syntheses of gold and silver nanoparticles of controlled dispersity using prokaryotic microorganism such as actinomycetes and

(iii) Harnessing and application of extracellularly synthesized gold nanoparticles supported on amorphous (fumed) silica used as catalysts in the oxidation reaction.

Chapter 1 presents a general introduction about nanoscience and nanotechnology and their consequences to different fields of science. Different physical, chemical and bio-based synthesis routes of nanomaterials and their characterization techniques are discussed. It also gives an account of different properties and applications of nanomaterials with particular emphasis to catalytic application. Based on literature survey, the scope and objectives of the present work have been summarized at the end of the chapter.

Chapter 2 deals with the extracellular synthesis of metal (such as gold and silver) and bimetallic (gold silver) alloy nanoparticles using the eukaryotic system such as fungi. The fungus, *Fusarium oxysporum*, when exposed to gold and silver solutions resulted in the formation of highly stable gold and silver nanoparticles, respectively, in the size range of 5–50 nm. However, exposure of an equimolar mixture of gold and silver salts simultaneously to *Fusarium oxysporum* resulted in the synthesis of bimetallic gold silver alloy nanoparticles of different compositions. The preliminary study of protein extract revealed the presence of

NADH dependent reductases in the extract. It has been observed that the composition of Au-Ag nano alloy is cofactor, NADH, dependent. The Au-Ag alloy nanoparticle of varying composition can be synthesized by controlling the release of amount of cofactor by using the controlled amount of biomass. The high stability of the nanoparticle solution is due to the secretion of capping protein by the fungus in the reaction mixture. The stability of capping protein was found to be pH dependent

Chapter 3 accounts the extra- and intracellular biosynthesis of gold and silver nanoparticles with controlled monodispersity using actinomycetes, *Thermomonospora* sp., and *Rhodococcus* sp., respectively. The exposure of metal salts to *Thermomonospora* sp. resulted in the release of enzyme and subsequent formation of fairly monodispersed nanoparticles in solution of dimensions 7–12 nm. The preliminary study of the secreted enzyme revealed their dependence on NADH cofactor. However, in case of *Rhodococcus* sp., the reduction of metal ions occur intracellurly with good monodispersity of diameter in the range of 5–15 nm by the reductase enzyme present on the cell wall as well as on the cytoplasmic membrane.

Chapter 4 deals with the extracellular biosynthesis of semiconductor metal sulfide nanoparticles using fungus, *Fusarium oxysporum*. The extracellular synthesis of metal sulfide is due to the release of NADH dependent sulfate reductase enzyme in solution, which results in the reduction of SO_4^{2-} ions to S^{2-} and subsequent formation of metal sulfide nanoparticles. The high stability of the metal sulfide nanoparticle solution is due to stabilization by proteins present in the reaction mixture. It was observed that the presence of protein moiety on the surface of the metal sulfide does not affect their optoelectronic property. The fluorescence measurements recorded from CdS solution reveal the small

stokes' shift indicating that the surfaces of sulfide are regular with most surface atoms satisfying the coordination or oxidation states of their bulk counterpart. However, the measurements recorded from other sulfides, PbS, ZnS, MnS and NiS exhibit broad emission band, indicating the surfaces of sulfides are irregular, which may arise due to the uncommon oxidation or missing of atom or adsorbed impurities on the surface of the particle.

Chapter 5 focuses on the application of extracelluarly synthesized gold nanoparticles by *Fusarium oxysporum* supported on amorphous (fumed) silica as catalysts in the aerial oxidation of cyclohexane in a solvent free system. The conversion of cyclohexane oxidation was ~ 5–6 % and was found to be dependent on reaction temperature, pressure and amount of catalyst. Among the products, amount of acids increases linearly with the decrease in nano gold particle size and among the acid products the selectivity of adipic acid was more than 90 %.

6.2. CONCLUSIONS

6.2.1. Extracellular Synthesis of Metal and Bimetallic Alloy Nanoparticles using *Fusarium oxysporum*

- The use of eukaryotic microorganism such as fungi, for the first time, in the synthesis of metal nanoparticles is established.
- The exposure of gold and silver ions to fungus, *Fusarium oxysporum*, results in the release of reductase enzyme and subsequent formation of highly stable gold and silver nanoparticles in solution of 5–50 nm dimensions. The secreted enzyme is found to be dependent on NADH cofactor.

- The high stability of nanoparticles in solution is due to capping of particles by the release of capping proteins by *Fusarium oxysporum*. The stability of capping protein is found to be pH dependent. At higher pH (>12) the nanoparticle solution remains stable while it aggregates at lower pH (<2) as the protein gets denatured.
- The exposure of equimolar mixture of gold and silver solution simultaneously to *Fusarium oxysporum*, lead to the formation of gold silver alloy nanoparticle of different compositions.
- The composition of gold silver alloy nanoparticles is cofactor, NADH, dependent. The alloy nanoparticles of varying composition can be synthesized by controlling the release of amount of cofactor by using the controlled amount of biomass of *Fusarium oxysporum*.

6.2.2. Extra- and Intracellular Synthesis of Metal Nanoparticles using Actinomycetes

- The use of prokaryotic microorganism such as actinomycetes, in the extracellular synthesis of nanomaterials is established for the first time.
- The exposure of gold solution to actinomycete, *Thermomonospora* sp. resulted in the formation of fairly monodispersed and highly stable nanoparticles of dimensions 7–12 nm. However, the same actinomycete, *Thermomonospora* sp., could not synthesize silver nanoparticles with similar monodispersity. This may be due to the difference in mode of interactions between different metal nanoparticles and the capping proteins. In this case also, the reductase was found to be NADH dependent, as in *Fusarium oxysporum*.

- The time taken for reduction of gold ions with actinomycete, *Thermomonospora* sp. (120 h), was longer compared to that using fungus, *Fusarium oxysporum*, (48 h) (chapter 2). However, the gold nanoparticles synthesized using the fungi were polydispersed of dimension 8–40 nm while with actinomycetes, the synthesized nanoparticles were fairly monodispersed of diameter in the range 7–12 nm. The size and dispersity control may be the consequence of different types and extent of proteins/enzymes secretion by actinomycetes in comparison with fungi and also may be due to use of different synthesis conditions. In the case of actinomycetes, *Thermomonospora* sp., the reaction is carried out under alkaline conditions and at slightly elevated temperatures. Under these extreme conditions, fungus, *Fusarium oxysporum*, cannot survive.
- The treatment of gold solution with actinomycete, *Rhodococcus* sp. lead to the formation of intracellular nanoparticles with good monodispersity in the size range of 5–15 nm. The intracellular formation of nanoparticles can be attributed to the reduction of the metal ions by the enzyme present in the cell wall membrane.

6.2.3. Extracellular Synthesis of Metal Sulfide Nanoparticles using *Fusarium oxysporum*

- The extracellular synthesis of semiconductor metal sulfide nanoparticles using fungus *Fusarium oxysporum* by a purely enzymatic pathway has been observed.
- The extracellular synthesis of metal sulfide is due to the release of NADH dependent sulfate reductase enzyme in solution, which resulted in reduction of SO_4^{2-} to S^{2-} ions and subsequent formation of highly stable metal sulfide nanoparticles. The high

stability of the metal sulfide nanoparticle solution is due to present of proteins in the reaction mixture.

- Cadmium sulfide solution revealed small stokes' shift in the fluorescence measurements, indicating that the surfaces of sulfide are regular with most surface atoms satisfying the coordination or oxidation states of their bulk counterpart.
- Fluorescence measurements of other sulfides, PbS, ZnS, MnS and NiS exhibited broad emission band, signifying the surfaces of sulfides are irregular, which may arise due to uncommon oxidation state or adsorbed impurities on surfaces of sulfide particles.

6.2.4. Aerial Oxidation of Cyclohexane to Adipic Acid

- Aerial oxidation of cyclohexane to adipic acid was demonstrated using extracellularly synthesized gold nanoparticles, by fungus, *Fusarium oxysporum*, supported on amorphous (fumed) silica, as a catalyst in an environmentally benign oxidation process in a solvent free system.
- The conversion of cyclohexane oxidation was ~ 5–6 %.
- The selectivity of acids was found to depend on reaction temperature, pressure and amount of catalyst.
- The gold particle size plays an important role in aerial oxidation of cyclohexane. The acid selectivity was found to be dependent on the size of gold nanoparticle.

6.3. FUTURE OUTLOOK

The ability of eukaryotic and prokaryotic microorganisms to reduce the inorganic metals has opened up a new exciting green chemistry approach towards the development of natural 'nano-factories'. However, a number of issues have to be addressed from the nanotechnology and microbiology point of view and require to be addressed before such a biosynthesis approach can compete with the existing physical and chemical protocols. The elucidation of biochemical pathways leading to metal ion reduction and formation of nanoparticles is essential in order to develop a rational bio-based nanoparticle synthesis procedure. Similarly, an understanding of the surface chemistry of the biogenic nanoparticles (i.e., the nature of capping surfactants/peptides/proteins) would be equally important. This would then lead to the possibility of genetically engineering fungi/actinomycetes to overexpress specific reducing molecules and capping agents, thereby controlling not only the size of the nanoparticles but also their shape. The rational use of constrained environments within cells such as the periplasmic space and cytoplasmic vesicular compartments (in case of actinomycetes, *Rhodococcus* sp.) to modulate nanoparticle size and shape is an exciting possibility. The range of chemical compositions of nanoparticles currently accessible by bio-based methods is currently extremely limited and confined to metals, metal sulfides and iron oxide. Extension of the protocols to enable reliable synthesis of nanocrystals of other oxides (TiO_2, ZrO_2, etc.) and nitrides, carbides etc. could make this synthesis protocol a commercially viable proposition.

The fungal and actinomycete-mediated green chemistry approach towards the synthesis of nanoparticles has many advantages such as ease with which the process can be scaled up, economic viability, possibility of easily covering large surface areas by suitable

growth of the mycelia, etc. Compared to bacterial fermentations, in which the process technology involves the use of sophisticated equipment for getting clear filtrates from the colloidal broths, fungal broth can be easily filtered by filter press of similar simple equipment, thus saving considerable investment costs for equipment. This shift from bacteria to fungi as a means of developing natural 'nano-factories' has the added advantage that downstream processing and handling of the biomass would be much simpler. Further, compared to bacteria; fungi and actinomycetes are known to secrete much higher amounts of proteins, thereby significantly increasing the productivity of this biosynthetic approach.

Equally intriguing are questions related to the metal ion reduction/reaction process in cellular metabolism and whether the nanoparticles formed as by-products of the reduction process or is there any possible roles of thus formed nanoparticles in a cellular activity (such as magnetite in magnetotactic bacteria). Microorganisms such as fungi are not normally exposed to high concentrations of metal ions such as Cd^{2+}, $AuCl_4^-$ and Ag^+. This stress induced cellular function such as secretion of enzymes when challenged, which is capable of metal-ion reduction and indeed conversion of sulfates to sulfides, may help in understanding of evolutionary processes.

The use of specific enzymes secreted by organisms such as fungi and actinomycetes in the extracellular synthesis of nanoparticles is exciting for the following reasons. The synthesis of nanoparticles would be of importance in catalysis and other applications such as non-linear optics. The nanoparticles can be immobilized in different matrices and used for different catalytic processes.

LIST OF PUBLICATIONS

1. Bioreduction of $AuCl_4^-$ ions by the fungus, *Verticillium* sp. and surface trapping of the gold nanoparticles formed

   P. Mukherjee, A. Ahmad, D. Mandal, **Satyajyoti Senapati**, S. R. Sainkar, M. I. Khan, R. Ramani, R. Parischa, P. V. Ajaykumar, M. Alam, M. Sastry and R. Kumar *Angewante Chemie International Edition*, **2001**, *40*, 3585-3588.

2. Fungus mediated synthesis of silver nanoparticles and their immobilization in the mycelial matrix: A novel biological approach to nanoparticle synthesis

   P. Mukherjee, A. Ahmad, D. Mandal, **Satyajyoti Senapati**, S. R. Sainkar, M. I. Khan, R. Parishcha, P. V. Ajaykumar, M. Alam, R. Kumar and M. Sastry

   Nano Letters, **2001**, *1*, 515-519.

3. Extracellular synthesis of gold nanoparticles by the fungus *Fusarium oxysporum*

   P. Mukherjee, **Satyajyoti Senapati**, D. Mandal, A. Ahmad, M. I. Khan, R. Kumar and M. Sastry

   ChemBioChem, **2002**, *3*, 461–463.

4. Enzyme mediated extracellular synthesis of CdS nanoparticles by the fungus *Fusarium oxysporum*

   Ahmad, P. Mukherjee, D. Mandal, **Satyajyoti Senapati**, M. I. Khan, R. Kumar and M. Sastry

   Journal of the American Chemical Society, **2002**, *124*, 12108–12109.

5. Extracellular biosynthesis of silver nanoparticles using the fungus Fusarium oxysporum

   Ahmad, P. Mukherjee, **Satyajyoti Senapati**, D. Mandal, M. I. Khan, R. Kumar and M. Sastry

   Colloids and Surfaces B: Biointerfaces, **2003**, *28*, 313–318.

6. Extracellular biosynthesis of monodisperse gold nanoparticles by a novel extremoplilic actinomycete, *Thermomonospora* sp.

   A. Ahmad, **Satyajyoti Senapati**, M. I. Khan, R. Kumar and M. Sastry

   Langmuir, **2003**, *19*, 3550-3553.

7. Intracellular synthesis of gold nanoparticles by a novel alkalotolarent actinomycete, *Rhodococcus* species

   A. Ahmad, **Satyajyoti Senapati**, M. I. Khan, R. Kumar, R. Ramani, V. Srinivas, M. Sastry

   Nanotechnology, **2003**, *14*, 824–828.

8. Fungus mediated synthesis of silver nanoparticles: a novel biological approach

   Satyajyoti Senapati, D. Mandal, A. Ahmad, M. I. Khan, M. Sastry and R. Kumar, *Indian Journal of Physics*, **2004**, *78A*, 101-105.

9. Biosynthesis of Extra/Intracellular Gold Nanoparticles from a Novel Fungus *Tricothesium* sp.

   A. Ahmad, **Satyajyoti Senapati**, M. I. Khan, R. Kumar and M. Sastry

   Journal of Biomedical Nanotechnology, **2005**, *1*, 47-53.

10. Extracellular biosynthesis of bimetallic Au-Ag alloy nanoparticles

    Satyajyoti Senapati, A. Ahmad, M. I. Khan, M. Sastry and R. Kumar

    Small, **2005**, *1*, 517–520.

11. Biosynthesis of Silver Nanoparticles using Fungi

    A. Ahmad, **Satyajyoti Senapati**, M. I. Khan, R. Kumar and M. Sastry

    In: *The Fungi: Bio-diversity and Biotechnology*, Ed: S. Deshmukh, Oxford IBH publisher, NewDelhi/ Science publisher enfield (NH) USA, **2005** (In press).

List of Manuscript Communicated

1. Aerial oxidation of cyclohexane to adipic acid using nano Au as catalyst in a solvent free system

   Satyajyoti Senapati, A. K. Kinage, A. A. Deshmush, A. Ahmad, M. I. Khan, M. Sastry and R. Kumar

   Applied Catalysis A: General (communicated)

2. Extracellular synthesis of metal sulfide quantum dots

   Satyajyoti Senapati, A. Ahmad, M. I. khan, M. Sastry and R. Kumar, *Nanotechnology* (communicated).

Contributions to National/International Symposia/Conferences

1. Fungus mediated synthesis of gold nanoparticles: a novel biological approach to nanoparticle synthesis

   D. Mandal, A. Ahmad, P. Mukherjee, **Satyajyoti Senapati**, S. R. Sainkar, M. I. Khan, R. Parischa, R. Kumar and M. Sastry

   Fourth National Symposium in Chemistry, 1-3 February, 2002

   Organized jointly by NCL and University of Pune, Pune. **(*Poster Presentation*)**

2. Isolation, purification and identification of gold nanoparticles produced by an endophytic fungus, *Verticillium* sp.

   A. Ahmad, P. Mukherjee, D. Mandal, **Satyajyoti Senapati**, M. I. Khan, R. Kumar and M. Sastry

   National Conference on Fungal Diversity and Biotechnology, 2-4 February, 2002

   K. V. Pendharkar College, Dombivli, University of Mumbai. **(*Oral Presentation*)**

3. TEM study of surface trapping of gold nanoparticles during bioreduction of chloroaurate ions by the fungus, *Verticillium* sp.

   R. Parischa, P. Mukherjee, A. Ahmad, **Satyajyoti Senapati**, D. Mandal, M. I. Khan, M. Sastry and R. Kumar

   XXV Annual conference of the Electron microscope society of India on electron microscopy and allied fields, February 19-22, 2002

   Indian Institute of Technology, Bombay. **(*Poster Presentation*)**

4. Isolation, purification and identification of silver nanoparticles produced by an endophytic fungus, *Verticillium* sp.

   A. Ahmad, P. Mukherjee, **Satyajyoti Senapati**, D. Mandal, M. I. Khan, R. Kumar and M. Sastry

   International Symposium on Milestones in the Development of Mycology and plant pathology, 28-30, March, 2002

   Centre for advanced studies in Botany, University of Madras, Madras (Chennai). **(*Oral Presentation*)**

5. Biocatalytic transformations of cyclic and aromatic ketones by the fungus *Fusarium oxysporum*

   D. Mandal, **Satyajyoti Senapati**, A. Ahmad, M. I. Khan and R. Kumar

   Catalysis: Concepts to practice a conference in honour of Dr. Paul Ratnasamy on his 60th Birth anniversary, 26-27 June, 2002

   Organized by NCL Research Foundation, Pune. **(*Oral Presentation*)**

6. Fungus mediated intra and extra cellular synthesis of gold nanoparticles: a novel biological approach to nanoparticle synthesis

   R. Kumar, **Satyajyoti Senapati**, A. Ahmad, P. Mukherjee, D. Mandal, M. I. Khan and M. Sastry

   International Symposium on "Nanobionics 2", September, 2002

   Marburg, Germany. **(Oral *Presentation*)**

7. Biosynthesis of inorganic nanomaterials using fungi

   A. Ahmad, P. Mukherjee, D. Mandal, **Satyajyoti Senapati**, M. I. Khan, R. Kumar, and M. Sastry

   National Symposium on Prospecting of Fungal Diversity and Emerging Technologies & 29th Annual meeting of Mycological Society of India. 6-7 February, 2003 Organized by Agharkar Research Institute, Pune. **(*Poster Presentation*)**

8. Fungus mediated synthesis of silver nanoparticles: a novel biological approach

   Satyajyoti Senapati, D. Mandal, A. Ahmad, M. I. Khan, M. Sastry and R. Kumar, *National symposium on Science and Technology of Nanomaterials*, 6-7 March, 2003

   Organized by Materials Research Society of India (Calcutta Chapter). **(*Poster Presentation*)**

9. Actinomycetes mediated synthesis of monodispersed gold nanoparticles: a novel biological approach

   Satyajyoti Senapati, D. Mandal, A. Ahmad, M. I. Khan, M. Sastry and R. Kumar, *International conference on Science and Nanotechnology*, 17-20 December, 2003, Organized by DST at Hyatt Regency, Kolkata. **(*Poster Presentation*)**